FACULTY OF SCIENCE AND TECHNOLOGY

BACHELOR THESIS

Study programme / specialisation:

Mechanical engineering

The spring semester, 2022

Open / ~~Confidential~~

Authors:
Lars Andreas Flesjå Genthner .....

(signature author)

Sondre Mikael Mikkelsen .....

(signature author)

Course coordinator: Prof. Dimitrios Pavlou
Supervisor: Prof. Dimitrios Pavlou

Thesis title: **Design of the steel frame of a racing car**

Credits (ECTS): 20 points

Keywords: Racing car, Torsional stiffness, Ansys Workbench, FEA

Pages: 87

+ appendix: 16

Stavanger, 15.05.2022

This page is intentionally left blank

Abstract

This thesis concerns the modeling and simulation of the steel frame of a racing car. A literature study on the fundamentals of racing car design, with particular attention to frame design, has been carried out. A considerable amount of time has been invested in 3-D modeling and simulation.

The main objective of this thesis was not to design and revise the best possible version of a racing car. The focus was instead on simulating and interpreting the results. However, it is worth mentioning that six frame iterations were made and improved. The design process was carried out using Autodesk Inventor Professional 2022. Ansys Workbench, Release 2020 R1 was used to analyze and simulate torsional stiffness, behavior under dynamic loading, and deformation during impact with a rigid wall. Simulation resulted in a torsional stiffness value of 13 531.8 Nm/degree and low values in bending, compressive, and tensile stress. Values for external loading were estimated using multiplication factors.

This page is intentionally left blank

Acknowledgments

This thesis is submitted for concluding our bachelor's degree in mechanical engineering at the University of Stavanger.

We want to express our gratitude to Professor Dimitrios Pavlou, our supervisor at the University, for his guidance, advice, and feedback on the project. His enthusiastic encouragement and helpful critique have been greatly appreciated. We would also like to extend our thanks to the rest of the professors and employees at the Department of Mechanical and Structural Engineering and Material Science for their knowledge and learning. We wish to acknowledge the help provided by Anders Engelsvold for his valuable suggestions and advice during the simulation process of this thesis.

A special thanks to our closest family for support and encouragement throughout our study.

Stavanger, 15.05.2022

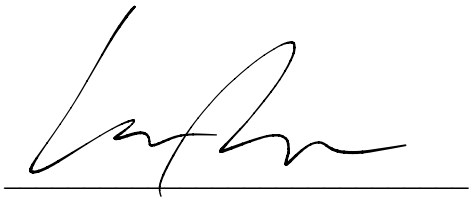

Lars Andreas Flesjå Genthner

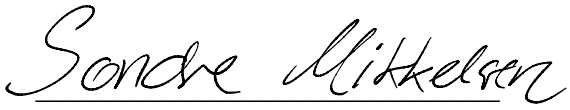

Sondre Mikael Mikkelsen

This page is intentionally left blank

Contents

List of figures

List of tables

Symbols

A	Reference area
A_{cs}	Cross sectional area
C_d	Coefficient of drag
C_l	Coefficient of lift
D	Downforce
D_F	Drag force
D_i	Inside diameter
D_o	Outside diameter
E	Young's modulus
F	Force
$\mathrm{F_E}$	Allowable Euler buckling load
F_t	Tensile Force
f_u	The nominal ultimate tensile strength of the weaker material joined
G	Shear modulus
g	Standard earth gravity
H	Height
h	Height
H_m	Height of CoG
I	Moment of inertia
I_x	Area moment of inertia

k	Torsional stiffness
L	Length
l	Length
L_k	Effective length
M	Momentum
m	Mass
M_i	Material index
n	Safety factor
R	Outer radius
r	Inner radius
T	Wheel track width
TS	Torsional stiffness
V	Velocity
W	Weight
Z	Elastic section modulus
β_w	Correlation factor
γ	Compressive strain
γ_{M2}	Partial safety factor for joints
ΔW_y	Total lateral weight transfer
ε	Tensile strain
μ	Coefficient of friction
ν	Poisson ratio

ρ	Density
σ	Stress
$\sigma_{allowable}$	Allowable stress
σ_e	Equivalent stress
σ_t	Tensile stress
σ_y	Yield stress
$\sigma_\perp$	The normal stress perpendicular to the throat
τ	Shear stress
$\tau_\parallel$	The shear stress parallel to the axis of the weld
$\tau_\perp$	The shear stress perpendicular to the axis of weld
ϕ	Angular rotation
°	Degree

Abbreviations

CAD	Computer-Aided Design
CFD	Computational Fluid Dynamics
CFRP	Carbon Fibre Reinforced Polymer
CoG	Centre of Gravity
FEA	Finite Element Analysis
FEM	Finite Element Method

1. Introduction

The chassis is one of the more essential parts of a racing car. Almost every component of the vehicle is attached to the chassis, and it primarily affects handling, weight, safety, and the ergonomics of the driver. Throughout the 20th century, the chassis formed the car's skeleton, where the motor, transmission, axle assembly, and steering were bolted on [1]. The body of the vehicle was then mounted on top of the chassis. This design is referred to as a ladder frame simply because it resembles a ladder. One can still find this used today on heavy-duty trucks and vehicles designed to haul big loads. Herb Adams mentions in his book Chassis Engineering [2] that ladder frames offer poor torsional stiffness and are not for performance racing cars.

The most popular chassis design seen in today's sportscars (except for carbon monocoque cars) is a spaceframe configuration. The main principle behind this idea is welding tubular members together in a triangular manner which places them in either tension or compression [3]. By ensuring the members do not suffer any torsion or bending, one can maximize weight reduction while obtaining adequate torsional stiffness. One of the main reasons for its popularity in the kit car market and Formula Student populace is the low cost of tooling and ease of production [3].

On the opposite end of the cost scale is the carbon monocoque chassis. In this design, there is no internal framing or support. The outer skin bears all the load, both compressive and tensile. The main design challenge here is to avoid point loads normal to the surface of the outer skin. To allow for safe mounting points for suspension, metal inserts are added to resist these concentrated loads [4]. Space frame and monocoque are the two most used chassis in racing.

Modern passenger sportscars are a combination where chassis and body are combined or unified, thereby the name "unibody" [1]. This design uses a steel body shell with carefully placed reinforcements and braces to adequately strengthen the construction.

The design of a race car chassis is a challenging and iterative process. There is usually a set of strict rules and regulations to abide by and several considerations to be made. Early on, the decision was made not to model a frame for the popular Formula Student event, but rather be more creative and freethinking. This allowed us to experiment with different designs, cross-sections and materials.

Figure 1 Ladder frame [5]

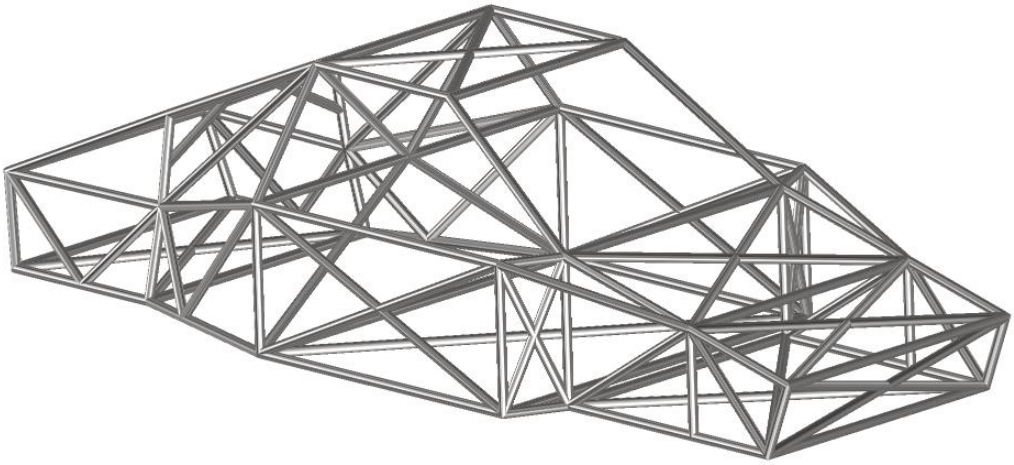

Figure 2 Space frame

2. Theory

To be able to design and simulate a racing car frame, we must familiarize ourselves with relevant theory and mathematical models relevant to car design. What follows presents the background for the thesis, a brief introduction to chassis theory, material and fabrication methods, essential design criteria and simulation theory, and design considerations.

2.1. Chassis

The essential functions of a chassis can be listed as follows [4]:

- Act as a secure mounting place for all other components such as engine, suspension, and fuel tank.
- To serve as a protective cover for the occupants, including the driver.
- To provide enough strength and stiffness to support the weight and forces applied by acceleration, bumpy roads, turning, aerodynamic forces, and passengers.

Although all these functions are important, criteria number three is the first one any car designer should focus on. It ensures that the car operates as expected when under normal or extreme use. It is also essential for the suspension to function as intended. This can only happen if the suspension mounting points remain as stationary as possible regarding the car's axis system [3].

To ensure these mounting points stay stationary, one must design the chassis to withstand three main types of dynamic loading:

1. Torsional loads
2. Bending loads
3. Longitudinal loads.

These three types of loading will most likely occur simultaneously, but torsional stiffness is the most critical parameter to focus on in the early design process [3]. But what shapes and materials will offer these qualities? To understand more about this, one must understand the principles of triangulation and shear plates. The latter can be found extensively in monocoque chassis.

2.1.1. Monocoque chassis

The monocoque chassis is typically constructed using carbon or glass fiber composites. It is the most commonly used chassis material in professional racing due to its ability to be stronger, lighter, and if designed correctly, safer than its metal counterpart [4]. In Race Car Design by Seward [4], it is stated that per unit weight, the carbon fiber composite is three times stronger than steel or aluminum. As the name composites states, it is made up of multiple parts. The reinforcement material is often in the form of a woven mat and a bonding resin. The flexible woven material is cut into pieces, placed in a prefabricated mold, and coated with bonding material or resin. There are many types of fiber and resin depending on what material properties are wanted. Phenolic resins offer better fire resistance; polyester resins are cheap but lack the strength needed in car chassis. The better choice is an epoxy resin for its strength and toughness [4].

On a spaceframe chassis, the members are placed in such a manner that they ideally only experience tension or compressing. However, on a monocoque, its design is based on plates or shells in shear [4]. Calculating the exact strength of these shells can be laborious as carbon fiber composites are anisotropic, meaning the characteristics rely on the direction of fibers. Two seemingly equal chassis can possess unequal properties depending on the stacking sequence and direction of the fibers.

2.1.2. Space-frame chassis

A space frame is a 3-D structure of elements connected at the ends, forming a geometric pattern. The strength in these frames comes from the strength of a triangle. This method of design has been popular in more than just the automotive industry. One of the more famous examples is the great Eiffel tower in Paris. The immense strength of these triangles can be seen in Figure 3 and Figure 4. The structures are both constructed using the same material and dimensions, with the main difference being triangulation. In both cases, supports are added in lower corners, and the same force is applied at the top right corner. We can observe a deflection of 5.36 mm in the unbraced frame and 0.16 mm in the braced frame. Adding one cross member has dramatically increased the stiffness of this simple structure. Both models are displayed with 4 times magnified deformation.

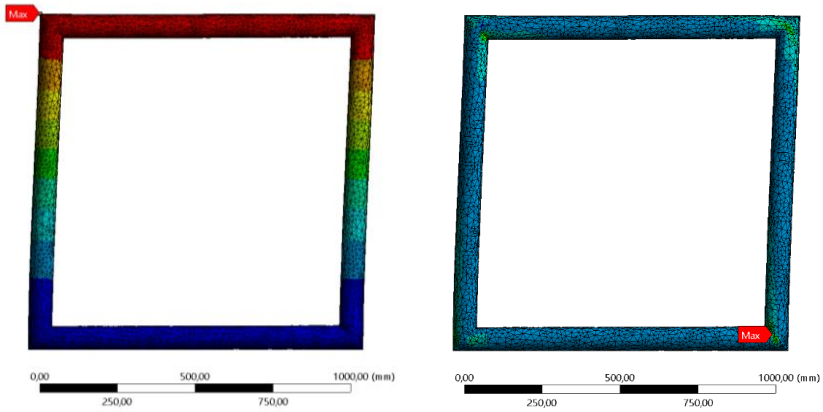

Figure 3 Non-triangulated 2-D frame

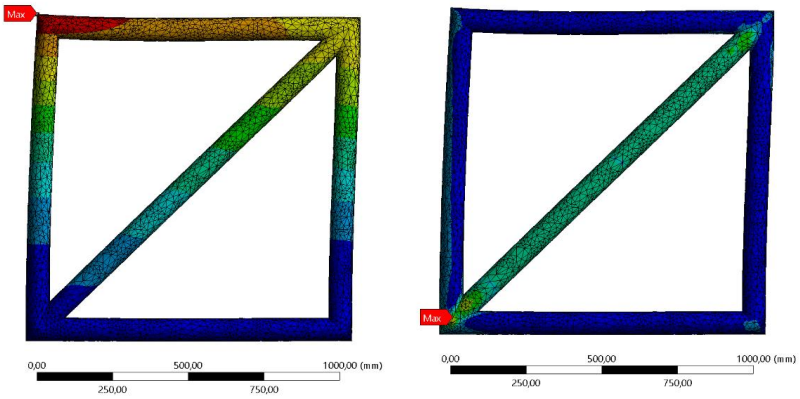

Figure 4 Triangulated 2-D frame

Table 1 Deflection and stress in braced and unbraced frame

	Deflection [mm]	**Max. stress [MPa]**
With diagonal bracing	0.16	24.9
Unbraced	5.36	326

The same principle applies when designing a race car frame. Ideally you want at least three elements passing through the same point, with the center of axis of each member meeting at this point. In a perfect world, the force applied to the structure is only on these points, nodes, resulting in the members only being subjected to pure tension or compression. This is one of the reason triangulations is so effective, by not having to designing the members to resist bending makes for a lighter structure. This is however not the case in real life; as the connections are welded, some bending will occur.

This type of chassis is immensely popular in the small sports car category, partly because of the ease of design, low cost in tooling, and substantially easier to manufacture than its carbon fiber counterpart.

A well-known race car that uses a true spaceframe is the Porsche 917, designed by Hans Mezger. The chassis was remarkably lightweight, weighing in at only 42 kg. Because it was so light and only meant to last one race, they pressurized the frame with gas to detect any cracks in the weld. The Porsche 917 succeeded in winning Le Mans in 1970 and 1971 [6].

2.2. Frame material

The construction material of a racecar significantly governs the behavior and is important in the design process. Materials range from high-tech aluminum plus composite constructions to tough thermoplastic matrix and stiff carbon fiber or Kevlar [3]. In the increasingly popular F1 Grand Prix, cars are made almost entirely of ultra-light carbon fiber composite materials, giving them astonishing power to weight ratio and exceptional stiffness [3].

However, it was the popular space-frame design that sparked our curiosity and motivated us to embrace this challenge. Its design is beautiful and enticing to look at; it is both industrial and elegant and often cheaper to produce than carbon monocoque chassis [3]. If designed correctly, the seemingly random placement of triangles and beams can create a strong and surprisingly lightweight chassis. This thesis will focus its efforts on a steel space-frame chassis and briefly mention the benefits and disadvantages of a monocoque chassis.

2.2.1. Elastic deformation

Understanding the material properties is essential when choosing a material for construction. Materials can have different properties with different advantages. In a spaceframe, the beams are subjected to forces and loads, resulting in deformation. This deformation can, if big enough, result in failure. Key properties of materials are stiffness, strength, hardness, ductility, and toughness [5].

When you supply force on an area of a beam, stress will occur. Molecules in the material gets squeezed together with the tension between them. If the deformation is elastic, the molecules spring back to their original positions, and the beam returns to its original shape. The stress σ can be set mathematically as [5]:

$$Stress, \sigma = \frac{F}{A_{cs}} \tag{1}$$

When the object is under stress it changes in one or more dimensions. The deformation caused by the stress is called strain. Engineering strain ε is defined by:

$$Strain, \varepsilon = \frac{\Delta l}{l} \tag{2}$$

The degree of the deformation, stress, depends on the magnitude of the imposed stress. Most metals subjected to low-level stress in tension have a proportional strain behavior, which is defined by Hooke's law:

$$\sigma = E\varepsilon, \qquad E = \frac{\sigma}{\varepsilon} \tag{3}$$

The constant E is the Modulus of elasticity or Young's modulus and is the slope of the graph from zero till yield strength, see Figure 5. One might think of E as the material stiffness or the resilience to elastic deformation. The higher the Young´s Modulus, the stiffer the material is, and the smaller the deformations will be for an applied load. The deformation until yield strength is elastic, meaning non-permanent deformation.

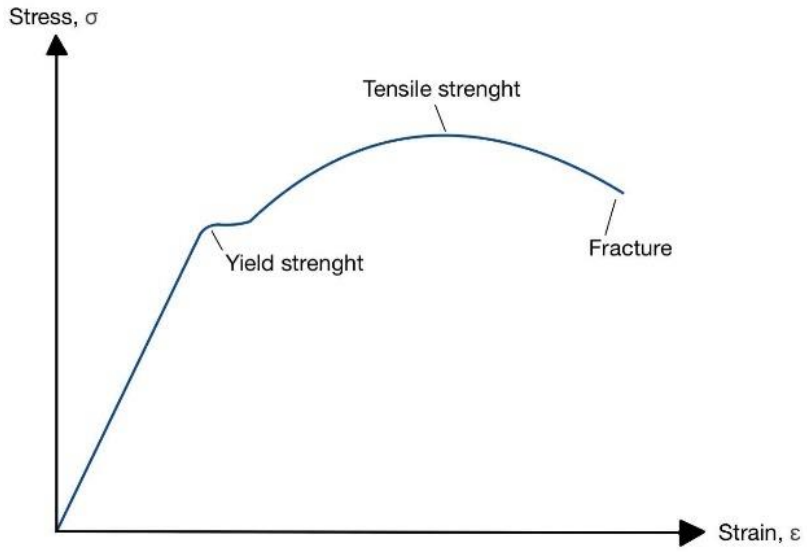

Figure 5 Stress strain curve

Compressive stress evokes elastic behavior, giving it shear or torsional stresses. The stress-strain behavior is the same as in tensile stress. The behavior of the shear stress τ and strain γ is expressed as the elastic modulus:

$$\tau = G\gamma, \qquad G = \frac{\tau}{\gamma} \tag{4}$$

Where G is the shear modulus, the slope of the linear region in the stress-strain curve.

2.2.2. Plastic deformation

When the material is deformed beyond the point of elastic deformation, Hooke's law is not valid. At this stage, plastic deformation occurs. When designing a structure, one must avoid plastic deformation. Therefore, it is essential to express where the material goes from elastic deformation to plastic deformation. This point, called the proportional limit, is hard to measure precisely. Therefore, a convention has been set to construct a parallel line to the elastic portion with a strain offset of usual 0.002. The intersection between the line and the stress-strain slope is defined as the yield strength as displayed left in Figure 6.

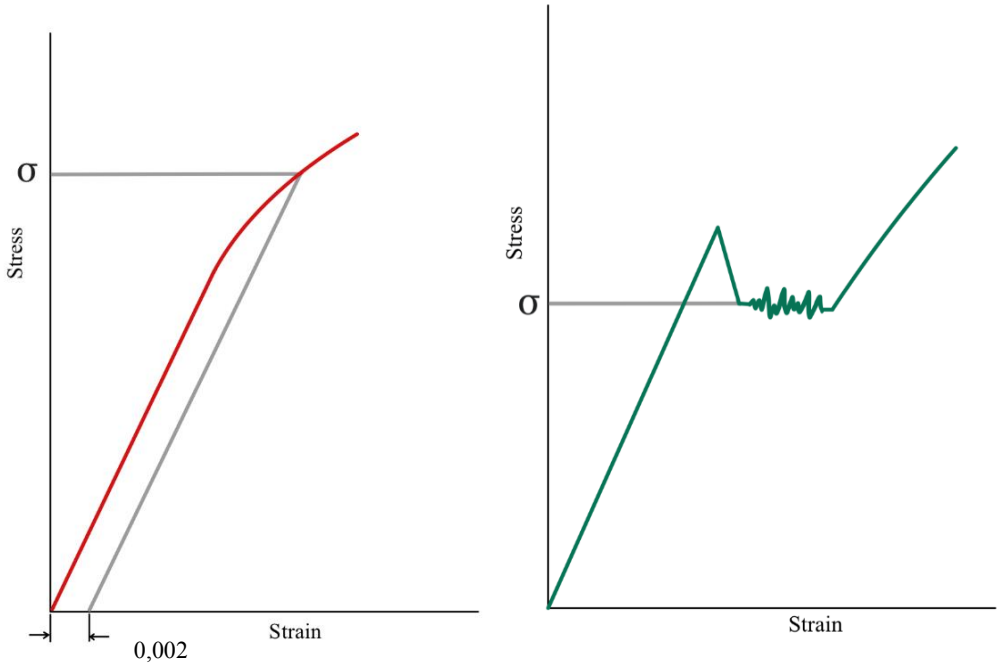

Figure 6 Yield strength using the 0.002 strain method (left) and the yield point phenomenon (right)

For some materials, the elastic-plastic transition is very well defined. This is displayed in Figure 6 and is termed a yield point phenomenon. The plastic deformation is initiated at the upper yield point, and the continued deformation happens at a lower yield point. The yield strength is the average value in the lower yield point in materials with these properties.

After the yield strength, the stress necessary to continue to deform the metals comes to a maximum point. This point is called tensile strength and is the point with the maximum absorbed stress in the material in tension. If the stress is applied and maintained, it will result in fracture.

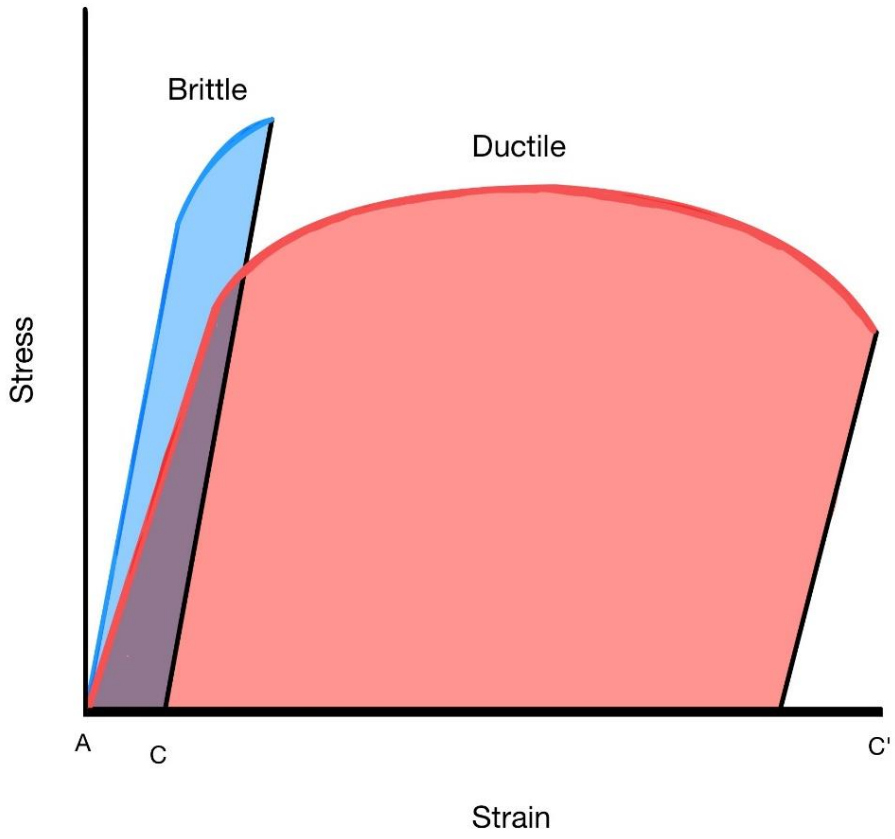

Figure 7 Stress strain curve of brittle and ductile material

2.2.3. Energy absorption

Ductility is an important property of the material. Callister and Rethwish [5] describe it as: “the measure of the degree of plastic deformation that has been sustained at fracture”. The material is brittle if it has a low level of ductility. Figure 7 shows the difference in a brittle and ductile material. When the material is under load below yield strength it absorbs the energy and deforms. Upon unloading, releasing the energy goes back to its original form. This is called Resilience and the associated property is the modulus of resilience which is the strain energy per unit volume required to stress up to the yield point [5]. If the racecar frame is not stiff enough, it will act as a spring, absorbing energy under loading and releasing energy during de-loading. This results in an unpredictable racecar. It is therefore crucial to make the frame stiff enough to where it can be safely ignored [7].

The toughness of the material can be used in several contexts as described by Callister and Rethwish [5]. For one, toughness, more specifically fracture toughness, can be described as the property of the material to ensure no fracture by cracks or imperfection. It is almost impossible to make a material without any imperfections, therefore it is vital to have a tough material. Toughness can also be described as the ability of a material to absorb energy and plastically deform before fracturing. For a racecar, it is crucial to absorb large amounts of energy during a crash. The combination of stiffness, flexibility, strong in some places, and weaker in others, is challenging in race car design. Therefore, one needs to make a stiff chassis that absorb energy during plastically deformation.

For a low strain situation, one can measure the toughness by the result of the stress-strain test. The toughness is then the area under the stress-strain curve up to the fracture point. Figure 7 shows that the stress-strain curve area differs for a brittle and ductile material. The brittle material might have higher tensile strength but will not absorb nearly as much energy as a ductile material at fracture.

The toughness can be measured by an impact test for a high strain situation, specifically the Charpy V-notch test. The CVN-test can measure the toughness at the state of low temperature, high strain, and triaxial stress. A bar shaped with a square cross-section test specimen is used, where a V-notch is machined. The apparatus for the test, displayed in Figure 8, has a pendulum with a mass of m. It gets released from the start point at the height H. Then, the pendulum hits

the test specimen, absorbs energy, and reaches a height of h. The difference in height is the energy absorbed by the test specimen. This can be expressed as:

$$E = mg(H_i - H_f) \tag{5}$$

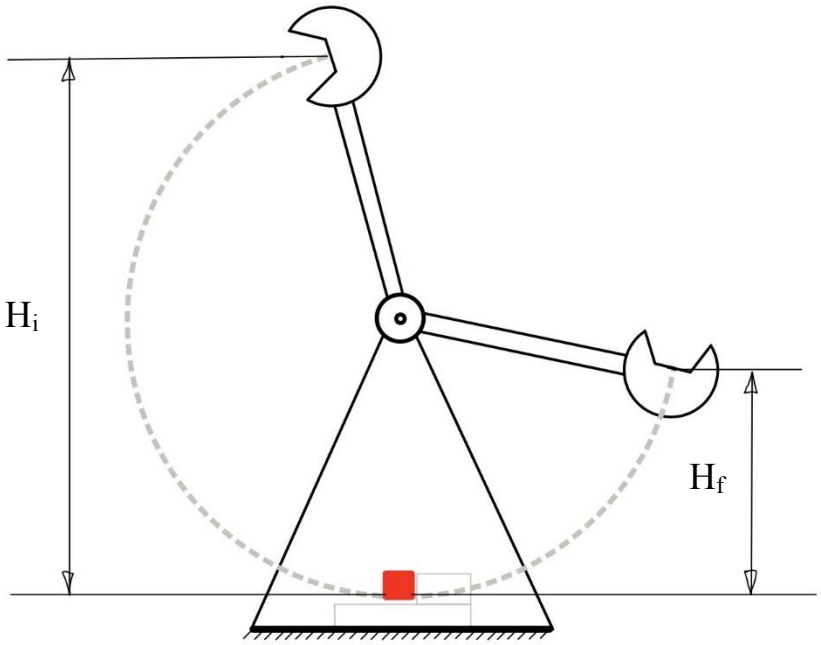

Figure 8 Charpy v-notch test

Designing a car chassis as rigid and stiff as possible can have some disadvantages. One of which shows itself during a crash. When a vehicle is involved in a collision, forces are at play. How much depends on the car's speed and mass, and the mass of the object it hits. The aim is to maximize the time it takes for the vehicle to decelerate, thereby minimizing the force transmitted to the passengers.

The worst-case scenario would be that all the kinetic energy of a moving vehicle was transmitted to its occupants. Modern passenger cars solve this by utilizing crumple zones, i.e. parts of the construction whose only purpose is to deform and "absorb" some of the energy from the crash.

Material selection also plays a big role in the ability to deform and shield passengers from high-energy crashes. A look at the material's stress-strain curve lets us calculate the amount of energy absorbed by said material. The integrated area under the entire stress-strain curve is the energy absorbed [5]. Figure 9 shows a graph comparing two fictional materials of different composition and properties, where one resembles properties found in carbon fiber, and the other resembles construction steel. No calculation is needed to see which material absorbs the most amount of energy under deformation.

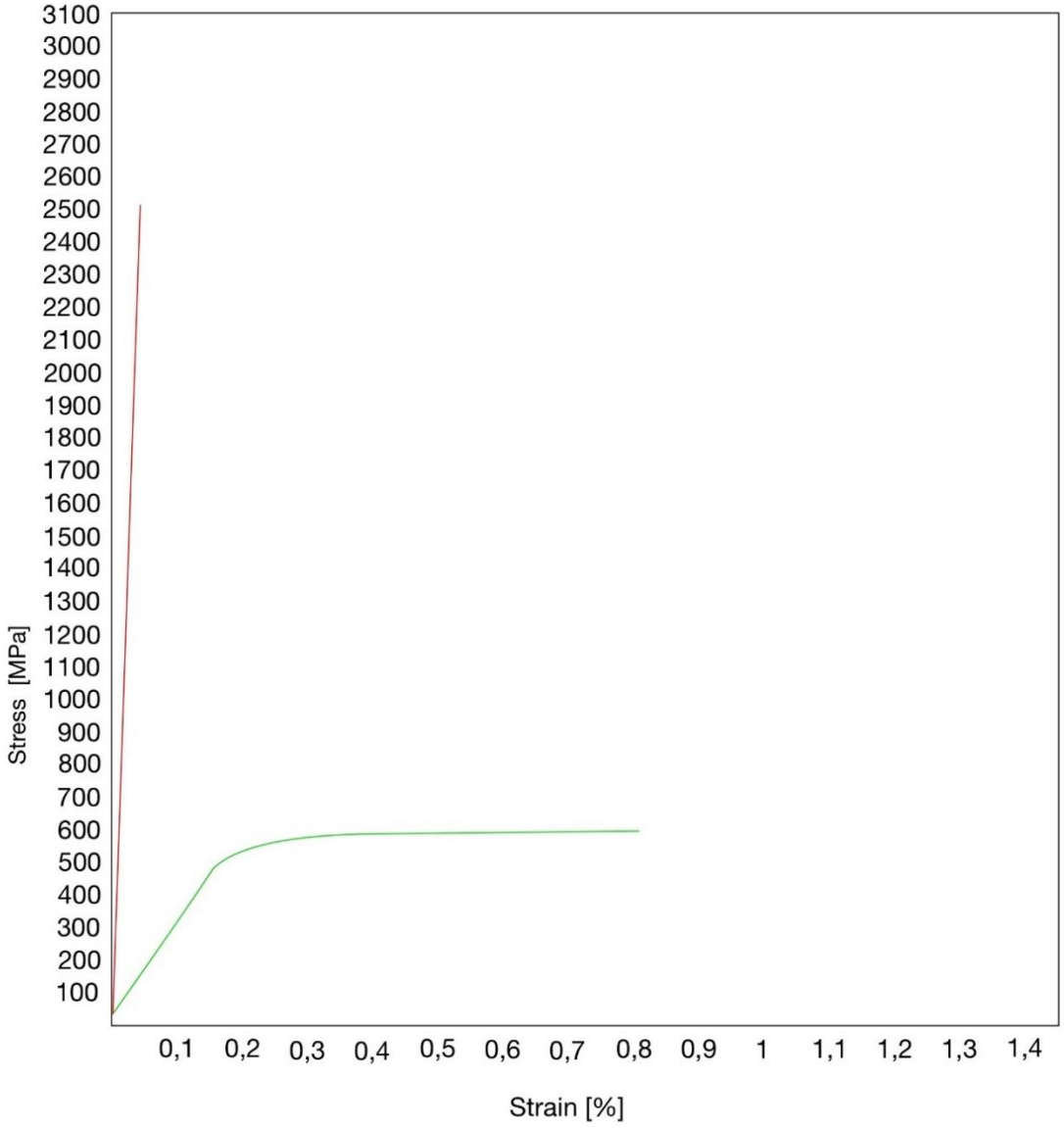

Figure 9 Material properties of brittle and ductile material.

Despite not being able to absorb significant amounts of energy, carbon fiber is still the most used material in modern formula 1 cars. The design takes advantage of entire sections of the car breaking off in a controlled fashion to decelerate the vehicle. One example of the breakaway sections in formula 1 doing what they are intended to do, can be found looking at Carlos Sainz`s crash in the Russian Grand Prix in 2015 [8]. He reportedly crashed into the barrier at 150 km/h. Crash data indicated that the total deceleration time was 0.09 seconds. Using simple equations of motion this results in a peak rate of deceleration of 463 m/s^2. Assuming Carlos weighed 70 kg at the time of the crash, his body weighed (albeit only for a split second) over three tons. That is over 4 times more than his own formula 1 car. Carlos raced the next day, a great testimony to the capabilities of a carbon fiber.

2.2.4. Material selection

Choosing the right material means taking a closer look at its attributes. Its attributes include density, strength, and weldability. A project my demand certain of these attributes, such as corrosion resistance over low weight, or strength rather than low cost. With today's extensive list of materials, a systematic approach is needed to assure that the designer is left with the material best suited for his needs. Not evaluating all possibilities may lead to missed opportunities.

One way of doing this is by [9]:

1. Establishing the desired attribute profile and then
2. Comparing it with those of real engineering material to find the best match.

The first step in narrowing down the vast number of materials is screening out the ones that do not meet the desired specifications. One would not consider glass when designing a hammer. The second step is scoring and ranking the remaining candidates to your set of requirements.

Matching the desired attributes to those of real materials can according to Ashby [9] be further divided in to four steps. Translation, screening, ranking and supporting information.

Translation can be described as identifying the criteria needed for the material. Depending on the project, some criteria may be answered by yes/no questions, further eliminating the ones not

meting these goals (screening). You will be left with a group of materials all inhibiting the needed criteria. Some materials will outperform others, you rank them according to this. Lastly an in-depth review will give you the supporting information you need regarding each material. The process of translation can be set up as a table of function, constraints, objective and free variables. Table 2 defines the boundary conditions for choosing a material for a race car frame.

Table 2 Function, constraints, objective and free variables for the frame

Function	**Race car frame**
Constraints	- Material must be strong - Must support axial tensile load, compressive and bending without failing.
Objective	- Maximize strength of car while minimizing weight
Free variables	- Choice of material - Cross-sectional area

When a mechanical component is under load, may it be tension, compression, bending or torsion, the condition can be written as a mathematical function. Rearranging that equation for the quantity you want to maximize gives you the material index for that problem.

If we solve for the material index M_i of a light, stiff beam we get:

$$M_i = \frac{E^{\frac{1}{2}}}{\rho} \tag{6}$$

More material indices can be found in Figure 10 and Figure 11. This is an easy process, if you understand which constraints are considered, and what you are trying to maximize.

Function and constraints	Maximize
Tie (tensile strut)	
Stiffness, length specified; section area free	E/ρ
Shaft (loaded in torsion)	
Stiffness, length, shape specified, section area free	$G^{1/2}/\rho$
Stiffness, length, outer radius specified; wall thickness free	G/ρ
Stiffness, length, wall-thickness specified; outer radius free	$G^{1/3}/\rho$
Beam (loaded in bending)	
Stiffness, length, shape specified; section area free	$E^{1/2}/\rho$
Stiffness, length, height specified; width free	E/ρ
Stiffness, length, width specified; height free	$E^{1/3}/\rho$
Column (compression strut, failure by elastic buckling)	
Buckling load, length, shape specified; section area free	$E^{1/2}/\rho$
Panel (flat plate, loaded in bending)	
Stiffness, length, width specified, thickness free	$E^{1/3}/\rho$
Plate (flat plate, compressed in-plane, buckling failure)	
Collapse load, length and width specified, thickness free	$E^{1/3}/\rho$
Cylinder with internal pressure	
Elastic distortion, pressure and radius specified; wall thickness free	E/ρ
Spherical shell with internal pressure	
Elastic distortion, pressure and radius specified, wall thickness free	$E/(1-\nu)\rho$

Figure 10 Stiffness-limited design at minimum mass [9]

Function and constraints	Maximize
Tie (tensile strut)	
Stiffness, length specified; section area free	σ_f/ρ
Shaft (loaded in torsion)	
Load, length, shape specified, section area free	$\sigma_f^{2/3}/\rho$
Load, length, outer radius specified; wall thickness free	σ_f/ρ
Load, length, wall-thickness specified; outer radius free	$\sigma_f^{1/2}/\rho$
Beam (loaded in bending)	
Load, length, shape specified; section area free	$\sigma_f^{2/3}/\rho$
Load length, height specified; width free	σ_f/ρ
Load, length, width specified; height free	$\sigma_f^{1/2}/\rho$
Column (compression strut)	
Load, length, shape specified; section area free	σ_f/ρ
Panel (flat plate, loaded in bending)	
Stiffness, length, width specified, thickness free	$\sigma_f^{1/2}/\rho$
Plate (flat plate, compressed in-plane, buckling failure)	
Collapse load, length and width specified, thickness free	$\sigma_f^{1/2}/\rho$
Cylinder with internal pressure	
Elastic distortion, pressure and radius specified; wall thickness free	σ_f/ρ
Spherical shell with internal pressure	
Elastic distortion, pressure and radius specified, wall thickness free	σ_f/ρ
Flywheels, rotating disks	
Maximum energy storage per unit volume; given velocity	σ
Maximum energy storage per unit mass; no failure	σ_f/ρ

Figure 11 Strength-limited design at minimum mass [9]

The process, is as mentioned, simple. Finding the material index for your problem, applying that to the appropriate chart and parallel shifting the line until a small group of materials are above it. The material last touched by the moving line is the one with the largest value for M_i, and the one most appropriate for the condition you set. As a designer or engineer you must decide which of the appropriate material are best suited for your application.

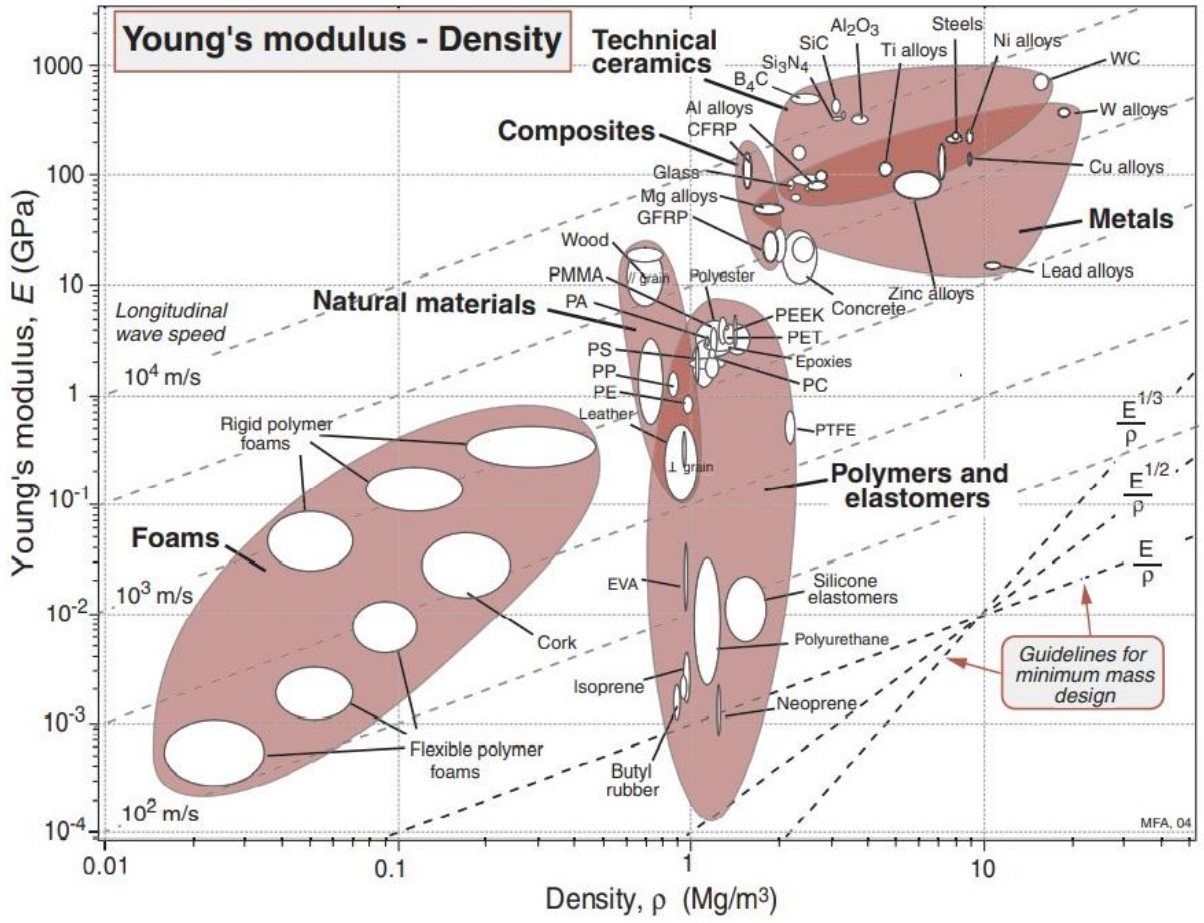

Figure 12 Youngs modulus, E, plotted against density [9]

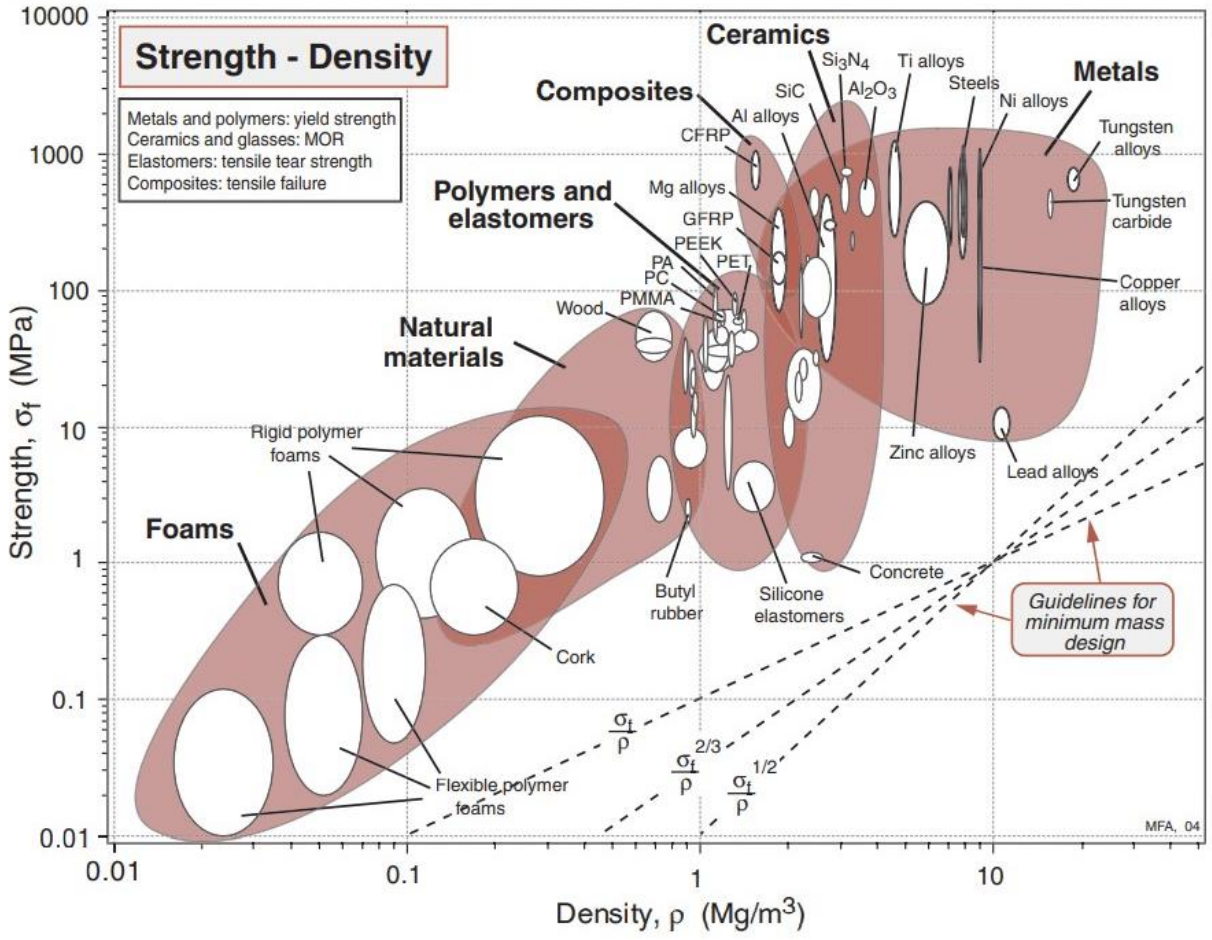

Figure 13 Strength, plotted against density [9]

Table 3 Material for race car frame

Material	Index $M = \frac{E^{\frac{1}{2}}}{\rho}$	Comment
Steels	61	Heavy, but cheaper. Strong enough.
CFRP	214	Light, strong, not suited for space frames.
Aluminum	98	Light, strong, but difficult to weld
Titanium	80	Strong, light, expensive

Ranking the materials results in several possible candidates for a race car frame. Steels, CFRP and aluminum alloys all scored high.

The final deciding factor between possible candidates will often come down to conditions such as local expertise, equipment and availability. For this specific thesis the deciding factors was ease of manufacturing, availability, cost, and local expertise in structural engineering.

2.2.5. Material and safety factor

It is a common practice to apply a safety factor *n* to construction materials. This will account for material imperfections such as:

- Quality
- Straightness
- Dimensional deviations
- Uneven load distribution

The safety factor is defined by the following equation[10]:

$$safety\ factor, n = \frac{yield\ stress}{design\ stress} \tag{7}$$

It is suggested to use a value of **1.5** as a safety factor [4].

2.3. Welding

The world of welding is vast and complicated. There are several popular welding techniques, but at its core, it is the process of joining two or more pieces of metal together. In other words, this is unavoidable when constructing a metal frame. If done correctly, a weld is strong, if done incorrectly, a weld is unreliable.

> "Like chess, however, welding is easy to learn yet hard to master" Atteberry [11]

It is normal to add filler material when melting the two existing materials together. This is done to avoid gaps or voids in the weld. Heat is quite naturally generated in this process, which can greatly alter the properties of the material. The significance of this effect is fairly difficult to determine for each weld, but must be taken into account. Rapid cooling of the heated material can both harden it and make it more brittle. If the material was hard to begin with (i.e., cold drawn or heat-treated) further heating can change these characteristics and diminish the effects of heat treatment. Welding can be done in various ways but can be narrowed down to two main methods.

The two main types of welds are:

Fillet weld

Fillet welds are used when the strength requirement is moderate [10]. It is used when two pieces of material meet at an angle or are in contact with each other in any way. The parent material will in this case physically melt together and form a strong bond. In welding science, this is called penetration. To achieve good penetration, it is useful to bevel the workpiece and ensure you are using the appropriate current.

Butt weld

In this type of welding, there is usually a gap between the materials being bonded together. This gap is then filled up with filler material, making it one piece. The pieces are placed end to end in the same plane and have no overlap with the parent material. The ends of the materials to be welded are “butted” against each other. It is easy to machine and inspect after welding, but can be prone to incomplete penetration and porosity. To get full penetration of a butt weld, the thickness and width must be equal to or greater than the lesser thickness of the materials welded together.

The challenge welders are faced with is that melting metal produces heat. Heat causes metal to expand, warping the intended shape of the part, and as mentioned, can alter the material properties. Both butt and fillet welds can be carried out in two manners: continuous and intermittent welding.

Continuous weld:

As the name suggests this is a continuous weld from one end of the joint, till the welder reaches the full length of the workpiece. This technique is often used when joining piping or tubes [12].

Intermittent weld:

An intermittent weld is often sectioned off and carried out in multiple lines. The metal pieces appear to be tacked together with alternating patches of welded and unwelded sections over the length of the material. This technique puts less thermal stress on the material and is cheaper as a result of using less filler material.

The two welding techniques to consider when fabricating a steel frame is MIG and TIG welding. Both techniques are based on the same principle, an electrical current is generating heat that melts the base material and bonding material. There are however some differences worth mentioning.

TIG welding:

The most versatile of the two is Tungsten Inert Gas welding. It is used by professionals in a wide variety of industries, including the aircraft industry, aerospace industry, and automobile industry [13]. It offers great control and allows the user to weld thick and thin material with only small adjustments to the equipment. This technique requires skilled workers, as the filler material is deposited by hand into the weld pool. The result is a slag-free, strong, and aesthetically pleasing result that shares the same corrosion resistance as the parent material [13]. It is often used on pipes.

MIG welding:

Unlike TIG welding where the filler material is fed by hand, MIG uses a wire that flows continuously through the handle of the welding tool simultaneously with shielding gas. This allows for the production of larger and longer continuous welds as the operator is not forced to stop and change the filler rod.

Navigating the jungle of filler materials can be a daunting task for the inexperienced welder, and sometimes even for the experienced professional, but there are some guidelines to help with this. Numerous variables determine what filler material is best suitable: Composition of base material, joint type, thickness and material properties of base material, amperage, gas flow, cup size, etc.

A rule of thumb is to choose a filler material with similar properties to the metals which you are welding, and a rod diameter less than the thickness of the stock material [14].

The filler material is often of higher strength than the metals being welded together, and a welded connection often surpasses the strength of the base material. This means that the design is

governed by this, and there are no procedures required for the weld [15]. Therefore, it is common practice to assume the same material properties in the weld as in the base material. Eurocode 3 requires that butt welds have greater or equal properties to those of the metals welded [15].

Table 4 Material properties [10, 16]

Material	Yield Strength [MPa]	Ultimate Tensile Strength [MPa]
Lincoln Electric Kryo 3 electrode	min. 460	530-680
S355 Steel tube	355	510

2.3.1. Welding calculations

The allowable stress in a fillet weld is given by the following equation [17].

$$\sigma_e = \sqrt{\sigma_\perp^2 + 3(\tau_\perp^2 + \tau_\parallel^2)} \leq \sigma_{allowable} = \frac{f_u}{\beta_w \gamma_{M2}} \tag{8}$$

and:

$$\sigma_\perp \leq \frac{f_u}{\gamma_{M2}\beta_w} \tag{9}$$

Where:

$\sigma_\perp$- The normal stress perpendicular to the throat

$\tau_\perp$- the shear stress perpendicular to the axis of the weld

$\tau_\parallel$ - the shear stress parallel to the axis of the weld

β_w - correlation factor

γ_{M2}- partial safety factor for joints = 1.25

f_u- the nominal ultimate tensile strength of the weaker material joined

Table 5 Correlation factor for fillet welds, and partial safety factor [17].

Material EN10025	**Correlation factor β_w**	**Partial safety factor γ_{M2}**
S235 **S235W**	0.8	1.25
S275 **S275 N/NL** **S275 M/ML**	0.85	1.25
S355 **S355 N/NL** **S355 M/ML** **S355 W**	0.9	1.25
S420 N/NL **S420 M/ML**	1.0	1.25
S460 N/NL **S460 M/ML** **S460 Q/QL/QL1**	1.0	1.25

2.4. Torsional stiffness

According to Seward [4], torsional stiffness refers to twisting throughout the length of the car. It is simply how much a car frame will flex as it is loaded with one front wheel up and the other down, and both rear wheels level. A condition that occurs at every corner of the racetrack.

One can think of a chassis as a large spring twisting and bending as the car accelerates and turns. Having an extra spring added to the already complex system of springs and dampeners complicates an already difficult calculation. Making this spring as stiff as possible will allow the designer to safely eliminate it from the equation when setting up the suspension [7]. It is therefore obvious that torsional stiffness is of utmost importance.

Torsional stiffness is also important when cornering hard. In hard cornering, the chassis obtain strain energy. The frame twists like a spring in a mechanical watch, and when the car is at the critical point of a cornering, straightening up, the stored energy gets released. This makes the car behave and handle unpredictably.

The torsional stiffness of a frame is measured in Nm/degree. Historically this was done by fixing three corners of the car and applying a load to the fourth. This was usually the left or right front suspension mounting point, or directly on the frame. With the advance of CAD programs and powerful analyzing software, this is often done computationally to save time and money on production.

Multiplying the added force with the width of the frame equals the moment about the support point. From the momentum you get a downward displacement used to calculate the angular rotation with the formula:

$$Angular\ rotation, \phi = tan^{-1}\left(\frac{H}{L}\right) \tag{10}$$

With the angular rotation ϕ and the momentum M, the torsional stiffness k can be calculated [10]:

$$Torsional\ stiffness, k = \frac{M}{\phi} \tag{11}$$

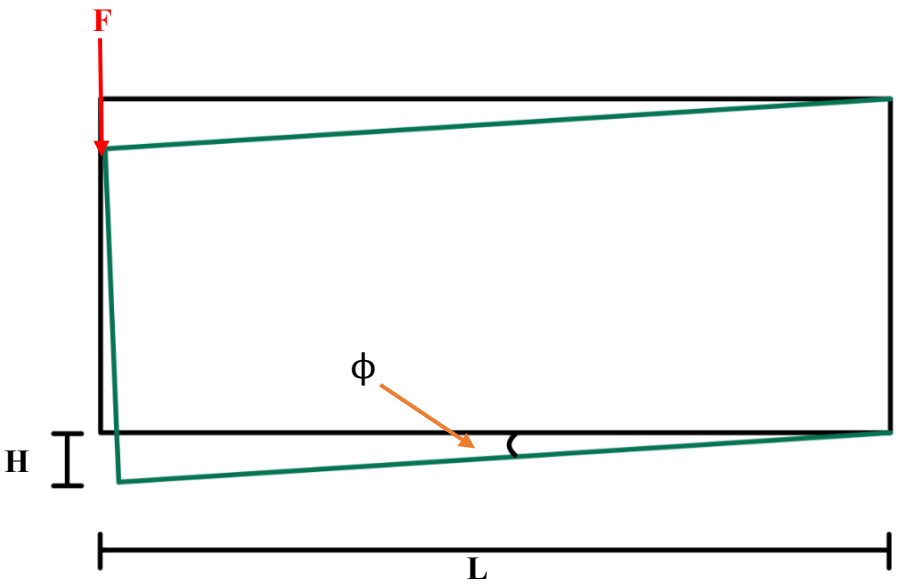

Figure 14 Angular rotation

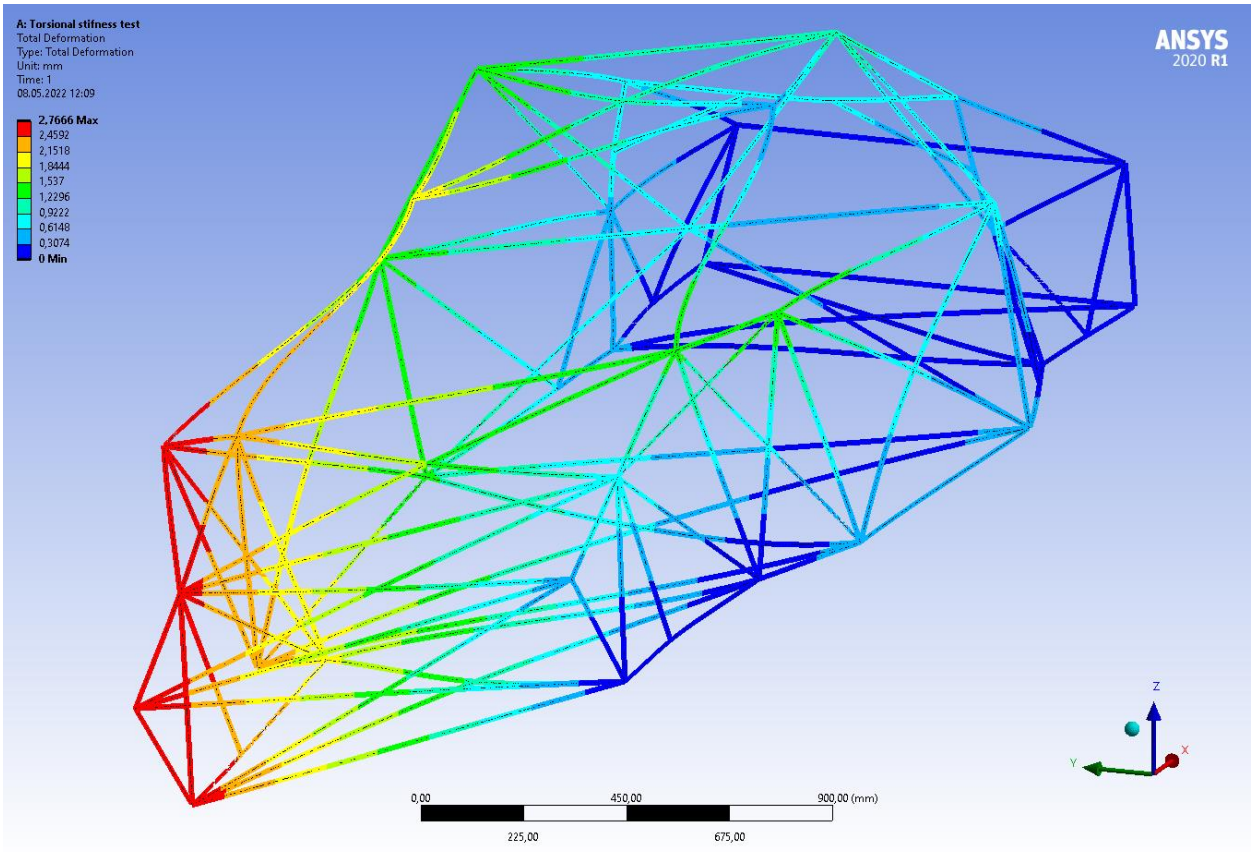

Figure 15 Torsion

There are four common ways to measure torsional stiffness in a race car frame. All of them can be done physically as well as computationally.

Option 1.

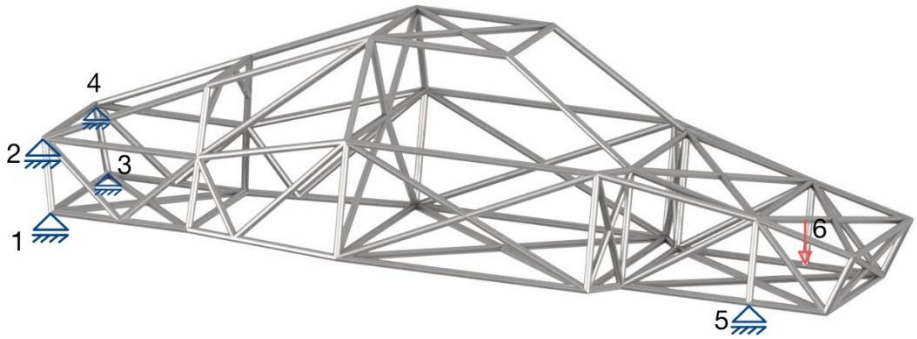

Figure 16 Constraints and forces for option 1

Constraints: *Point 1, 2, 3, 4, 5 – Fixed translation (x, y, z)*

Forces: *Point 6 – downward forced*

Measurement: *Vertical displacement of probe on node 6*

Option 2.

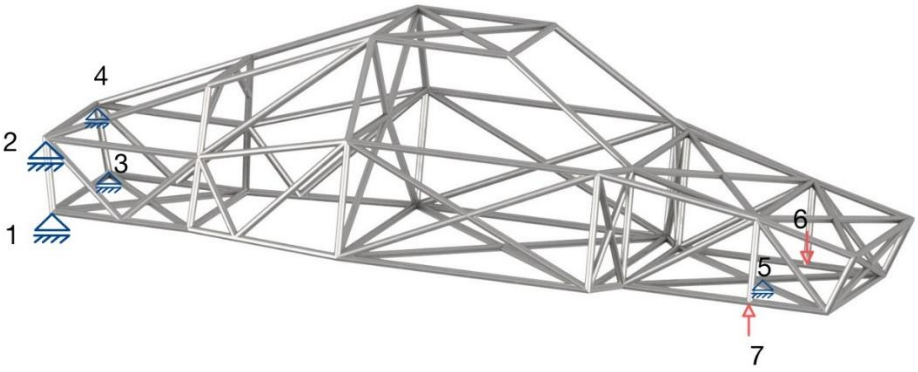

Figure 17 Constraints and forces on option 2

Constraints: *Point 1, 2, 3, 4, 5 – Fixed translation (x, y, z)*

Forces: *Point 6 – downward forced, Point 7 – upward force*

Measurement: *Vertical displacement of probe on node 6*

Option 3.

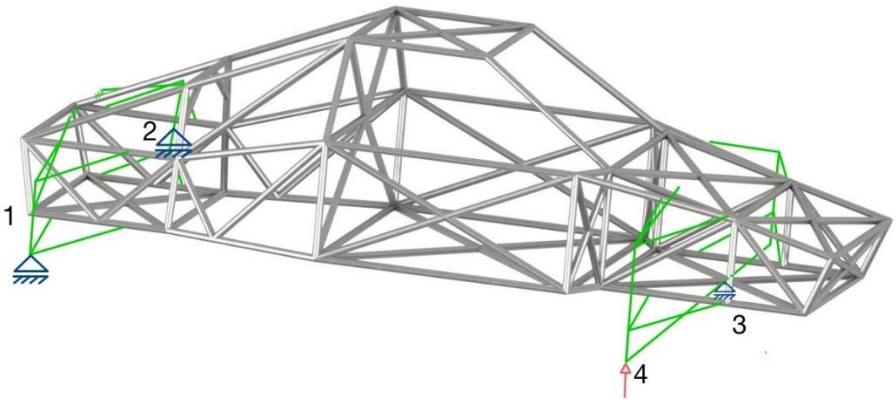

Figure 18 Constraints and forces on option 3

Constraints:	*Point: 1, 2, 3 - Fixed translation (x, y, z)*
Forces:	*Point 4 – downward forced*
Measurement:	*Vertical displacement of probe on point 4, Suspension modeled as rigid links*

Option 4.

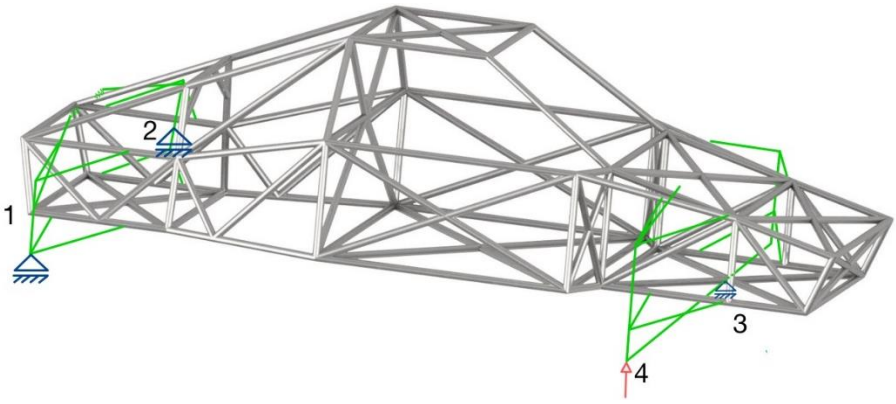

Figure 19 Constraints and forces on option 4

Constraints:	*Points 1, 2, 3, 4 – Fixed constraint (x, y, z)*
Forces:	*Point 4 – Upward force*
Measurements:	*Vertical displacement of probe on point 4. Suspension modeled as flexible links*

They all offer different advantages and disadvantages and can yield slightly different results of torsional stiffness for the same frame. Skovajsa and Sedlaeck [18] found the maximum difference to be 1112.4 Nm/deg between respective methods two and three. It was concluded that modeling the suspension as rigid links increased the stiffness to unrealistic levels. Considering this, and in close corporations with our supervisor we have decided that option 1 is best suited for this thesis. It is a configuration that resembles real-world conditions as a car turns, and one wheel lifts off the ground.

Option three and four may yield more realistic results, but moves the load away from the frame, and may require additional modeling of wheel and suspension systems. Since this is beyond the scope of this thesis no further investigation was invested in perusing these results.

2.5. Bending stiffness

The frame is exposed to bending in both vertical and horizontal directions. The vertical bending comes from the weight of the car and its components. Figure 20 displays the vertical load with the wheels as reaction forces. This loading is present both when the car stands still or drives in a straight line but multiplies when turning or driving over uneven roads.

The lateral bending is due to the centrifugal force acting on the car while cornering. In Figure 20 you can see the centrifugal force acting from the center of mass of the car while the wheels act as reaction forces. The amount of acceleration load depends on the mass and the cornering speed.

The bending stiffness can be expressed as:

$$Bending\ stiffness = \frac{Total\ applied\ load}{Deflection\ accured\ after\ applied\ load} \tag{12}$$

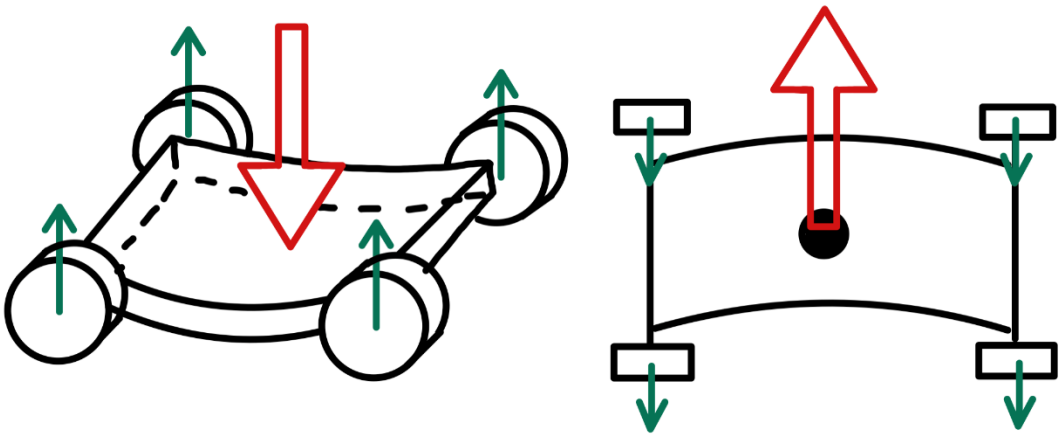

Figure 20 Vertical bending (left) and lateral bending (right)

2.6. Finite element method

Finite element analysis (FEA) can be used to make a racing car space frame as strong and light as possible. FEA is the simulation of any physical phenomenon using the numerical technique called the Finite Element Method (FEM) [19]. It can be used to analyze a wide range of engineering problems such as structural engineering, heat transfer, thermal loading, fluid mechanics aerodynamics, and electrostatics. Performing such an analysis help predict how certain objects perform, and to predict mechanical behavior.

This can be done manually using large systems of equations, or computationally using software such as MATLAB or Ansys.

What follows are the equations used to calculate bending moments, shear stress and axial forces in beams. Equation 13 below conforms to the deformation in a beam in the x-y plane.

Equation 13 Element equation[20]

$$\begin{Bmatrix} f_{1x} \\ f_{1y} \\ m_{1x} \\ m_{1z} \\ f_{2x} \\ f_{2y} \\ m_{2x} \\ m_{2z} \end{Bmatrix} = \begin{bmatrix} \frac{EA}{L} & 0 & 0 & 0 & \frac{-EA}{L} & 0 & 0 & 0 \\ 0 & \frac{12EI_z}{L^3} & 0 & \frac{6EI_z}{L^2} & 0 & \frac{-12EI_z}{L^3} & 0 & \frac{6EI_z}{L^2} \\ 0 & 0 & \frac{GJ}{L} & 0 & 0 & 0 & \frac{-GJ}{L} & 0 \\ 0 & \frac{6EI_z}{L^2} & 0 & \frac{4EI_z}{L} & 0 & \frac{-6EI_z}{L^2} & 0 & \frac{2EI_z}{L} \\ \frac{-EA}{L} & 0 & 0 & 0 & \frac{EA}{L} & 0 & 0 & 0 \\ 0 & \frac{-12EI_z}{L^3} & 0 & \frac{-6EI_z}{L^2} & 0 & \frac{12EI_z}{L^3} & 0 & \frac{-6EI_z}{L^2} \\ 0 & 0 & \frac{-GJ}{L} & 0 & 0 & 0 & \frac{GJ}{L} & 0 \\ 0 & \frac{6EI_z}{L^2} & 0 & \frac{2EI_z}{L} & 0 & \frac{-6EI_z}{L^2} & 0 & \frac{4EI_z}{L} \end{bmatrix} \begin{Bmatrix} u_{1x} \\ u_{1y} \\ \theta_{1x} \\ \theta_{1z} \\ u_{2x} \\ u_{2y} \\ \theta_{2x} \\ \theta_{2z} \end{Bmatrix}$$

This should then be combined with the beam element as displayed in the Equation 14 below.

Equation 14 Beam element equation [20]

$$\begin{Bmatrix} f_{1z} \\ m_{1y} \\ f_{2z} \\ m_{2y} \end{Bmatrix} = \begin{bmatrix} \frac{12EI_y}{L^3} & \frac{6EI_y}{L^2} & \frac{-12EI_y}{L^3} & \frac{6EI_y}{L^2} \\ \frac{6EI_y}{L^2} & \frac{4EI_y}{L} & \frac{-6EI_y}{L^2} & \frac{2EI_y}{L} \\ \frac{-12EI_y}{L^3} & \frac{-6EI_y}{L^2} & \frac{12EI_y}{L^3} & \frac{-6EI_y}{L^2} \\ \frac{6EI_y}{L^2} & \frac{2EI_y}{L} & \frac{-6EI_y}{L^2} & \frac{4EI_y}{L} \end{bmatrix} \begin{Bmatrix} u_{1z} \\ \theta_{1y} \\ u_{2z} \\ \theta_{2y} \end{Bmatrix}$$

Further expanding the element equation to a 3-D system containing axial forces as well as bending moments and shear forces ultimately yields:

Equation 15 3-D element equation of a beam [20]

$$\begin{Bmatrix} f_{1x} \\ f_{1y} \\ f_{1z} \\ m_{1x} \\ m_{1y} \\ m_{1z} \\ f_{2x} \\ f_{2y} \\ f_{2z} \\ m_{2x} \\ m_{2y} \\ m_{2z} \end{Bmatrix} = \begin{bmatrix} \left[K_{fu}^{11}\right] & \left[K_{f\theta}^{11}\right] & \left[K_{fu}^{12}\right] & \left[K_{f\theta}^{12}\right] \\ \left[K_{mu}^{11}\right] & \left[K_{m\theta}^{11}\right] & \left[K_{mu}^{12}\right] & \left[K_{m\theta}^{12}\right] \\ \left[K_{fu}^{21}\right] & \left[K_{f\theta}^{21}\right] & \left[K_{fu}^{22}\right] & \left[K_{f\theta}^{22}\right] \\ \left[K_{mu}^{21}\right] & \left[K_{m\theta}^{21}\right] & \left[K_{mu}^{22}\right] & \left[K_{m\theta}^{22}\right] \end{bmatrix} \begin{Bmatrix} u_{1x} \\ u_{1y} \\ u_{1z} \\ \vartheta_{1x} \\ \theta_{1y} \\ \theta_{1z} \\ u_{2x} \\ u_{2y} \\ u_{2z} \\ \theta_{2x} \\ \theta_{2y} \\ \theta_{2z} \end{Bmatrix}$$

Where the sub-matrices are defines as:

Equation 16 Sub-matrices in the 3-D element equation of a beam [20]

$$\left[K_{fu}^{11}\right]=\begin{bmatrix}\frac{EA}{L} & 0 & 0\\ 0 & \frac{12EI_z}{L^3} & 0\\ 0 & 0 & \frac{12EI_y}{L^3}\end{bmatrix} \quad \left[K_{f\theta}^{11}\right]=\begin{bmatrix}0 & 0 & 0\\ 0 & 0 & \frac{6EI_z}{L^2}\\ 0 & \frac{6EI_y}{L^2} & 0\end{bmatrix} \quad \left[K_{fu}^{12}\right]=\begin{bmatrix}\frac{-EA}{L} & 0 & 0\\ 0 & \frac{-12EI_z}{L^3} & 0\\ 0 & 0 & \frac{-12EI_y}{L^3}\end{bmatrix} \quad \left[K_{f\theta}^{12}\right]=\begin{bmatrix}0 & 0 & 0\\ 0 & 0 & \frac{6EI_z}{L^2}\\ 0 & \frac{6EI_y}{L^2} & 0\end{bmatrix}$$

$$\left[K_{mu}^{11}\right]=\begin{bmatrix}0 & 0 & 0\\ 0 & 0 & \frac{6EI_y}{L^2}\\ 0 & \frac{6EI_z}{L^2} & 0\end{bmatrix} \quad \left[K_{m\theta}^{11}\right]=\begin{bmatrix}\frac{GJ}{L} & 0 & 0\\ 0 & \frac{4EI_y}{L} & 0\\ 0 & 0 & \frac{4EI_z}{L}\end{bmatrix} \quad \left[K_{mu}^{12}\right]=\begin{bmatrix}0 & 0 & 0\\ 0 & 0 & \frac{-6EI_y}{L^2}\\ 0 & \frac{-6EI_z}{L^2} & 0\end{bmatrix} \quad \left[K_{m\theta}^{12}\right]=\begin{bmatrix}\frac{-GJ}{L} & 0 & 0\\ 0 & \frac{2EI_y}{L} & 0\\ 0 & 0 & \frac{2EI_z}{L}\end{bmatrix}$$

$$\left[K_{fu}^{21}\right]=\begin{bmatrix}\frac{-EA}{L} & 0 & 0\\ 0 & \frac{-12EI_z}{L^3} & 0\\ 0 & 0 & \frac{-12EI_y}{L^3}\end{bmatrix} \quad \left[K_{f\theta}^{21}\right]=\begin{bmatrix}0 & 0 & 0\\ 0 & 0 & \frac{-6EI_z}{L^2}\\ 0 & \frac{-6EI_y}{L^2} & 0\end{bmatrix} \quad \left[K_{fu}^{22}\right]=\begin{bmatrix}\frac{EA}{L} & 0 & 0\\ 0 & \frac{12EI_z}{L^3} & 0\\ 0 & 0 & \frac{12EI_y}{L^3}\end{bmatrix} \quad \left[K_{f\theta}^{22}\right]=\begin{bmatrix}0 & 0 & 0\\ 0 & 0 & \frac{-6EI_z}{L^2}\\ 0 & \frac{-6EI_y}{L^2} & 0\end{bmatrix}$$

$$\left[K_{mu}^{21}\right]=\begin{bmatrix}0 & 0 & 0\\ 0 & 0 & \frac{6EI_y}{L^2}\\ 0 & \frac{6EI_z}{L^2} & 0\end{bmatrix} \quad \left[K_{m\theta}^{21}\right]=\begin{bmatrix}\frac{-GJ}{L} & 0 & 0\\ 0 & \frac{2EI_y}{L} & 0\\ 0 & 0 & \frac{2EI_z}{L}\end{bmatrix} \quad \left[K_{mu}^{22}\right]=\begin{bmatrix}0 & 0 & 0\\ 0 & 0 & \frac{-6EI_y}{L^2}\\ 0 & \frac{-6EI_z}{L^2} & 0\end{bmatrix} \quad \left[K_{m\theta}^{22}\right]=\begin{bmatrix}\frac{GJ}{L} & 0 & 0\\ 0 & \frac{4EI_y}{L} & 0\\ 0 & 0 & \frac{4EI_z}{L}\end{bmatrix}$$

As shown these systems of equations get quite large rather quickly, thus making them ideal to solve using a computer.

2.6.1. Mesh

Selecting the correct mesh setting for analysis is crucial for extracting the correct result. When meshing, the model is divided into increments that contain nodes, these nodes represent the shape of your geometry. Quite often a three-dimensional model consists of irregular shapes which can be troublesome for an FEA program to process. A shape more suited for an FEA solver is cubes and tetrahedrons, these volumes are called elements. Calculations are then made for every element, sometimes ranging in the millions, then combining the result. Selecting which element is the correct one for your model requires experience.

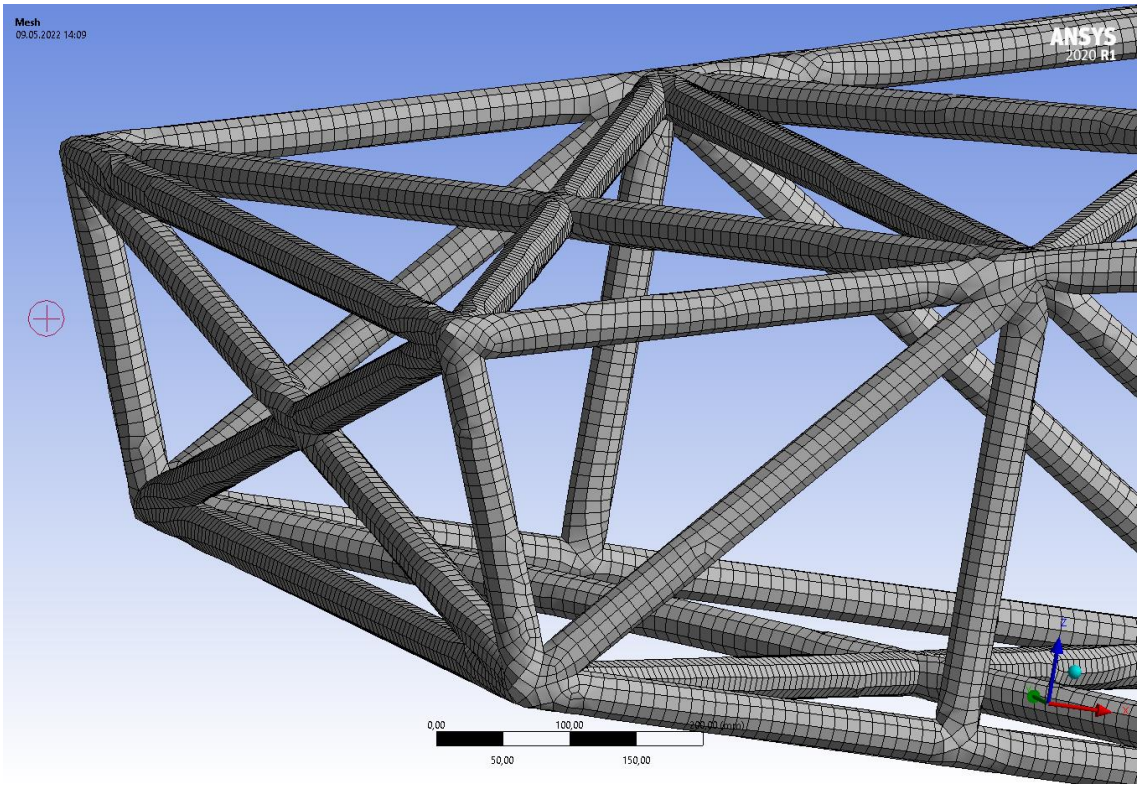

Figure 21 Meshing of chassis

After choosing the correct mesh begins the process of mesh refinement. This process boils down to using finer and finer meshes and comparing the results. The quality of the mesh can greatly impact the results obtained by the analysis. Decreasing the element size is often related to a higher level of accuracy in the results, but only down to a certain level. At one point the results will not depend on the number of elements, but rather converge to give the same result. This is known as mesh convergence. Further decreasing the mesh size after the convergence limit is reached will only increase the computational time and complexity of the model, with only minor insignificant changes to the result.

2.6.2. Weld

The meshing of welded connections is hard to accurately calculate due to several variables mentioned in chapter 2.3. A space frame can consist of several dozen welds, making it a time-consuming task to correctly simulate and generate a good mesh. Structured quadrilateral mesh is well suited for welds [21]. If done correctly it can capture the peak stress at the toe of the weld.

2.6.3. Crash

While the regular graded mesh is suited for simulating the durability of a weld, it is not ideal for crash simulation. For computational efficiency, it is preferred to use a uniform-sized mesh [21]. Using Hooke´s law relies on one assumption, that the model in question returns to its original shape, not realistic in a car crash. Since the deformations a car experiences remain after the crash it is not possible to simulate it using linear equations. It is evaluated using nonlinear dynamics and explicit time steps. The forces are calculated for each specified time step, with the forces from the previous timestep determining the next iteration.

2.6.4. FEA results

When solving a FEA using software, the results are worthless without the correct interpretation. Not knowing what the values imply, or how to use them, renders the simulations pointless. Solving a Static Structural problem using Ansys Mechanical Beam Tool gives the following result:

Table 6 Explanation of Ansys solver results [22]

Direct stress	The stress component of a beam caused by axial load.
Minimum bending stress	The lowest of four bending stresses that arise from bending loads
Maximum bending stress	The highest value of the four bending stresses
Minimum combined stress	The linear combination of Direct stress and Minimum bending stress
Maximum combined stress	The linear combination of Direct stress and Maximum bending stress
Axial force	The force along the x-axis of a beam element
Bending moment	The moment in the plane perpendicular to the beam element axis
Torsional moment	The moment about the beam element axis (x component).
Shear force	The force acting perpendicular to the beam element axis (y and z components)

2.7. Center of mass of a vehicle

To get the weight distribution of the axels we need the center of mass, also known as the center of gravity. The weight distribution determines how the car rolls while cornering and the weight transfer between wheels when braking, accelerating, and cornering [4]. The different components have a weight of m and their location for center mass, l and h, can either be measured or estimated. By combining all the components one can calculate the center of mass of the car.

$$m_m = \sum(m_1 + m_2 + \cdots m_n) \tag{17}$$

The combined center of mass by length l and height h is given by:

$$l_m = \frac{\sum(l_1 m_1 + l_2 m_2 + \cdots l_n m_n)}{m_m} \tag{18}$$

$$h_m = \frac{\sum(h_1 m_1 + h_2 m_2 + \cdots h_n m_n)}{m_m} \tag{19}$$

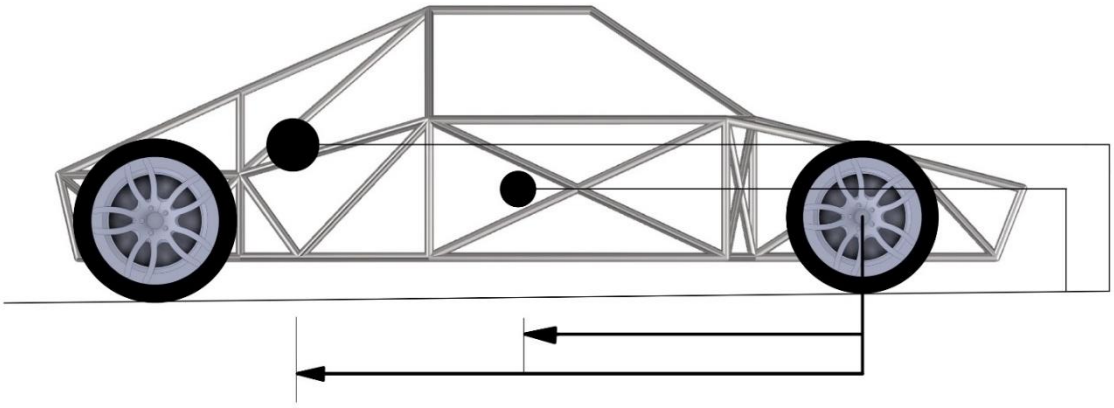

Figure 22 Center of mass

2.8. Aerodynamic and Downforce Fundamentals

Aerodynamics is the science and study of forces on objects moving through the air [23]. Closely monitoring how air moves around an object allows an engineer to determine the ideal shape of wings, propellors, ships, and racing cars. Altering the shape of a car greatly governs the behavior during acceleration, high speed, and cornering. Drag depends on the density of air, the velocity of the moving object, the drag coefficient C_d and a reference area. A flat brick held perpendicular to the flow of air has a drag coefficient of approximately 1.1, compared to a raindrop with the drag coefficient of approximately 0.05. The drag coefficient is often determined experimentally using wind tunnels, or computationally using CFD.

Table 7 Coefficients of drag and lift [4]

Shape	C_d	C_l
Passenger car	0.35	
Open-wheel race car	0.6	
Racecar with wings	0.7 – 1.2	0.3 – 1.2
Dolphin	< 0.01	

Listed above are some realistic drag coefficients for various shapes.

The aerodynamic drag force increases rapidly with the increase of speed. One can observe from equation 20 that by doubling the velocity it will result in quadrupling the drag forces [24]. Therefore, the designer needs to consider different load cases at different velocities.

$$D_F = C_d * \frac{\rho V^2}{2} * A \tag{20}$$

In addition to aerodynamic drag, we must mention lift and side forces. If designed correctly a car can have minimum amount of drag while obtaining maximum amount of lift. To avoid

confusion, it is common to refer to this as negative lift. It's not optimal to have a car that "lifts" off the ground. The downforce equation is almost identical to the drag equation, however the value for reference area changes. For aerodynamic downforce the area in question is taken as the width and chord length of the wing. Also, the coefficient of drag is substituted for the coefficient of lift.

$$Downforce \ = C_l * \frac{\rho V^2}{2} * A \tag{21}$$

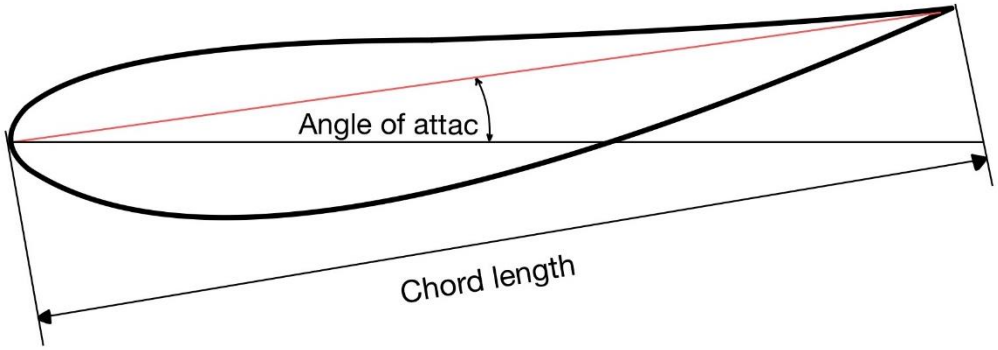

Figure 23 Terminology for aerofoil

On race cars, aerodynamics plays a vital role in the performance and is crucial at high speed for traction. One example is the Swedish designed Koenigsegg Jesko, delivering a downforce payload of 800 kg at 250 km/h, and an astonishing 1400 kg maximum downforce. At this level of car design, nothing is left to chance. Even the rear-view mirrors add 20 kg of downforce and is directing air to the massive rear spoiler [25].

Many race cars can be seen sporting a big rear wing, as this is a certain way of improving downforce. All this downforce often comes with a drawback, which is more drag. It is estimated by Miliken and Miliken [7] that a rear spoiler can increase downforce by 20 %, but at the same time increase drag by 50 %. You then need more engine power to overcome the added drag.

Contradictory to race cars, the aim of passenger cars is often to minimize the coefficient of drag to boost fuel efficiency. This comes at the expense of reduced downforce, this is not a big concern for normal road use.

Downforce has a significant effect on high-speed cornering. It adds additional g-force on the car which transforms into more grip. Mathematically it can be written as:

$$Maximum\ cornering\ force, F = (W + D) * \mu \tag{22}$$

When viewing the maximum cornering force in light of the downforce, it is obvious that increasing downforce D will yield a greater maximum cornering force, thereby resulting in faster lap times and better results.

2.9. Dynamic loads

As a race car is rarely standing still, it is not enough to analyze it using static forces only. One must consider dynamic forces to ensure a more realistic result and a safer vehicle. These dynamic forces occur during the entire duration of a race. As previously mentioned, a race car is ideally in either an accelerating phase or a decelerating phase. The objective is to carry the maximum amount of speed through a corner and onwards to the straights. This will quite naturally result in weight being shifted from the front wheels to the rear wheels, and from left to right. In some instances, the car might even get airborne. Accurately calculating all these forces is very challenging, the design procedure, however, is quite manageable.

A multiplication factor is applied to account for uneven roads, hitting curbs, cornering, and aerodynamic downforce. The multiplication factor of **3** is stating that the mass of the car is subjected to an acceleration of **3 g**.

Below is a table with suggested load cases with their assigned multiplication factors [4].

Table 8 Multiplication factors and load cases [4]

Load case	**Multiplication factor**
Max. vertical load	3.0
Max. torsion	1.3 on vertical loads
Max. cornering	1.3 on vertical and lateral loads
Max. decelerating	1.3 on vertical and longitudinal loads
Max. acceleration	1.3 on vertical and longitudinal loads

2.10. Design considerations

Structures such as beams and spaceframes experience three types of loading, and effort must be made to ensure all elements of the structure can withstand said loads.

2.10.1. Elements in tension

Ideally all members in a triangulated structure are loaded in either compression or tension. Adding the material safety factor of 1.5 mentioned above gives [4] :

$$Tensile\ stress\ \sigma_t = \frac{Force, F_t}{Area, A} \leq \frac{Yield\ stress, \sigma_y}{1.5} \tag{23}$$

$$Min.\ area, A\ = \frac{1.5 \times F_t}{\sigma_y} \tag{24}$$

2.10.2. Elements in compression

Thin and slender members often fail by buckling long before the material yield strength is reached. In the case of a spaceframe, the beams are connected by welds. The weld connection gives us the Euler critical load case IV. This results in reducing the effective length L_K to be equal to 0.5 times the original length L. Using the material safety factor of 1.5 the allowable Euler buckling load can be defined as[10]:

$$Allowable\ Euler\ buckling\ load\ F_E = \frac{\pi^2 EI}{1.5L_k^2} \tag{25}$$

The moment of inertia I, for a hollow tube can be mathematically derived as [26]:

$$Moment\ of\ inertia, I = \frac{\pi}{4}(R^4 - r^4) \tag{26}$$

2.10.3. Elements in bending

If the applied load does not act directly on the intersection of triangles bending moment will occur. This will in turn generate bending stress. Using the same material factor we can write [4]:

$$Bending\ stress, \sigma_b = \frac{bending\ moment, M}{Elastic\ section\ modulus, Z} \leq \frac{Yield\ stress, \sigma_y}{1{,}5} \tag{27}$$

$$Min. elstic\ modulus = \frac{1.5\ \times M}{\sigma_y} \tag{28}$$

$$Elastic\ section\ modulus, Z = \frac{\pi}{4R} \cdot (R^4 - Ri^4) \tag{29}$$

3. Concept selection

Choosing between the previously mentioned chassis was difficult. Available literature showed popularity among both monocoque design and steel space frames. The vast use of 3-D trusses in civil engineering was the winning argument that led us to pursue this concept. Bridges, stadiums, and perhaps even more relevant to our geographical location, offshore structures all use framed structures. This was a great opportunity to further our knowledge on this topic and learn more about both strengths and weaknesses of trussed structures.

4. Preliminary Design

The goal of the preliminary design process is to get the bigger picture of all the components, and their placement in the car. In motor racing, there are often strict rules to abide by concerning the weight, length, and width of the car. In this thesis there is taken no consideration of this. Since there are no rules limiting our design, the body shape, or the geometry of the car, we have simply designed a race car with estimated dimensions and external shape of our pleasing.

In this stage of the design process, we start by gathering data on all components used in the car. Some data will be assumptions and some estimates.

To produce a more realistic simulation, we have decided to include the weight of a motor, gearbox, and one passenger. To not exceed the scope of the task and exceed our capabilities we have chosen estimates in both size and weight of these components.

4.1. Design

The CAD software used for designing the spaceframe was Autodesk Inventor. The university of Stavanger holds an educational license for this program and both students are avid users of the program. The chassis was drawn as a 3-D sketch of lines as a part file, as displayed in Figure 24. The part file was then imported to an assembly where tubes were generated using frame generator. The model on the right in Figure 24 shows the chassis with the generated tubes in Inventor.

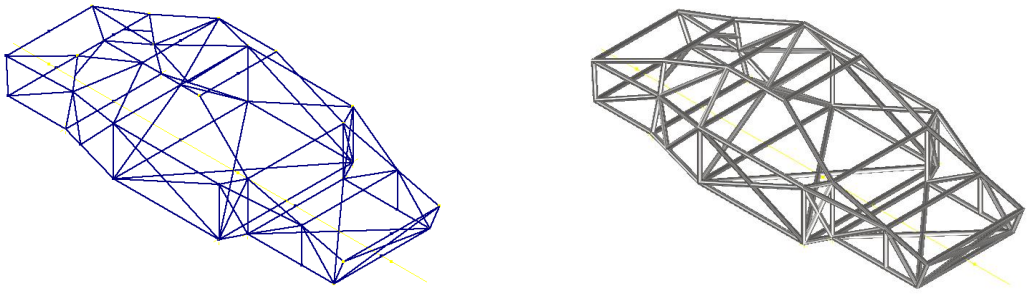

Figure 24 3-D frame of lines (left) and frame with tubes (right).

4.1.1. Design concepts

Below are the different design concepts made in Autodesk Inventor. The initial design was purely based on aesthetics, but later iterations were designed to improve torsional stiffness. Design 1 is the first iteration made with limited knowledge to triangulation and frame design. One can track the progress throughout the design process from iteration 1 all the way to iteration 6. The reason for these designs was to make a frame that could be simulated and improved further in Ansys with different beams and cross-sections.

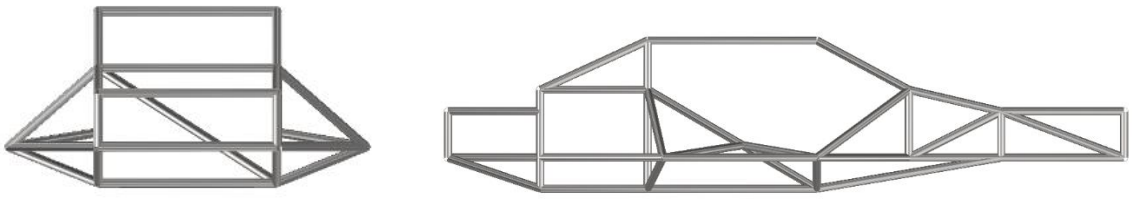

Figure 25 Design 1

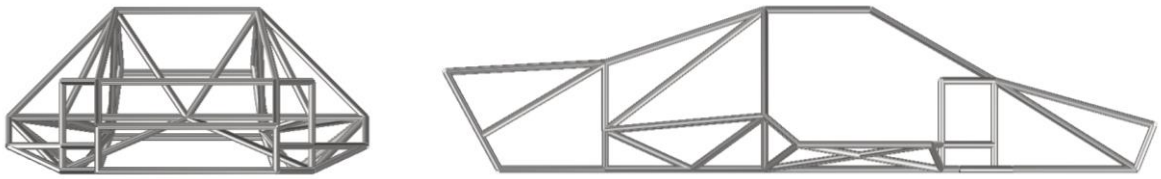

Figure 26 Design 2

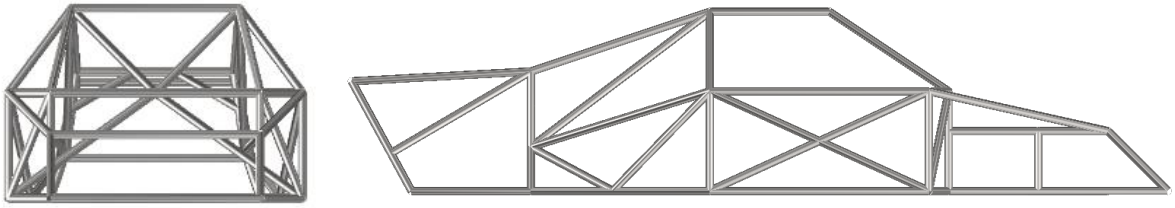

Figure 27 Design 3

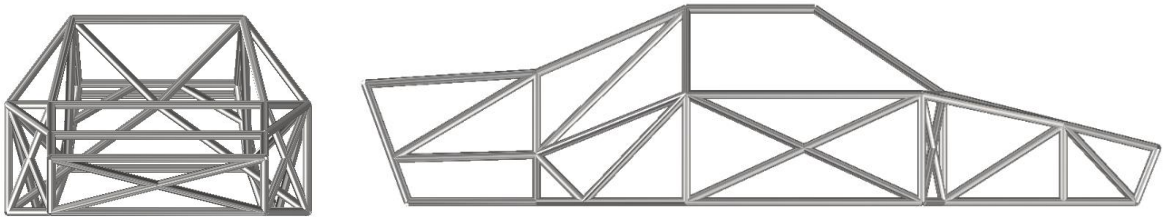

Figure 28 Design 4

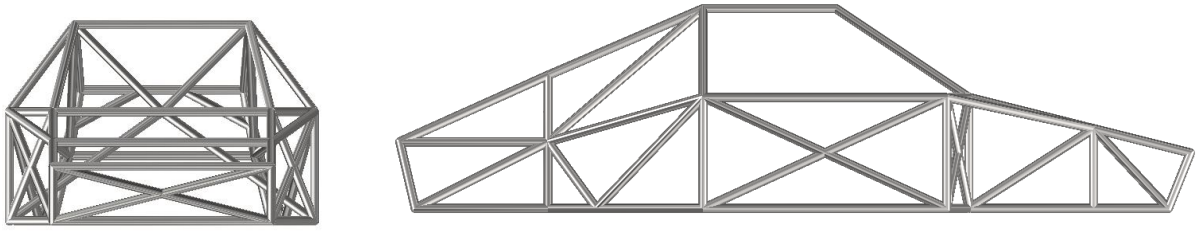

Figure 29 Design 5

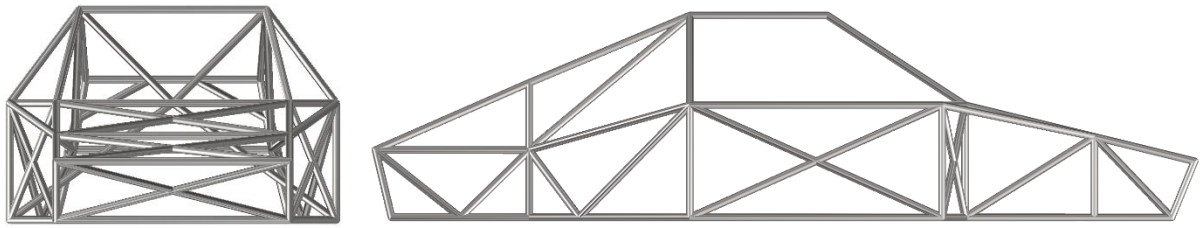

Figure 30 Design 6

Table 9 Frame properties of design 6

Description	**Units**
Mass	123.93 Kg
Material	S355
Cylindrical tubes	33.7 x 2 mm

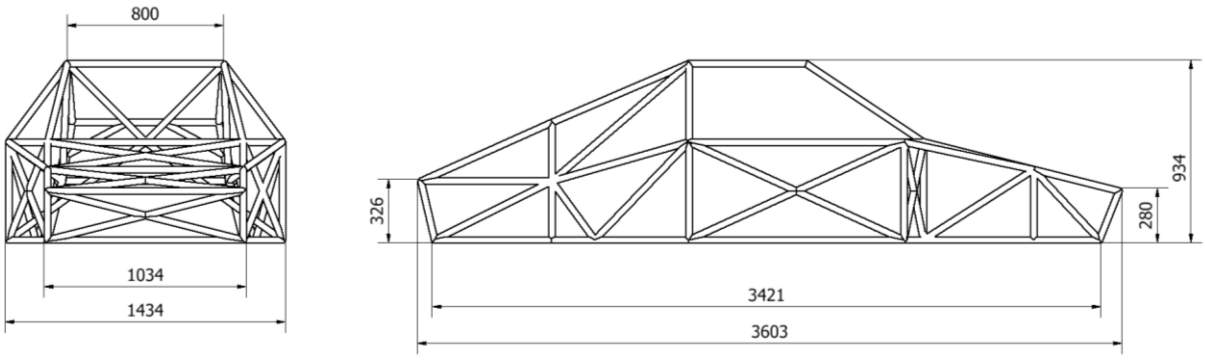

Figure 31 General dimensions of design 6

4.2. Assumptions and limitations

Assumptions are defined by Cambridge Dictionary as something that you accept as true without question or proof [27]. The assumptions and limitations of this thesis will be represented in this chapter.

4.2.1. Static forces

To retain a more realistic result, a mass for the car engine, gearbox and passenger had to be added. Research showed that average engine sizes ranged from 140 to 200 kg. Assuming high output race car engines weigh more than average we settled on 200 kg. This is a conservative estimate and will only contribute to a conservative result during simulations. The mass of the gearbox is set to be approximately 100 kg, that of a standard size gearbox [28]. The driver is set to be 85 kg.

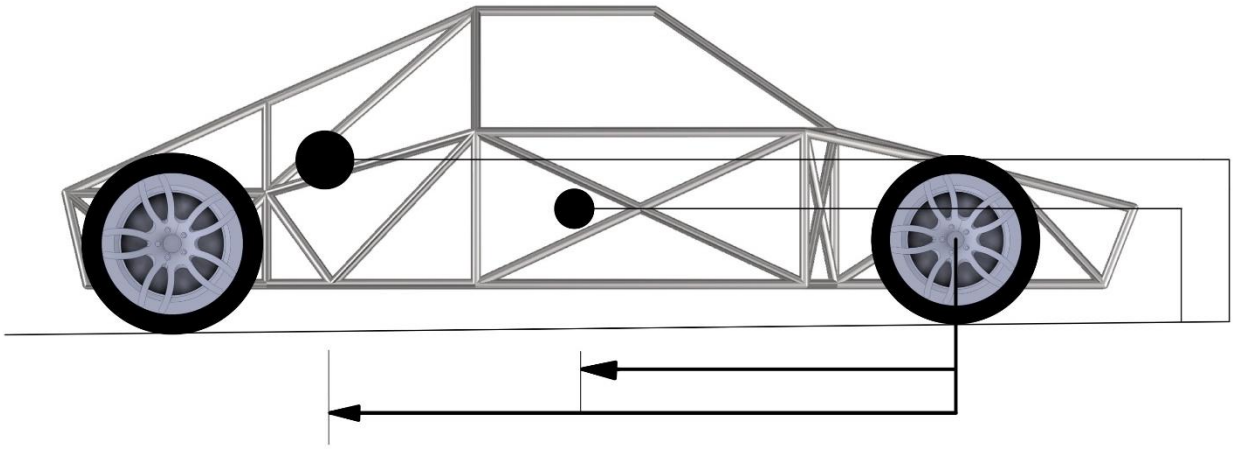

Figure 32 Location of center of mass of engine and driver

Table 10 Weight and center gravity of components

Component	Weight [kg]	CG length [mm]	CG height [mm]
Engine + Gearbox	300	2375	484
Driver	85	1363	375

4.2.2. Aerodynamics

The science of aerodynamics is complicated and cumbersome and not the main concern of this thesis, therefore no calculations were made to obtain real numbers.

It is however, important to consider the additional loading applied by aerodynamic downforce both under straight-line driving as well as in cornering speed. This can be done using estimates and tables of similar shapes. As mentioned in chapter 2.8, Table 7, a race car with a wing will commonly have a coefficient of drag between 0.7 – 1.2. We have opted for a C_d value of 1. This is a realistic estimate, one can say even a bit optimistic. Since aerodynamic downforce is outside the scope of this project, an estimated reference area of 2.8 m^2 was chosen. This area was calculated using the length and width of the frame. Further assuming that the shape of the car resembles a one element airfoil of width 0.8 m and length 3.6 m.

Table 11 Estimated downforce with increasing velocity

Velocity [km/h]	**Downforce [N]**
50	397
100	1588
150	3573
200	6352

To account for additional uncertainties such as road conditions and real aerodynamic values it was decided to use dynamic load factors found in Table 8.

4.2.3. Material

It is important to use a material that is both strong and tough for our racecar frame. We choose to use S355 from the standard EN-NS10025. This is weldable construction steel. From Table 12 , where the thickness is under 40 mm, the yield strength is 355 MPa and the tensile strength is 510 MPa.

Table 12 Material properties

Properties	*EN S275*	*EN S355*	*EN S420*	*25CrMo4*
Tensile strength [MPa]	275	355	420	740
Yield point [MPa]	430 (370-530)	490 (470-630)	550	590
Density [g/cm^3]	7.85	7.85	7.85	7.85
Young's modulus [GPa]	210	210	210	210

4.2.4. Weld

It is assumed that all welds exhibit the same material properties as the parent material. The weld geometry changes around the circumference of pipes. Accurately modeling this is time-consuming and challenging and may not considerably influence the result.

5. Ansys modeling

The finite element analysis was performed using the FEA software *Ansys® Workbench, Release 2020 R1*. The newest version at the time of writing this thesis was *Release 2022 R1,* but this was not available for use for students at the University of Stavanger. The figures regarding modeling and simulation in the thesis are all from *Ansys® Workbench, Release 2020 R1*.

Two different simulations were carried out, one for static structural problems, the other for explicit dynamics. Torsional stiffness, dynamic loading lateral and vertical were all simulated using Static structural, while crash simulation was done using Explicit dynamics.

5.1. Static Structural Simulation

The static structural simulation was divided into three stand-alone systems with shared engineering data and geometry. This eliminates the possibility of human errors when entering engineering data or preparing the geometry. Each system with different setups according to the loading type are displayed in Figure 33.

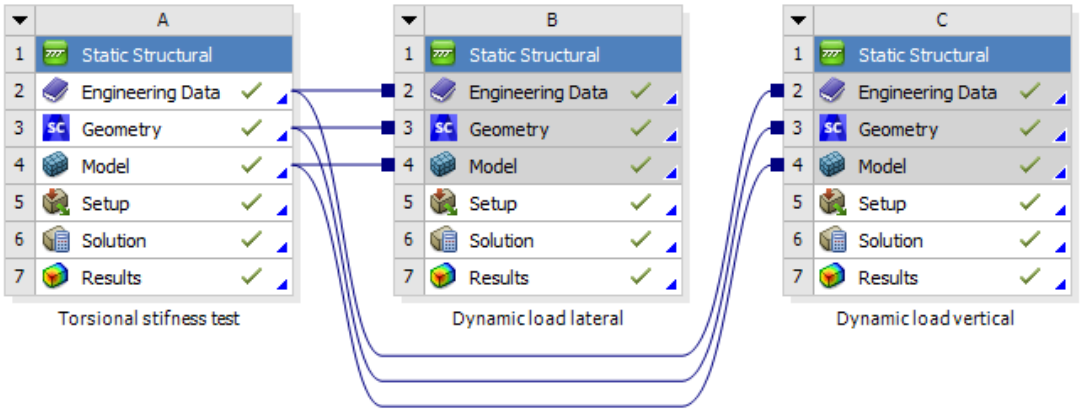

Figure 33 Setup of Static Structural

5.1.1. Engineering data

The built-in material library of Ansys did not feature the material S355. Therefore, it had to be entered manually as a new material. The European structural steel standard EN 10025:2004 was used to collect the material properties for the S355 [29]. The material has a Tensile Yield strength of 355 MPa and a tensile ultimate strength of 470 MPa. The young's modulus is 210 GPa and the Poisson's ratio is 0.3. The material has a density of 7850 kg/m^3. The material added in Ansys is displayed in Figure 34.

Properties of Outline Row 3: S355

	A	B	C	D	E
1	Property	Value	Unit		
2	Material Field Variables	Table			
3	Density	7850	kg m^-3		
4	Isotropic Elasticity				
5	Derive from	Young's Mo...			
6	Young's Modulus	2,1E+11	Pa		
7	Poisson's Ratio	0,3			
8	Bulk Modulus	1,75E+11	Pa		
9	Shear Modulus	8,0769E+10	Pa		
10	Tensile Yield Strength	3,55E+08	Pa		
11	Tensile Ultimate Strength	4,7E+08	Pa		

Figure 34 Material properties for S355.

5.1.2. Geometry preparation

The CAD file was converted to STEP format, imported to Ansys workbench, then edited in Ansys SpaceClaim. In SpaceClaim the “extract beams” tool was used. This allowed us to extract the beams from the solid model. Further improvement was needed to clean the CAD file. Lines were connected, overhanging lines deleted. These improvements were needed to smoothly mesh the model, and to successfully run the simulation. Removing the complicated geometry of all the mitered and notched connections reduced the risk of failed mesh, or to small elements. The dimensions are standard 33.7 mm diameter with a 2.0 mm thickness. This equals an outer radius of 16.85 mm and an inner radius of 14.85 mm. The cross-section is displayed in Figure 35.

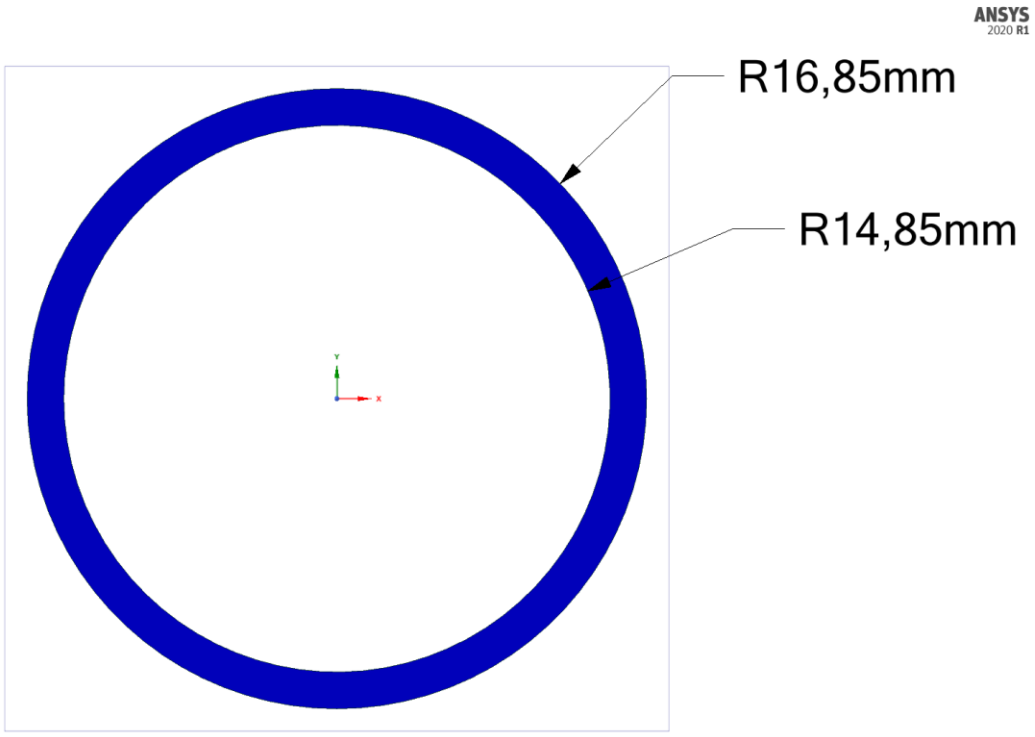

Figure 35 Cross section of frame material

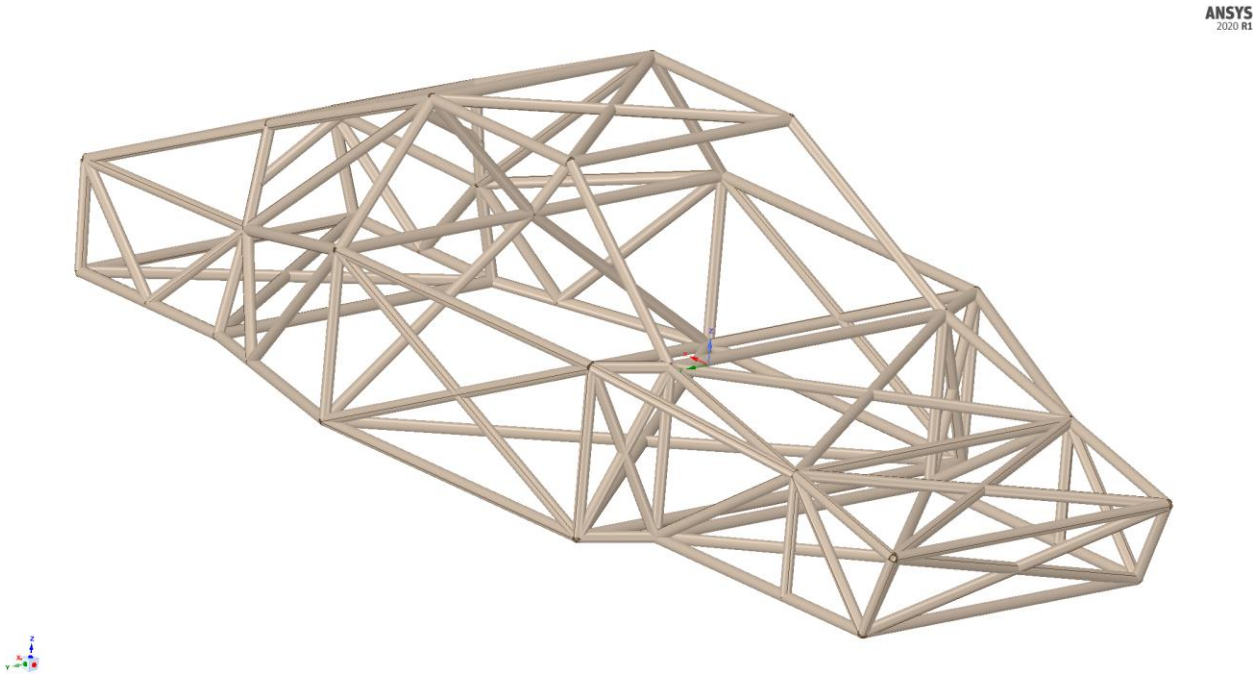

Figure 36 Solid frame in Ansys SpaceClaim

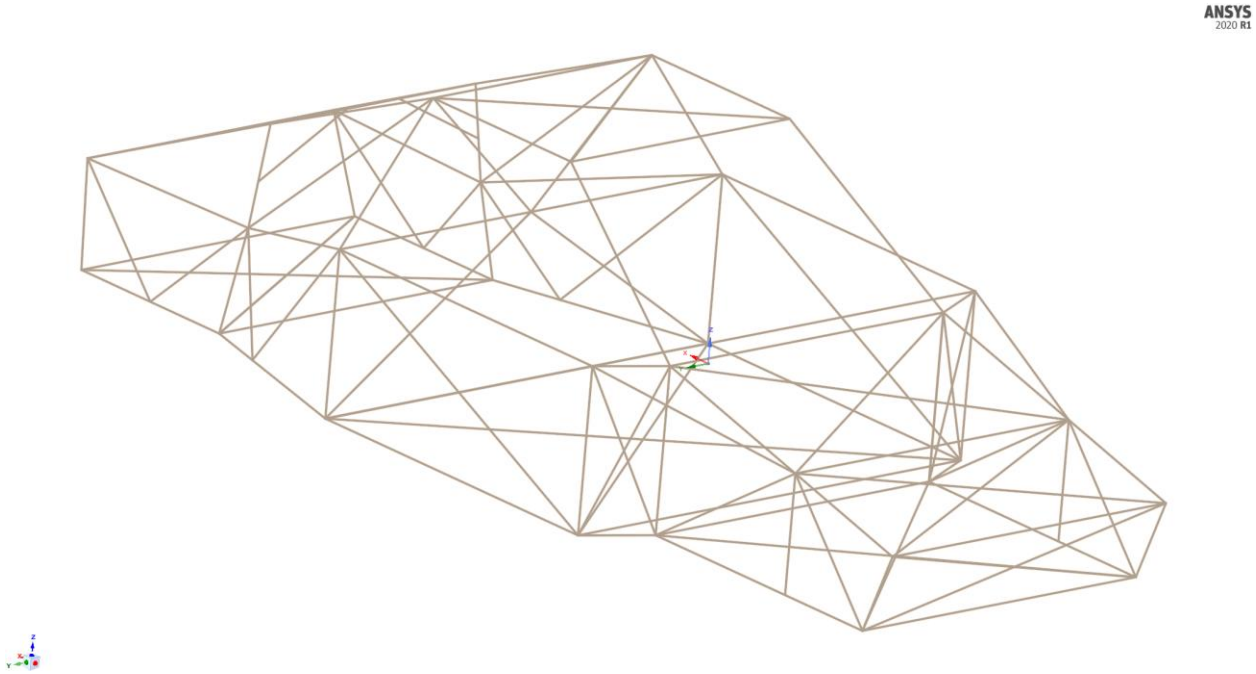

Figure 37 Beams extracted from frame in Ansys SpaceClaim

5.1.3. Mesh

A mesh convergence study was performed on the chassis. We used the maximum combined stress for the lateral dynamic load setup. The element size decreased with a ratio of 1.5 from 10 mm to 0.0343 mm. While decreasing the element size and increasing the number of elements, the combined stresses increased. The changes in stress were noted and plotted in an excel document. The results are displayed as a chart in Figure 38. From the chart, one can see the graph start converging around 450 000 elements. Further, we used the mesh size from point A in Table 13 and which gave the mesh size of 0.1156 mm.

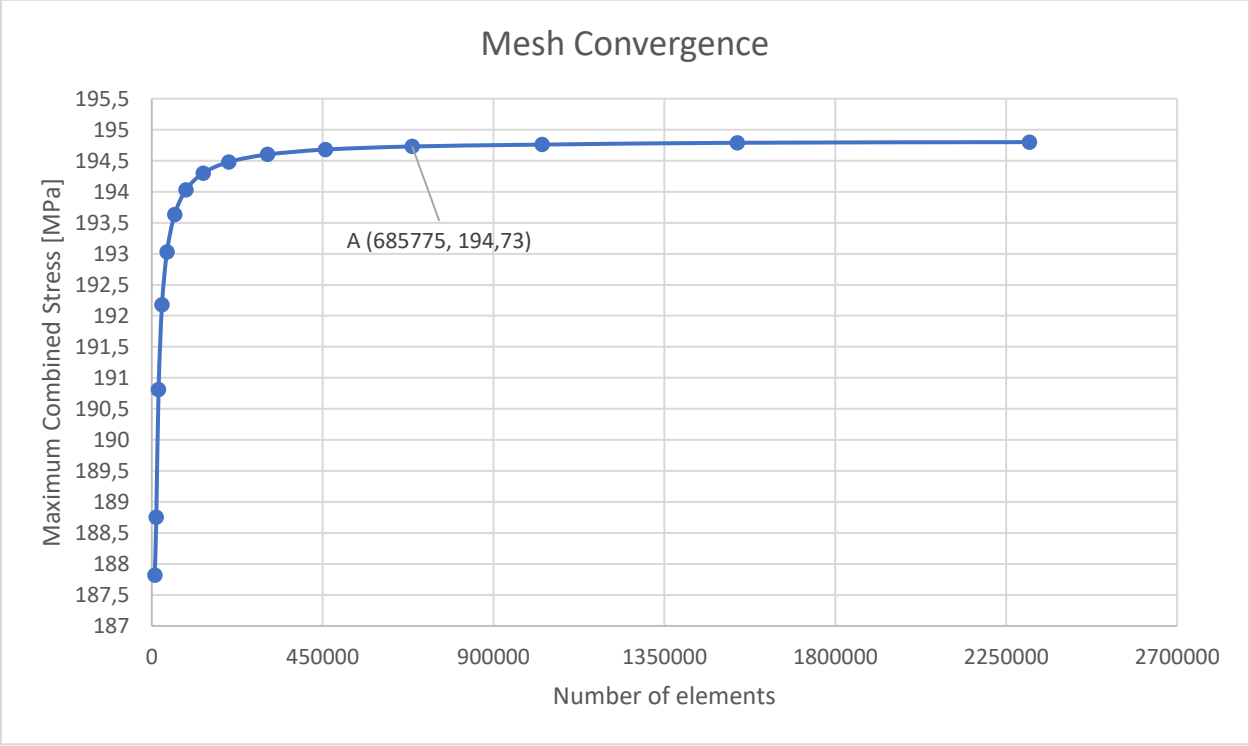

Figure 38 Mesh convergence study

Table 13 Mesh convergence test

Mesh size [mm]	Number of elements	Maximum Combined Stress [MPa]
10	7973	187.82
6,6667	11942	188.75
4,4444	17914	190.81
2,9630	27069	192.18
1,9753	40198	193.03
1,3169	60251	193.63
0,8779	90357	194.03
0,5853	135494	194.3
0,3902	203211	194.48
0,2601	304813	194.6
0,1734	457201	194.68
0,1156	685775	194.73
0,0771	1028182	194.76
0,0514	1542219	194.79
0,0343	2311035	194.8

5.1.4. Torsional stiffness

First step in Ansys Mechanical was to assign the material S355 to the geometry. For the torsional stiffness test, the frame was supported by simply supports at vertices 1-5 as displayed in Figure 39. This ensures no displacement of vertcies. A force of -1000 N was applied at vertex 6 in the z-direction.

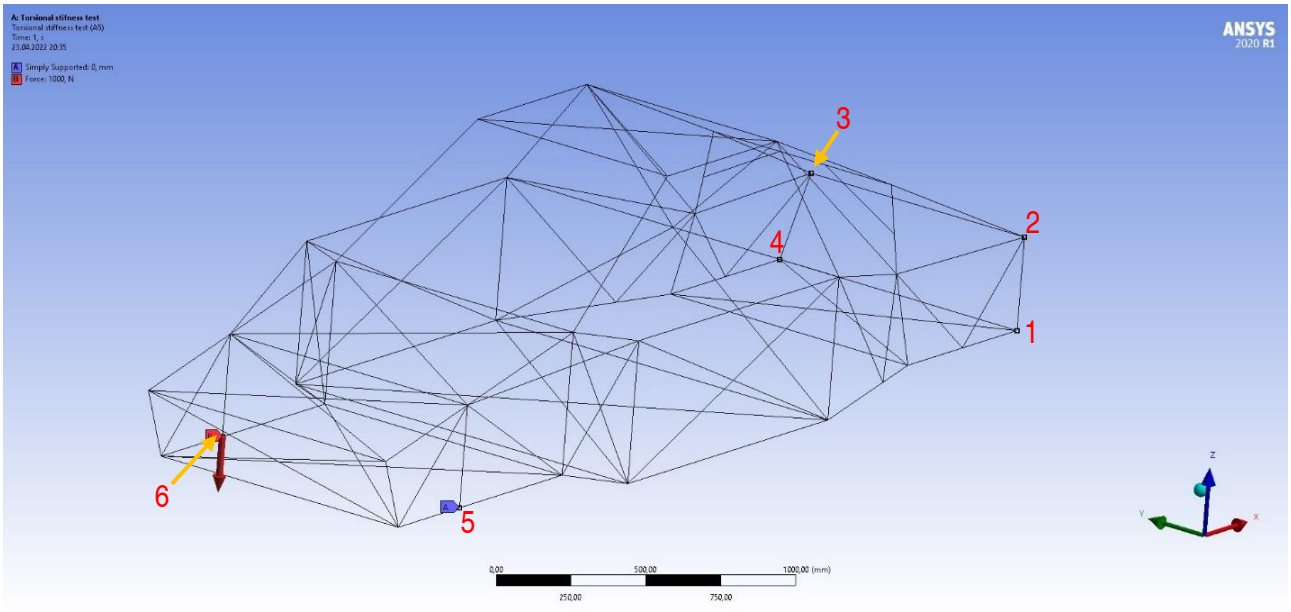

Figure 39 Supports and force on frame.

To calculate the torsional stiffness of the frame, the directional deflection was used. It is applied at vertex 6, the same vertex where the force is applied. Figure 40 shows the setup of the directional deformation.

Details of "Directional Deformation"

Scope	
Scoping Method	Geometry Selection
Geometry	1 Vertex
Definition	
Type	Directional Deformation
Orientation	Z Axis
By	Time
Display Time	Last
Coordinate System	Global Coordinate System
Calculate Time History	Yes
Identifier	
Suppressed	No
Results	
Minimum	
Maximum	
Average	
Minimum Occurs On	
Maximum Occurs On	
Information	

Figure 40 Directional deformation setup

5.1.5. Dynamic load lateral

The dynamic lateral load has the same material assignment as the torsional stiffness test. To add the mass of the motor, gearbox and driver the function *point mass* was used. A local coordinate system was set up at the front left lower corner as displayed in Figure 41. From the local coordinate system, the center mass of the engine, transmission, and the driver was located. The engine and transmission have the coordinates of x = 2712, y= 500 and z = 358.2 and are connected to the vertices shown in Figure 41. The driver has the coordinate points of x = 1700, y = 500, and z = 250 and are connected to the vertices displayed in Figure 42.

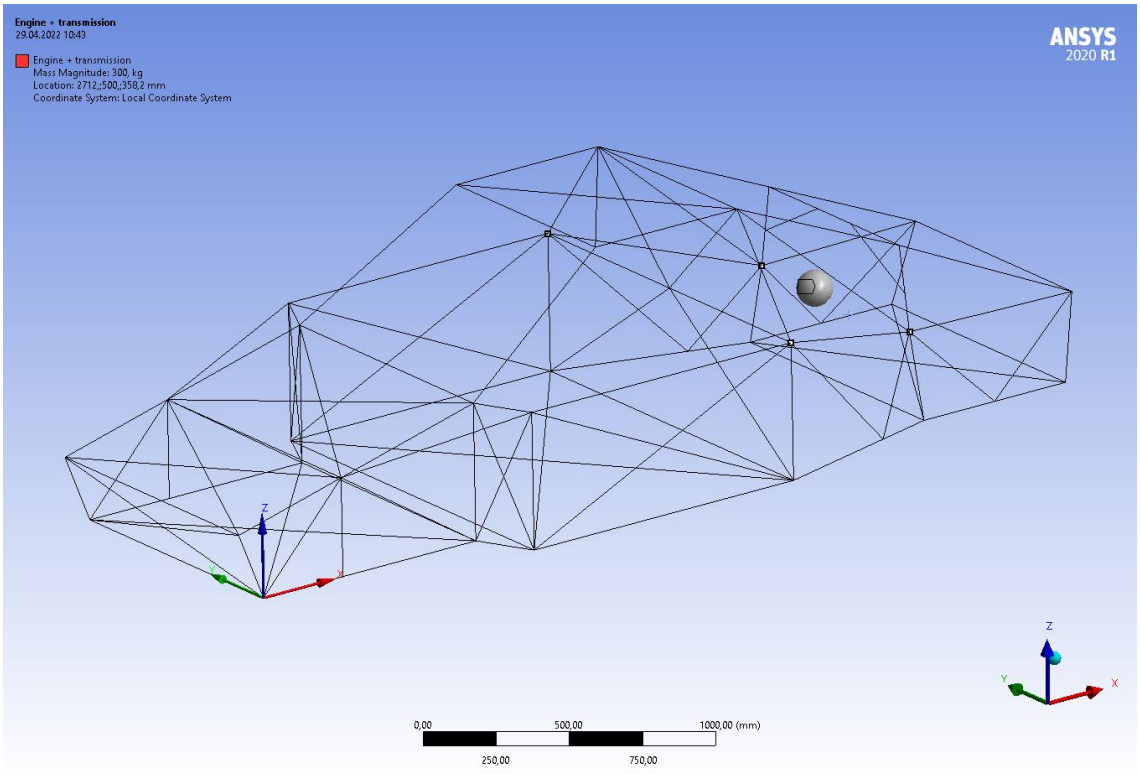

Figure 41 Point mass engine and transmission

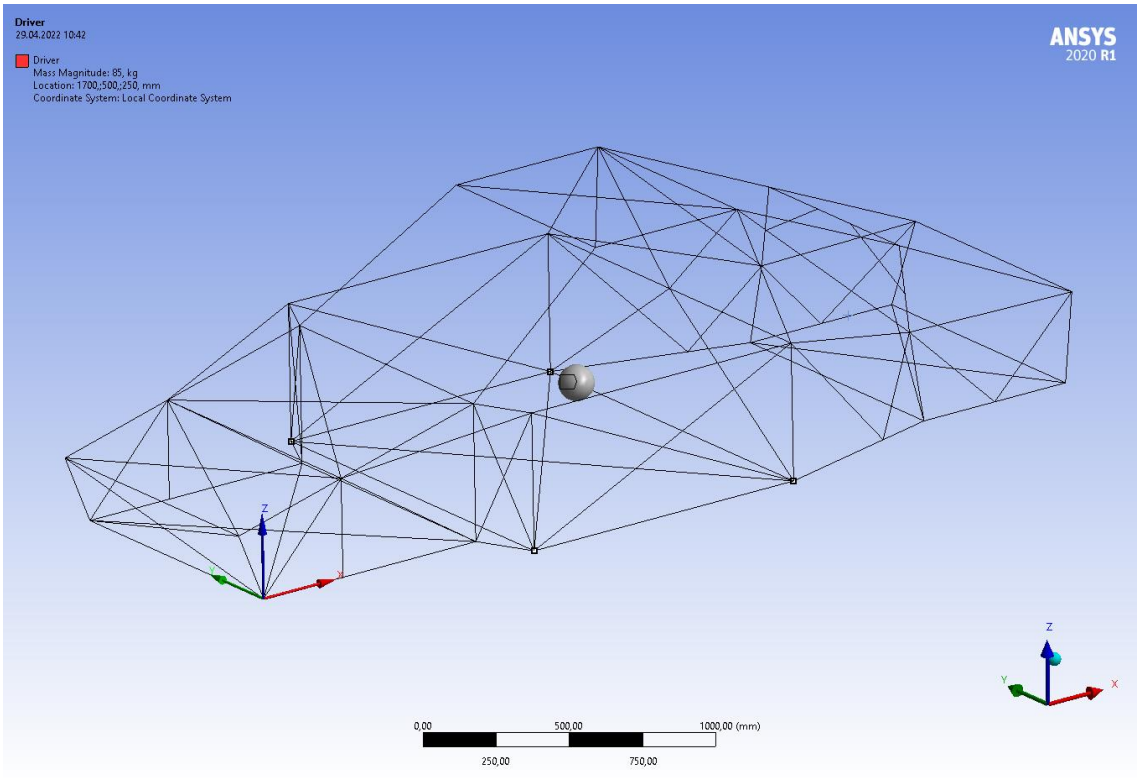

Figure 42 Point mass driver

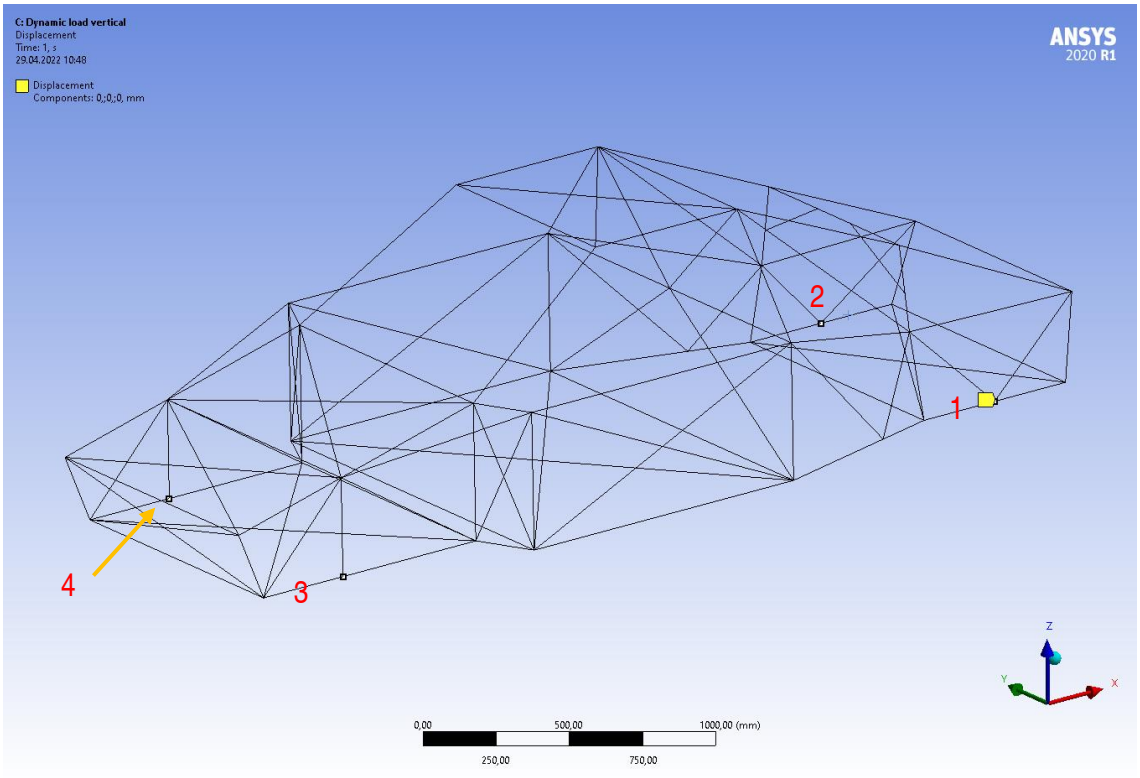

Figure 43 Supports dynamic load lateral

For the dynamic lateral load the frame was supported by simply supports on vertices 1-4 as displayed in Figure 43.

Standard earth gravity was then added in the negative Z-direction to achieve the weight of the frame and the point masses. The gravity is displayed as B in Figure 44. To simulate the stresses during a bump the acceleration of 29 430 mm/s^2 was added in the positive Z-direction, displayed as E in Figure 44. The value of 29 430 mm/s^2 comes from Table 8 and is equal to 3g.

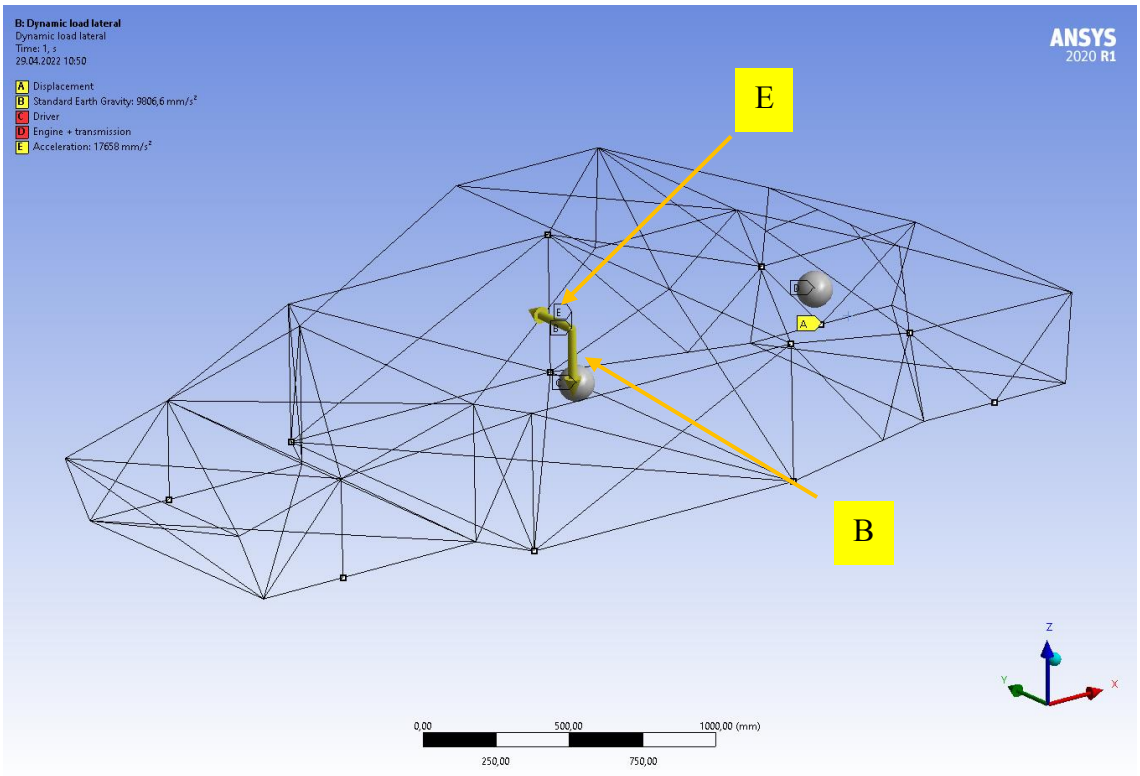

Figure 44 Dynamic load lateral setup

5.1.6. Dynamic load vertical

The dynamic load vertical simulates hard cornering of the vehicle with an acceleration of 17 658 mm/s^2 in the Y-direction. The supports, point masses and gravity are the same as the dynamic load vertical. Figure 45 shows the setup for the dynamic load setup.

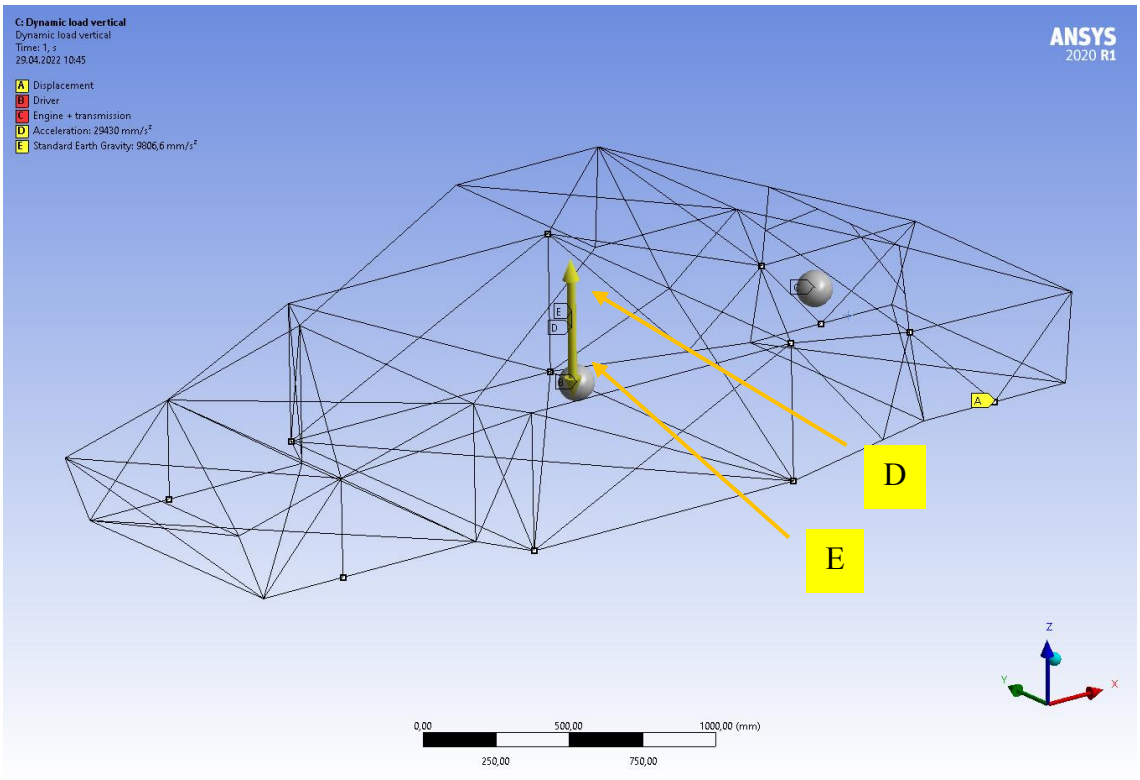

Figure 45 Dynamic load vertical setup

5.2. Explicit Dynamics Simulation

For the crash simulation the Explicit dynamics module in *Ansys® Workbench, Release 2020 R1* was used. This is ideal for capturing deformation and physics of high velocity evets of short duration. It lets us gather results when the steel frame undergoes highly nonlinear forces.

5.2.1. Engineering data

To achieve an explicit dynamic simulation, it is required to add a material with non-linear properties. The material properties of S355 steel had to be entered manually in Explicit Dynamics. The data for the non-linear properties was collected from Figure 46. Points were added along the length of the graph with great caution using WebPlotDigitizer [30]. The values were download to Microsoft Excel, formatted, and added to the multilinear isotropic hardening option in Ansys Workbench. The material *S355 multilinear isotropic* in Ansys can be seen in Figure 47 and Figure 48.

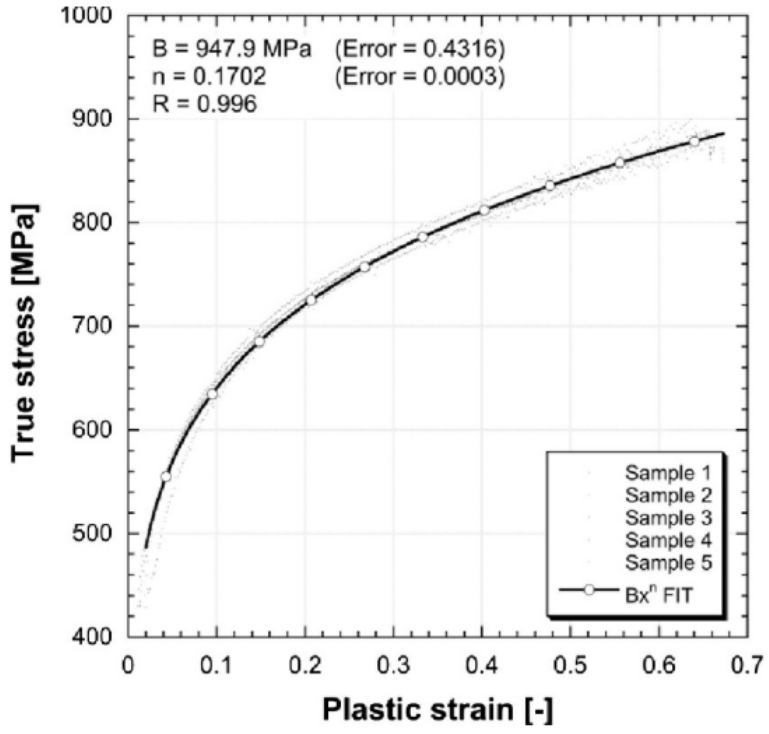

Figure 46 True stress Plastic strain data [31]

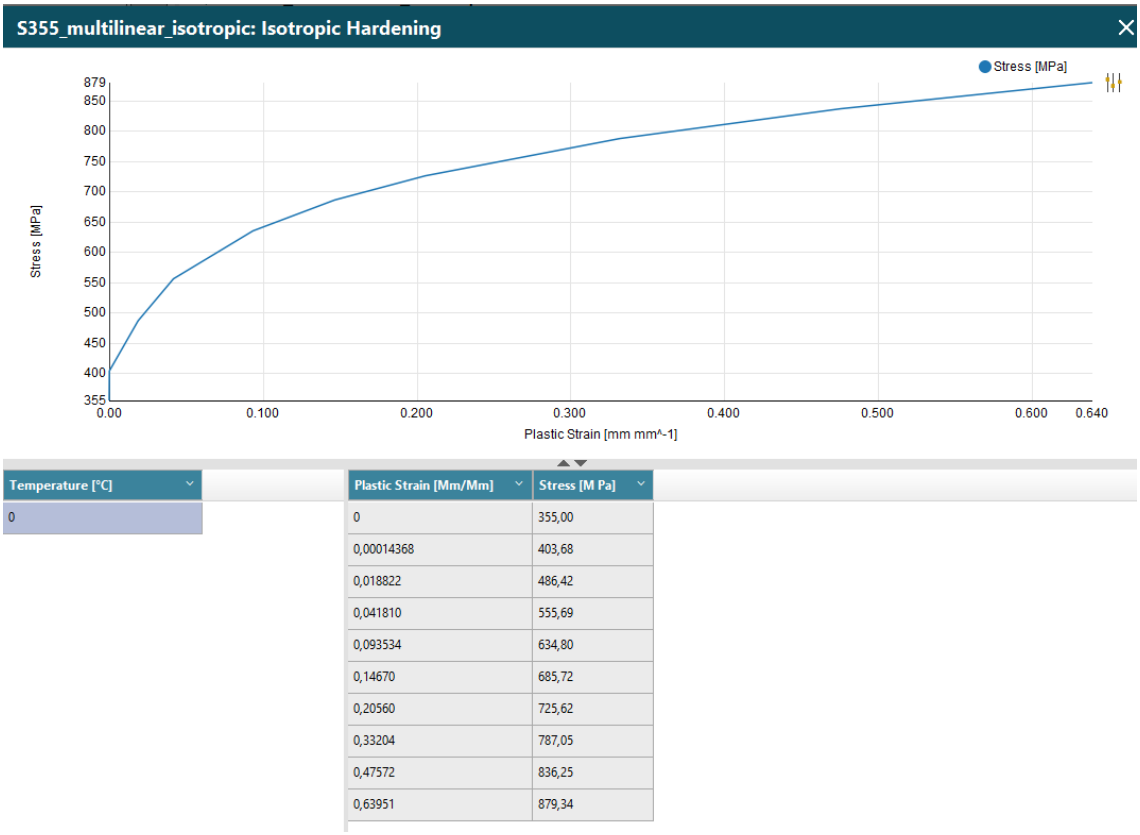

Figure 47 Multilinear Isotropic Hardening graph from extracted points and true stress and plastic strain values used to generate multilinear isotropic hardening graph

Properties of Outline Row 3: S355_multilinear_isotropic

	A	B	C	D	E
1	Property	Value	Unit		
2	Material Field Variables	Table			
3	Density	7850	kg m^-3		
4	Isotropic Elasticity				
5	Derive from	Young's Modulus and Poiss...			
6	Young's Modulus	2,1E+05	MPa		
7	Poisson's Ratio	0,3			
8	Bulk Modulus	1,75E+11	Pa		
9	Shear Modulus	8,0769E+10	Pa		
10	Multilinear Isotropic Hardening	Tabular			

Figure 48 Material properties for S355 Multilinear isotropic

5.2.2. Geometry preparation

To prepare the model and reduce computational time the frame was made to a shell model existing of surfaces. The surface of every member of the frame were copied and combined into one entity as shown in Figure 49. The thickness was added afterwards in Ansys Mechanical to equal the wall thickness of the frame.

For the frame to be able to crash, a wall was designed. The wall was dimensioned to be bigger than the crash surface of the frame. Figure 50 display the chassis and the wall. The wall was drawn on a surface tangent to the frame.

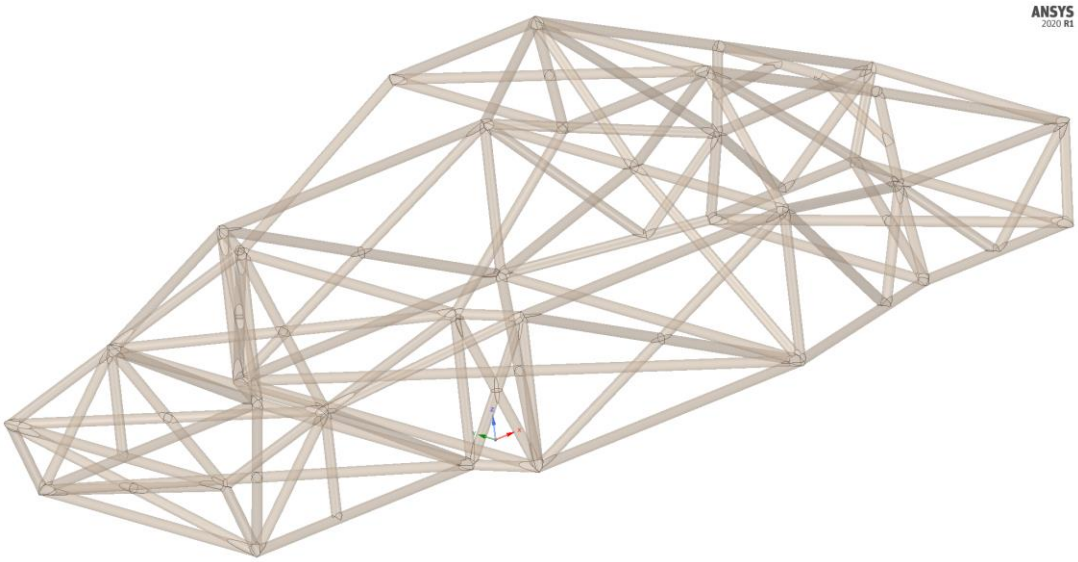

Figure 49 Surface extracted from frame in Ansys SpaceClaim

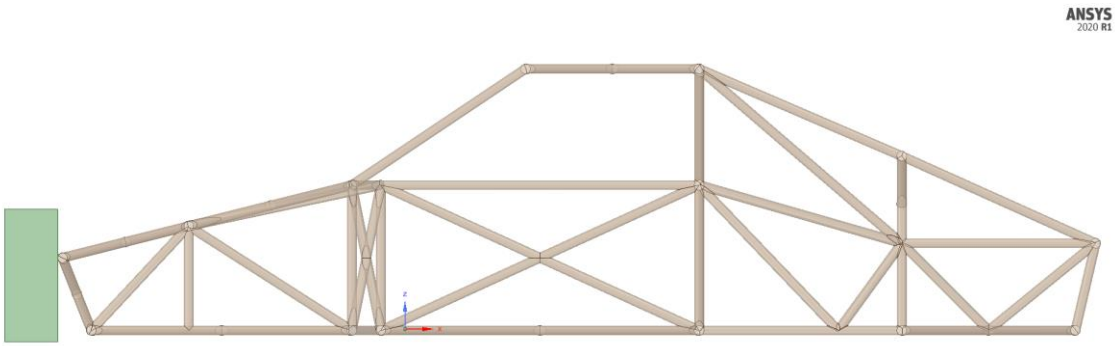

Figure 50 Frame and wall in Ansys SpaceClaim

5.2.3. Mesh

The element size selected for the frame was set to 10 mm, resulting in a total amount of elements of 79 467. The impact structure was modeled as rigid to reduce simulation time.

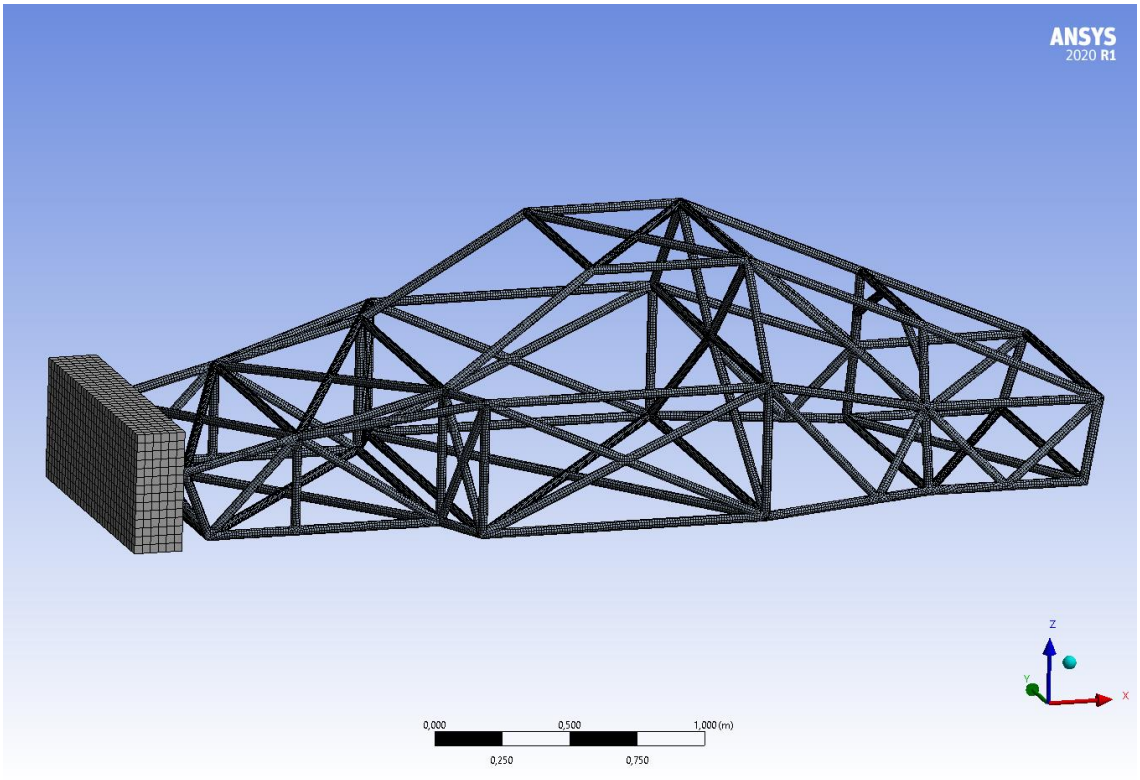

Figure 51 Mesh of frame and wall

5.2.4. Crash simulation

In the initial conditions, the velocity was scoped to the frame using body select. A value of 30 m/s in the negative x-direction was selected. The rigid “wall” was supported by fixed support. A surface contact was defined. The analysis settings can be seen in Figure 53.

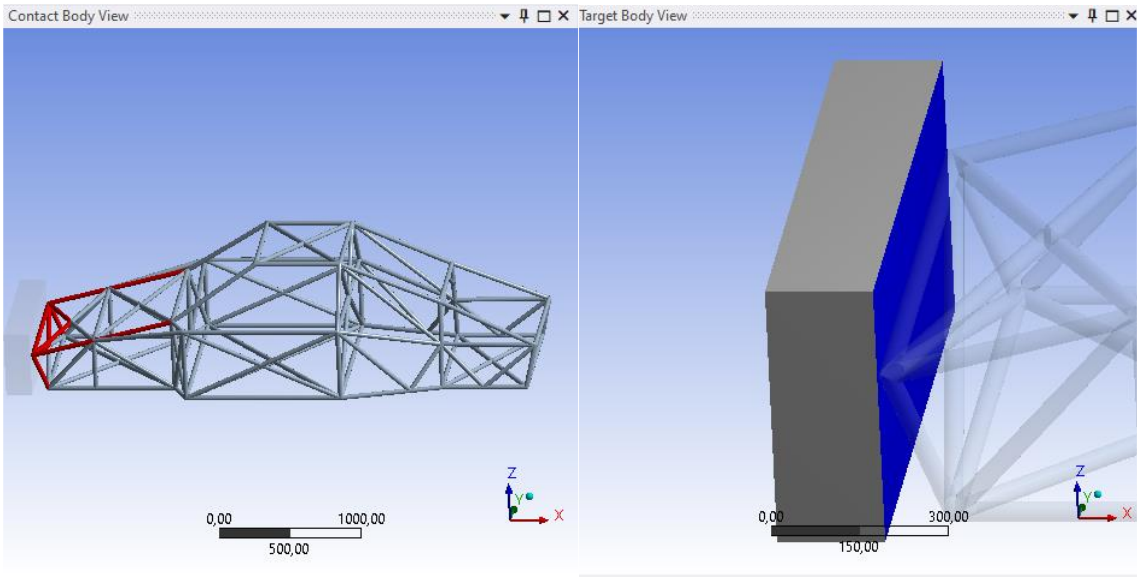

Figure 52 Contact body (left) and target body (right)

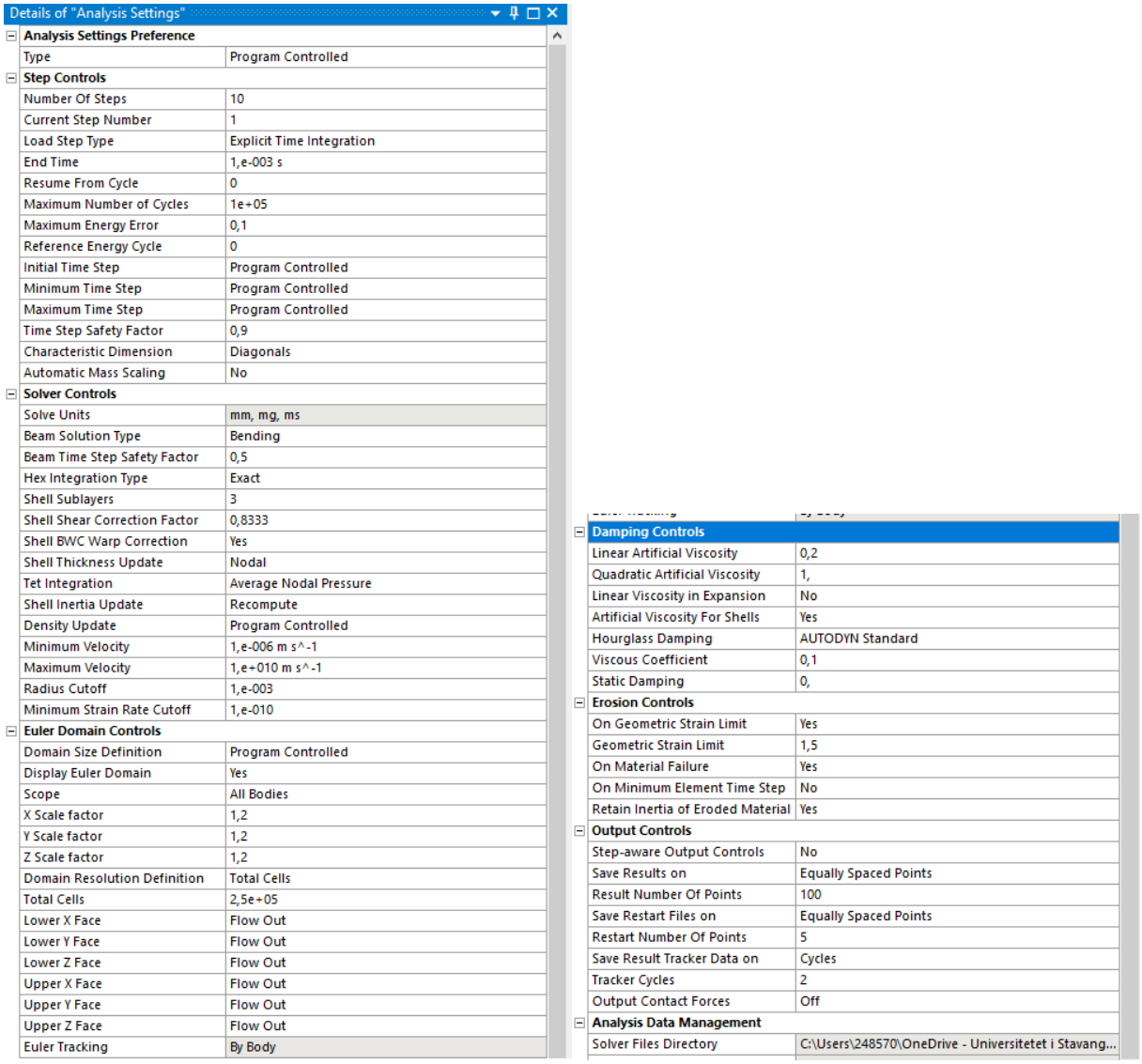

Details of "Analysis Settings"

Analysis Settings Preference	
Type	Program Controlled
Step Controls	
Number Of Steps	10
Current Step Number	1
Load Step Type	Explicit Time Integration
End Time	1,e-003 s
Resume From Cycle	0
Maximum Number of Cycles	1e+05
Maximum Energy Error	0,1
Reference Energy Cycle	0
Initial Time Step	Program Controlled
Minimum Time Step	Program Controlled
Maximum Time Step	Program Controlled
Time Step Safety Factor	0,9
Characteristic Dimension	Diagonals
Automatic Mass Scaling	No
Solver Controls	
Solve Units	mm, mg, ms
Beam Solution Type	Bending
Beam Time Step Safety Factor	0,5
Hex Integration Type	Exact
Shell Sublayers	3
Shell Shear Correction Factor	0,8333
Shell BWC Warp Correction	Yes
Shell Thickness Update	Nodal
Tet Integration	Average Nodal Pressure
Shell Inertia Update	Recompute
Density Update	Program Controlled
Minimum Velocity	1,e-006 m s^-1
Maximum Velocity	1,e+010 m s^-1
Radius Cutoff	1,e-003
Minimum Strain Rate Cutoff	1,e-010
Euler Domain Controls	
Domain Size Definition	Program Controlled
Display Euler Domain	Yes
Scope	All Bodies
X Scale factor	1,2
Y Scale factor	1,2
Z Scale factor	1,2
Domain Resolution Definition	Total Cells
Total Cells	2,5e+05
Lower X Face	Flow Out
Lower Y Face	Flow Out
Lower Z Face	Flow Out
Upper X Face	Flow Out
Upper Y Face	Flow Out
Upper Z Face	Flow Out
Euler Tracking	By Body

Damping Controls	
Linear Artificial Viscosity	0,2
Quadratic Artificial Viscosity	1,
Linear Viscosity in Expansion	No
Artificial Viscosity For Shells	Yes
Hourglass Damping	AUTODYN Standard
Viscous Coefficient	0,1
Static Damping	0,
Erosion Controls	
On Geometric Strain Limit	Yes
Geometric Strain Limit	1,5
On Material Failure	Yes
On Minimum Element Time Step	No
Retain Inertia of Eroded Material	Yes
Output Controls	
Step-aware Output Controls	No
Save Results on	Equally Spaced Points
Result Number Of Points	100
Save Restart Files on	Equally Spaced Points
Restart Number Of Points	5
Save Result Tracker Data on	Cycles
Tracker Cycles	2
Output Contact Forces	Off
Analysis Data Management	
Solver Files Directory	C:\Users\248570\OneDrive - Universitetet i Stavang...

Figure 53 Analysis settings for crash test

6. Results

In this chapter the results from the torsional test, vertical and lateral dynamic load simulation and crash simulation will be represented.

6.1. Torsional stiffness

From the torsional stiffness test we get a directional deflection of 2.437 mm. Using the equation 10, with the width of 1034 mm the angular rotation is:

$$angular\ rotation, \phi = \tan^{-1}(\frac{1.2901\ mm}{1000\ mm}) = \ 0.0739\ degree$$

The angular rotation result in a torsional stiffness:

$$Torsional\ stiffnes, k = \frac{1000\ Nm}{0.0739\ degree} = 13\ 531.8\ Nm/degree$$

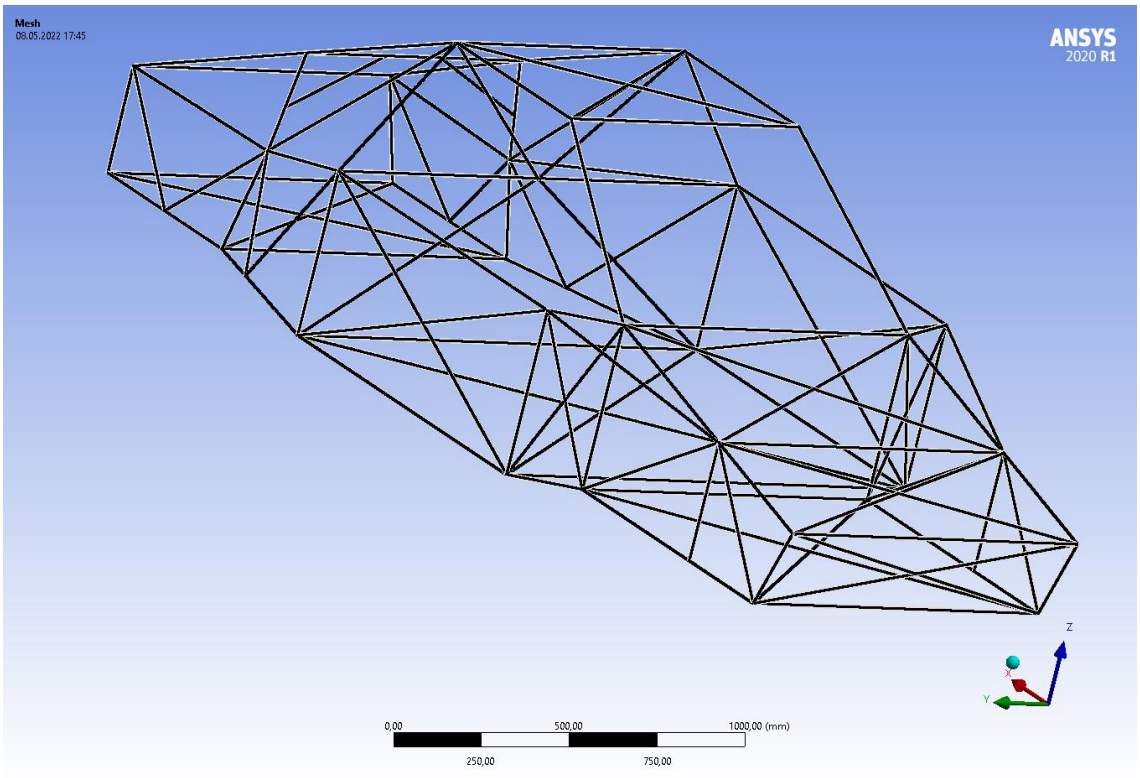

Figure 54 Chassis before torsional stiffness test

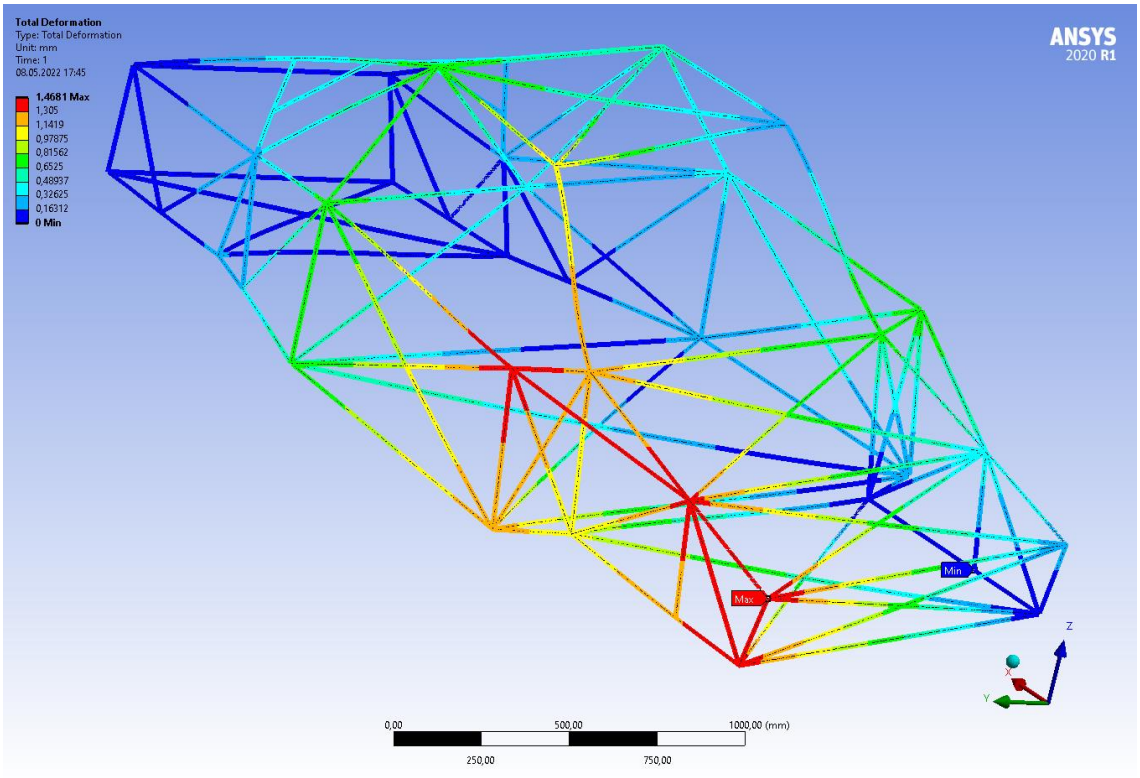

Figure 55 Total deformation, torsional stiffness test. Scale 140x

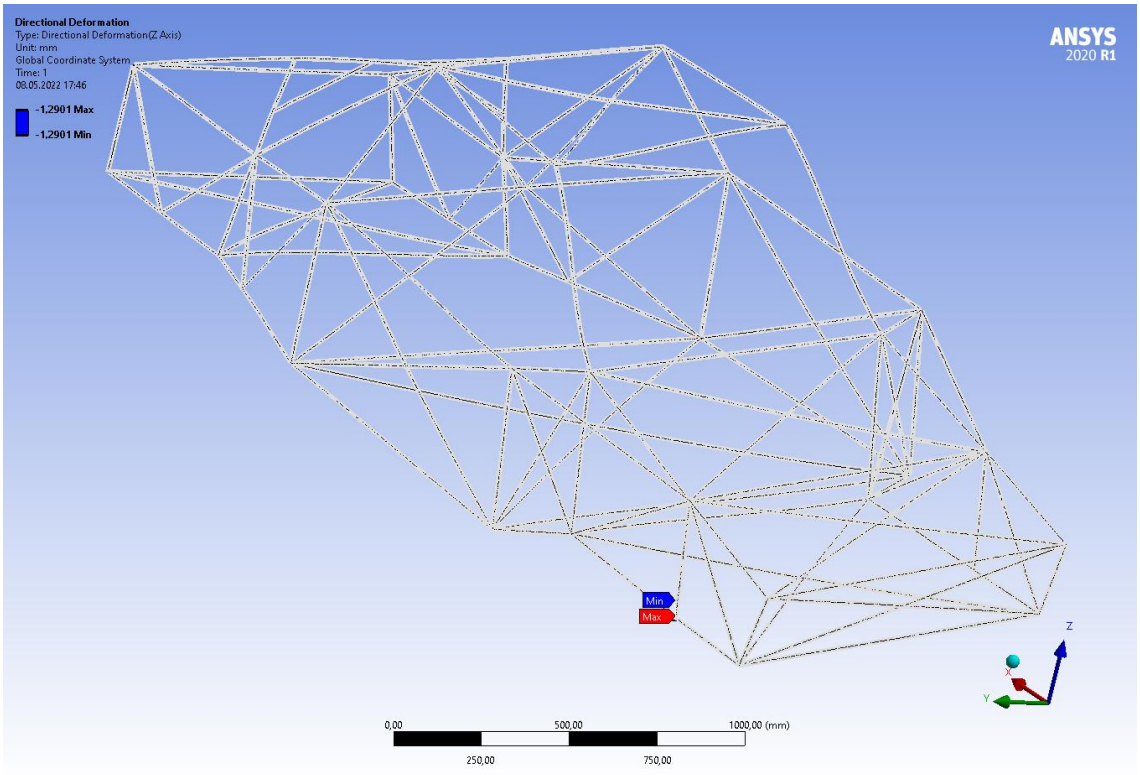

Figure 56 Directional deformation, torsional stiffness test. Scale 140x

6.2. Dynamic load lateral

The result from the dynamic load lateral simulation is expressed in Table 14.

Table 14 Results from lateral dynamic loading

Result	Max	Min
Total Deformation [mm]	0.89261	0
Axial Force [N]	5065	-7701
Total Shear Force [N]	893.87	7.7436e-7
Total Bending Moment [Nmm]	1.605e5	0.037535
Torsional Moment [Nmm]	22076	-24948
Direct Stress [MPa]	22.449	-38.694
Maximum Combined Stress [MPa]	115.84	-38.447
Minimum Combined Stress [MPa]	19.964	-110.21
Maximum Bending Stress [MPa]	106.92	2.2023e-5
Minimum Bending Stress [MPa]	-2.2023e-5	-106.92

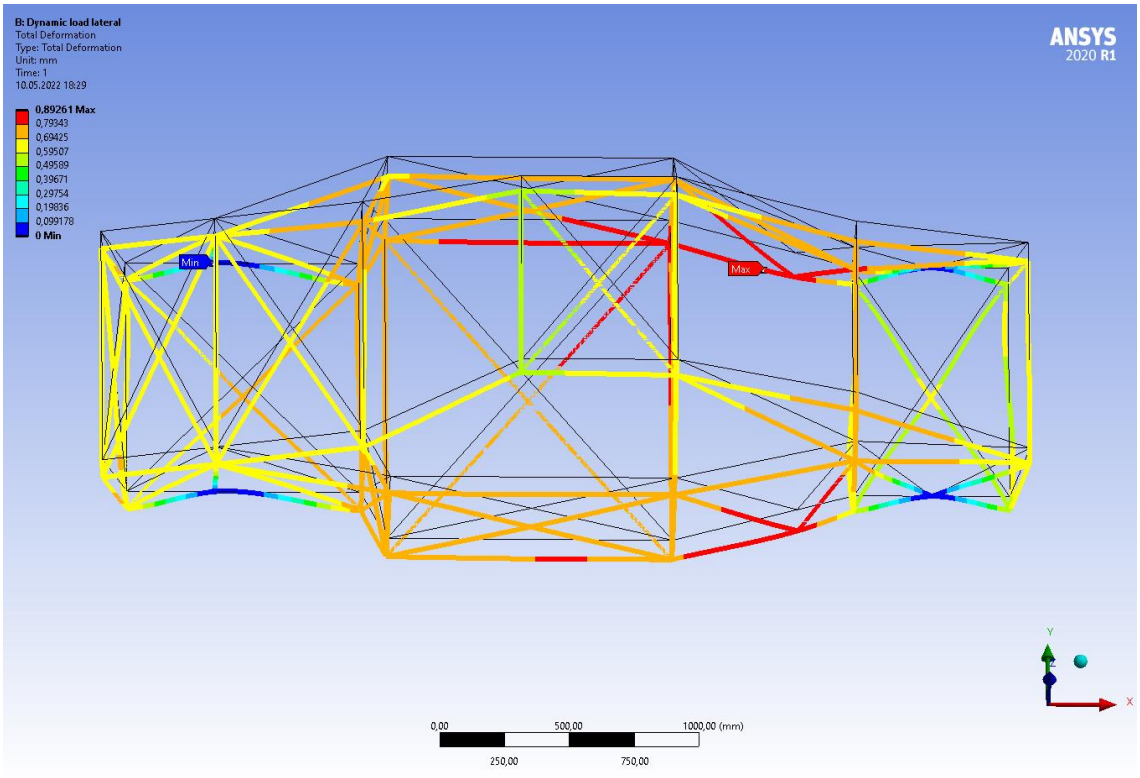

Figure 57 Total deformation at dynamic load lateral. Scale 110x

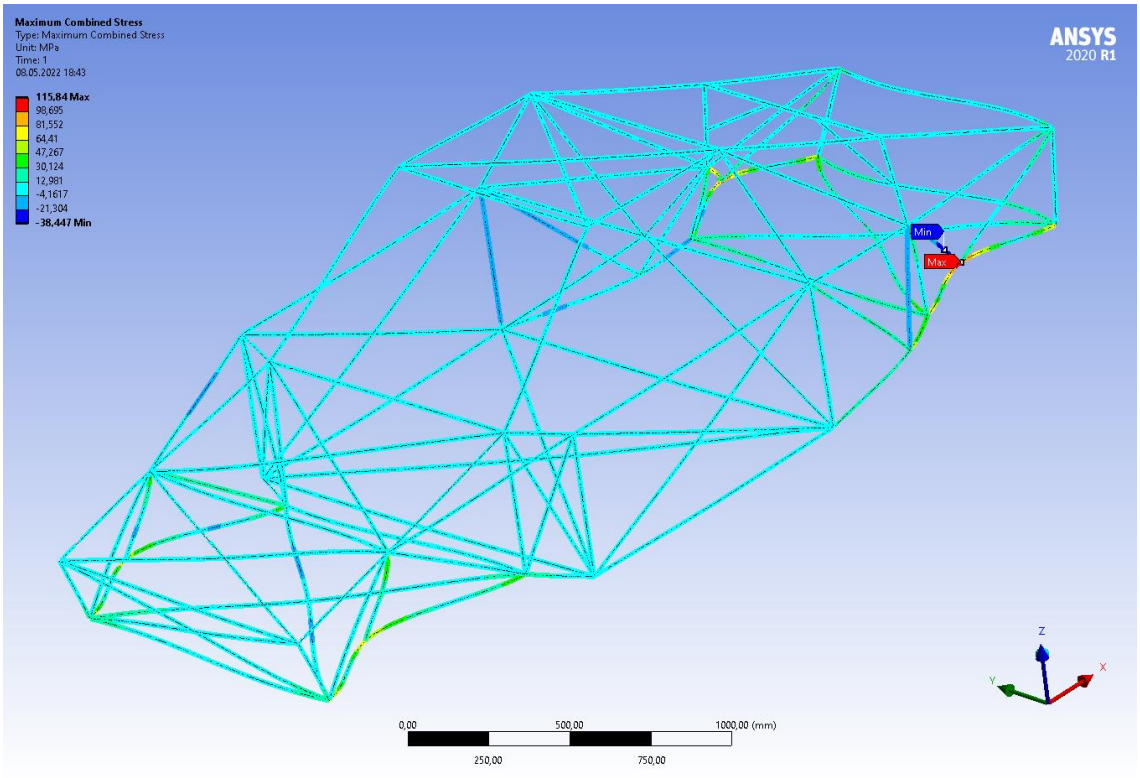

Figure 58 Maximum combined stress at dynamic load lateral. Scale 230x

6.3. Dynamic load vertical

Table 15 Results from vertical dynamic loading

Result	Max	Min
Total Deformation [mm]	0.58368	0
Axial Force [N]	3384.2	-8795.9
Total Shear Force [N]	183.13	7.1446e-8
Total Bending Moment [Nmm]	32926	0.0733377
Torsional Moment [Nmm]	3628.8	-3628.8
Direct Stress [MPa]	17.004	-44.196
Maximum Combined Stress [MPa]	28.406	-43.556
Minimum Combined Stress [MPa]	16.621	-54.524
Maximum Bending Stress [MPa]	22.102	4.9324e-5
Minimum Bending Stress [MPa]	-4.9324e-5	-22.102

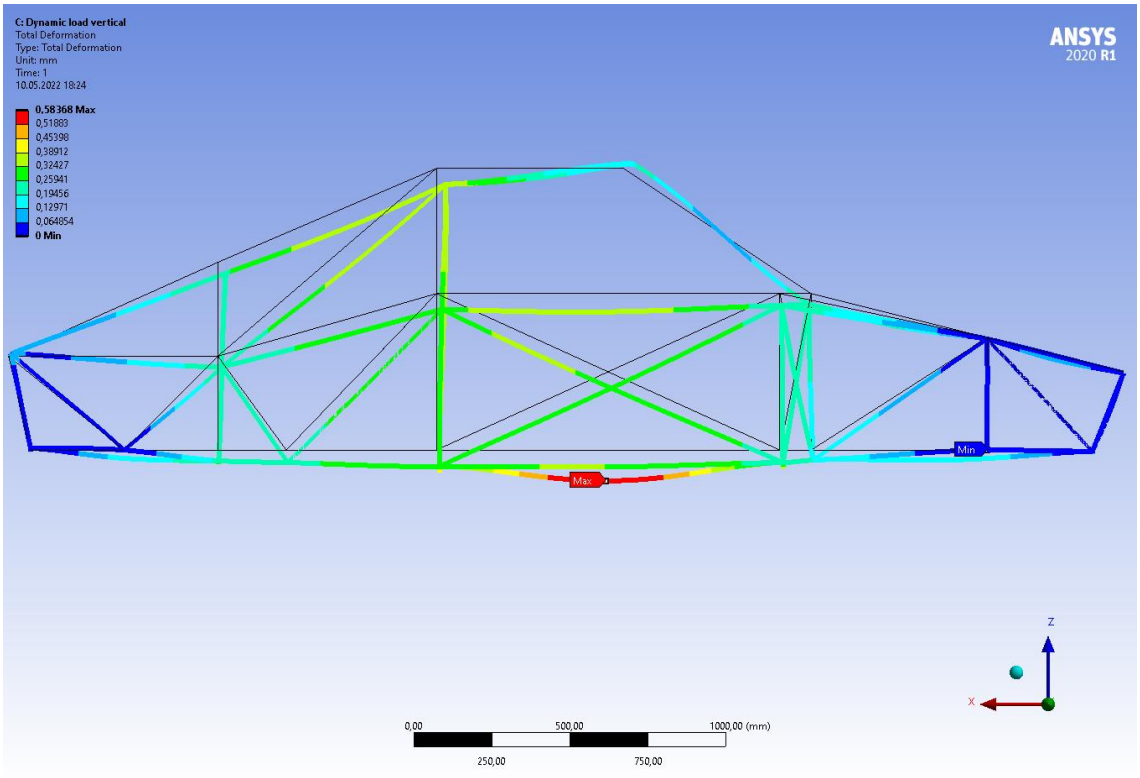

Figure 59 Total deformation at dynamic load vertical. Scale 170x

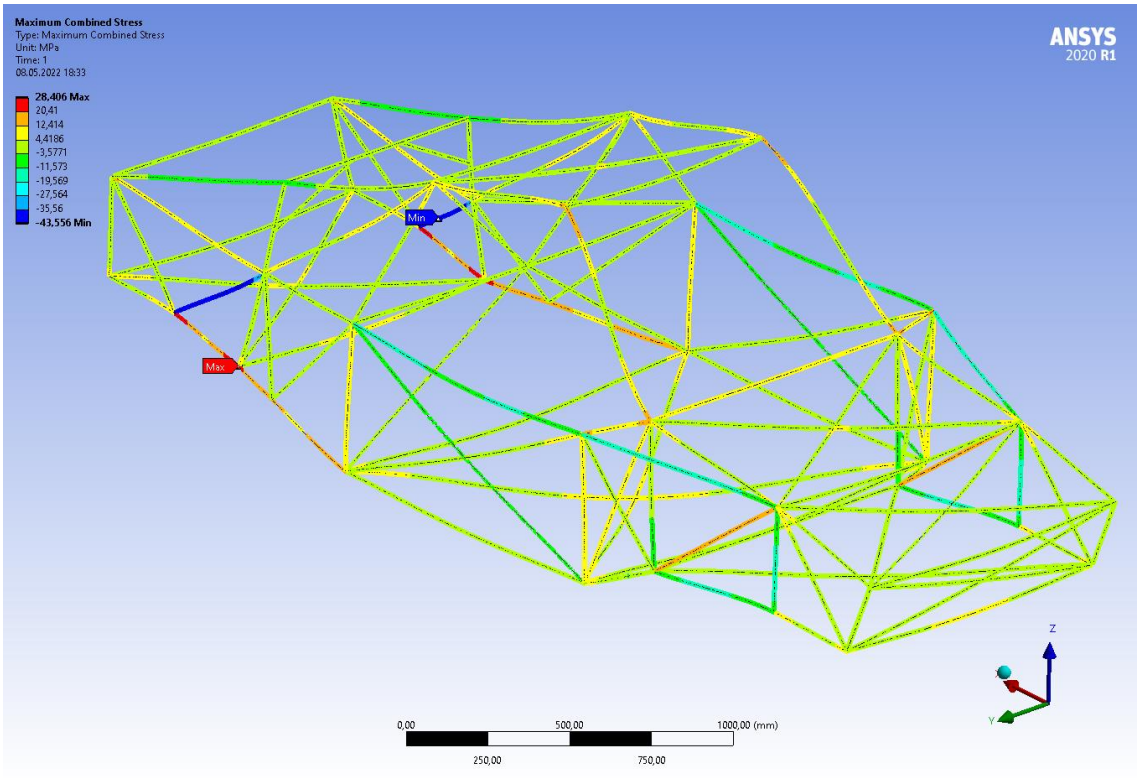

Figure 60 Maximum combined stress at dynamic load vertical. Scale 340x.

6.4. Tensile stress

With the S355 steel with yield strength of 355 MPa and the safety factor 1.5, we can derive the allowable tensile stress from the equation 23:

$$Allowable\ tensile\ stress, \sigma_t = \frac{355\ MPa}{1.5} = 236.67\ MPa$$

From the vertical load results, we get the direct stress, which is the tensile stress, of 17.004 MPa. Using the equation 7 we get the safety factor of:

$$safety\ factor\ vertical\ loading = \frac{355\ MPa}{17.004\ MPa} = 20.88$$

From the lateral load results, we get the direct stress of 22.449 MPa. Using the equation 7 we get the safety factor of:

$$safety\ factor\ vertical\ loading = \frac{355\ MPa}{22.449\ MPa} = 15.81$$

6.5. Compressive stress

Checking column buckling for the most critical member, that being the longest member in the frame. This value is 1400 mm, with a material factor of 1.5 and end-conditions L = 0.5L we get the maximum force before buckling from equation 25:

$$Allowable\ euler\ buckling\ load\ F_E = \frac{\pi^2 * 210 * \frac{\pi}{4}(16.85^4 - 14.85^4)}{1.5 * (0.5 * 1400)} = 70\ 831.2\ N$$

The maximum value of 8795.9 N of tensile compressive load was measured during vertical dynamic testing.

6.6. Bending stress

From equation 27, we get the bending stress during dynamic lateral test:

$$Bending\ stress, \sigma_b = \frac{160\ 500\ Nmm}{1491\ mm^3} = 107.65\ MPa$$

From the bending stress, we can calculate the safety factor:

$$safety\ factor\ bending = \frac{355\ MPa}{107.65\ MPa} = 3.30$$

During the dynamic vertical simulation, we get the following results:

$$Bending\ stress, \sigma_b = \frac{32\ 926\ Nmm}{1491\ mm^3} = 22.08\ MPa$$

Using the bending from the vertical load, we get the safety factor:

$$safety\ factor\ bending = \frac{355\ MPa}{22.08\ MPa} = 16.08$$

6.7. Crash test

Figure 61 display the deformation of the frame during the crash. The maximum total deformation is 43.453 mm. The time of the simulation is 0.0013722 s with maximum number of cycles set to 100 000. The maximum equivalent (Von-Mises) stress is 682 MPa, as displayed in Figure 62.

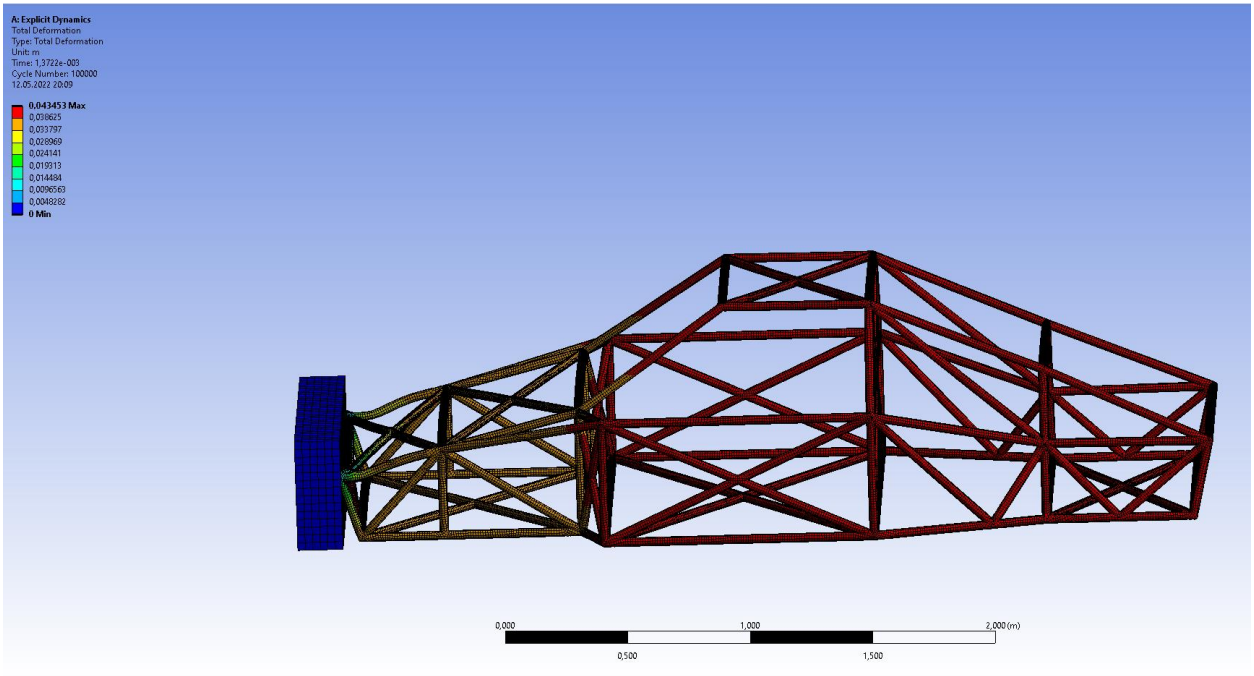

Figure 61 Total deformation crash test

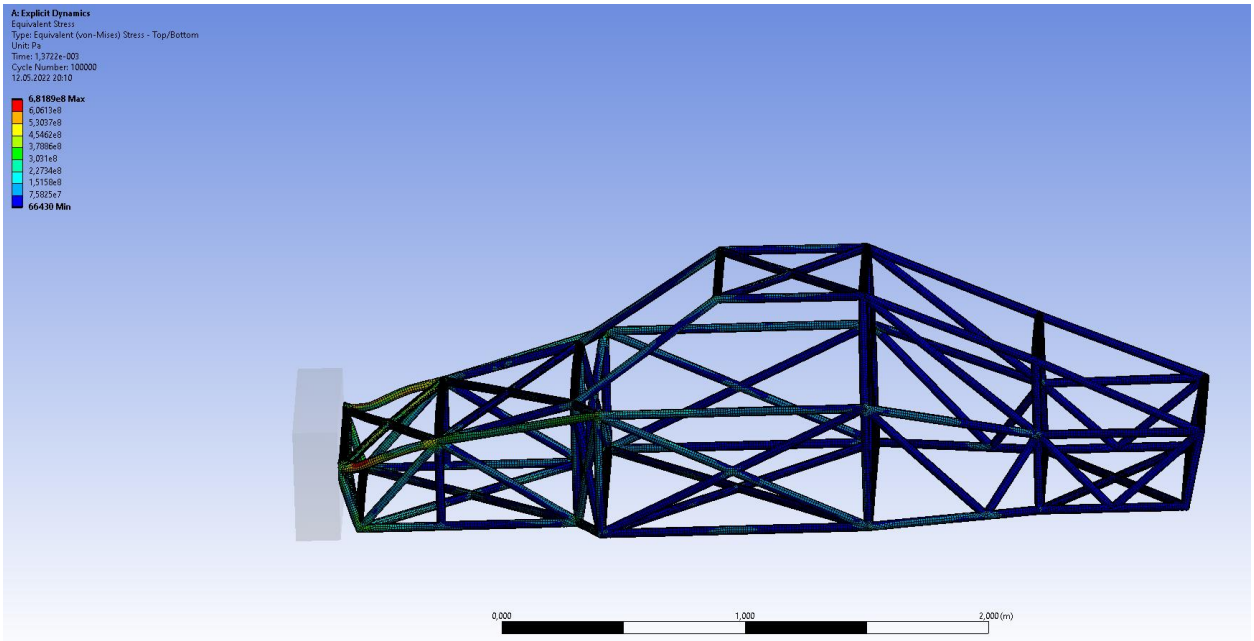

Figure 62 Von-Mises stress crash test

7. Discussion

The goal of this thesis was to design and simulate the frame of a racing car. In this chapter, we will discuss the results gathered from all simulations. We will evaluate the results against design criteria and allowable stresses. Lastly, we will mention areas of improvement, potential errors and point out how to further improve the frame.

7.1. Results

The torsional stiffness test was the first focus when simulating the frame in Ansys. Several possible test methods were available, but option 1 was chosen, as displayed in Figure 16 . The reason for using option 1 was that we didn't have any suspension setup. This gave us the best result when there without suspension added. From the analyses in Ansys, we got the torsional stiffness of 13 531.8 Nm/degree. The alternative methods for the torsional stiffness analyses would result in different values.

To get relevant loading for the dynamic loads, point masses were added for an engine with transmission and driver. In real life, these loads would differ and give different results. But for the meaning of this thesis, these loads and their center of gravity were only approximated.

A dynamic load in the vertical direction was applied to simulate driving over a bump. The load was approximated to be 3 g. From the material factor, we got allowable tensile stress of 236.67 MPa. The result from the vertical dynamic load gives maximum tensile stress of 17.004 MPa. This results in a safety factor of 20.88, which is significant compared to the material factor of 1.5.

The cornering was simulated with a lateral dynamic load of approximately 1.8 g. This resulted in the maximum tensile stress of 22.449 MPa. The stresses for the lateral dynamic load are well under the allowable stress and give a safety factor of 15.81. These results indicate that the frame will handle the applied load with a significant safety margin.

The maximum compressive axial force happens during the vertical dynamic loading, with a value of 8795.9 N. The allowable Euler buckling is 70 831.2 N, which indicates that the frame is safe for bending under compressive forces.

The maximum combined stress is 115.84 MPa, the linear combination of direct stress and maximum bending stress. This happens in the dynamic load lateral and is under the allowable stress of 236.67 MPa.

7.2. Crash test simulation

The car crash simulation was time consuming and problematic. Computational times were ranging from 7 to 200 hours. From Figure 61 we get a maximum deflection 43.5 mm, and we get the equivalent stress of 682 MPa. Because of the maximum cycle was set to 100 000, the simulation stopped before reaching a zero velocity. This resulted in the simulation stopping while the frame was still in motion. Because the crash simulation does not reach zero velocity, there is no real way of knowing the outcome of the crash. Further research and simulation are needed to determine the full effect of the crash, and to calculate the energy absorbed.

7.3. Potential problem areas

The frame consists of 107 members, where all of them are cut differently. The cutting would have had to be done using a computer-controlled laser cutter. Assembling all members in the correct order could impose some challenges.

Figure 63 display a connection at the front left side. This connection of tubes would be complex to weld. Small clearances and hard to reach areas will result in intermittent welding, and loss of weld strength. The complexity could transform to improper welds resulting in failure during loading. A resolution for further work could be changing the design of the joints, or there could be a "connecting part" for the tubes to be welded to.

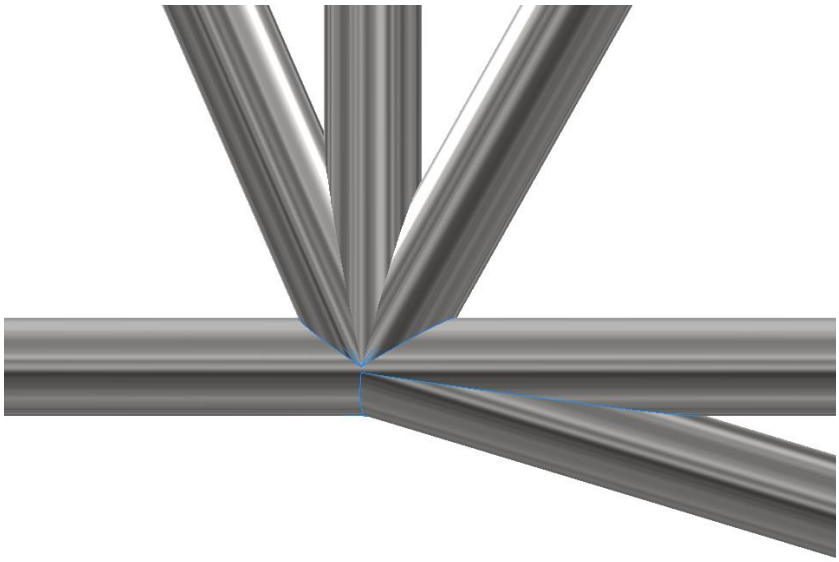

Figure 63 Complex joint

8. Conclusion

This thesis aimed to design and simulate a racing car frame. The first iteration was primarily based on aesthetic qualities and general design principles. The design of the frame was made in Autodesk Inventor using a 3-D line model, later beams were generated by frame-generator using the desired cross-section. The frame was imported to Ansys for simulation. The beams were extruded from the solid frame for the static structural analysis. A shell model of 2 mm thickness was used for the Explicit Dynamics simulation.

The torsional stiffness test and dynamic loading simulation indicate that the frame is sufficiently stiff and strong. One can argue that a torsional stiffness value of 13 531.8 Nm/degree and low values in bending, compressive and tensile stress indicate a successful frame design. However, it is worth mentioning that all loads were approximated. Additional loads from suspension, bodywork, and interior will affect the results. This indicates that triangulation increases strength and stiffness immensely and that no member is in danger of failing.

The benefits of designing a racing car frame using CAD software become evident when the complexity and size of the frame increase. This design would be infinitely more time-consuming and challenging if all calculations and measurements had to be done manually. Further, destructive testing, such as crash testing, can be undesirable and expensive to do physically. The benefit of explicit dynamics simulations can be of great value.

In further work, it would be interesting to see how suspension mounting points would affect the strength of certain frame members. It would also be interesting to observe the change in torsional stiffness and how springs and dampeners would influence simulation results. We would also like to invest time in modeling and simulation of the strength of welded connections. Further work could be done to minimize weight while maintaining an acceptable amount of stiffness and strength.

9. References

[1] Britannica. "Chassis." https://www.britannica.com/technology/automobile/Chassis (accessed.

[2] H. Adams, *Chassis Engineering*. New York: Berkley Publishing Group, 1992.

[3] D. C. Barton and J. D. Fieldhouse, *Automotive Chassis Engineering*. Cham: Cham: Springer International Publishing AG, 2018.

[4] D. Seward, *RACE CAR DESIGN*, 1. ed. Lancaster University: Macmillan Education UK, 2014.

[5] W. D. Callister and D. G. Rethwish, *Materials Science and Engineering*, 10th ed. Asia: John Wiley Sons Inc, 2020.

[6] R. S. Cars. "Le Mans 24 Hours." https://www.racingsportscars.com/results/Le_Mans-1970-06-14.html (accessed 25.03.2022.

[7] W. F. Miliken and D. L. Miliken, *Race Car Vehicle Dynamics*, 1. ed. Warrendale Pa.: SEA International, 1997.

[8] A. Benson. "Carlos Sainz suffers heavy crash in Russian Grand Prix practice." BBC. https://www.bbc.com/sport/formula1/34495586 (accessed 03.03, 2022).

[9] M. F. Ashby, *Materials Selection in Mechanical Design*, 3. ed. Oxford: Butterworth-Heinemann Ltd, 2005.

[10] H. G. Lemu, Ed. *Kompendium i fag MSK210 Maskinkonstruksjon*. 2020.

[11] J. Atteberry. "How Welding Works." https://science.howstuffworks.com/welding2.htm (accessed 25.01, 2022).

[12] B. Wiley. "Stitch Welding vs. Seam Welding For Your Metal Fabrication Product." https://www.wileymetal.com/stitch-welding-vs-seam-welding-for-your-metal-fabrication-product/ (accessed 22.03, 2022).

[13] O. Nguyen. "What Is TIG Welding?" Tulsa Wlding School. https://www.tws.edu/blog/welding/what-is-tig-welding/ (accessed 24.03, 2022).

[14] J. Grill. "TIG Welding Filler Rods: Selection Size With Chart." https://weldguru.com/tig-filler-rods/ (accessed 28.03, 2022).

[15] N. S. Trahair, M. A. Bradford, D. A. Nethercot, and L. Gardner, *The Behaviour And Design of Steel Structures to EC3*, 4. ed. Oxfordshire: Taylor & Francis, 2008.

[16] *Sveiseteknikk — Dekkede elektroder for manuell buesveising av bløtt lavlegert stål — Symbolkode for identifikasjon*, NS 5540:1977, 1977.

[17] *Prosjektering av stålkonstruksjoner. Beregnings- og konstruksjonsregler*, NS 3472, N. Standardiseringsforbund, 2001.

[18] M. Skovajsa and F. Sedlaeck, "Analytic Determination and Numerical Simulation of Torsional Stiffness of a Racing Car Frame," presented at the Proceedings of the 28th DAAAM International Symposium, Vienna, Austria, 2017, Online.

[19] SIMSCALE. "What Is FEA | Finite Element Analysis?" https://www.simscale.com/docs/simwiki/fea-finite-element-analysis/what-is-fea-finite-element-analysis/ (accessed.

[20] D. G. Pavlou, *Essentials of the Finite Element Method*. London, England: Academic Press, 2015.

[21] H. Radhakrishnan. "How to Mesh and Simulate Welds with Ansys Mechanical." Ansys https://www.ansys.com/blog/how-to-simulate-welds (accessed 06.04, 2022).
[22] ANSYS. "Beam Tool." https://ansyshelp.ansys.com/account/secured?returnurl=/Views/Secured/corp/v201/en/wb_sim/ds_Beam_Tool.html (accessed 13.05, 2022).
[23] E. Tandberg and T. h. Johansen. "aerodynamikk." Store Norske Leksikon. https://snl.no/aerodynamikk (accessed 16.03, 2022).
[24] N. A. A. S. Administration. "The Drag Equation." N.A.S.A. https://www.grc.nasa.gov/www/k-12/airplane/drageq.html (accessed 17.03, 2022).
[25] "Koenigsegg Jesko." Koenigsegg. https://www.koenigsegg.com/car/jesko/ (accessed 06.04, 2022).
[26] F. P. Beer, E. J. Russell Johnston, J. T. DeWolf, and D. F. Mazurek, *Mechanics of Materials*, 6. ed. New York: McGraw-Hill, 2012.
[27] Cambridge Dictionary. "assumption." https://dictionary.cambridge.org/dictionary/english/assumption (accessed 22.03, 2022).
[28] B. Valeski. "Average Transmission Weight (With 7 Examples)." https://www.survivaltechshop.com/transmission-weight/ (accessed 14.02, 2022).
[29] *NS-EN 10025-2:2004*, Standard Norge, 2004.
[30] A. Rohatgi. "WebPlotDigitizer." https://automeris.io/WebPlotDigitizer/ (accessed 26.04.2022.
[31] C. Ezio, D. Forni, R. Gieleta, and L. Kruszka, "Tensile and compressive behaviour of S355mild steel in a wide range of strain rates," *The European Journal Special Topics*, vol. 227, pp. 29-43, 10.09.2018, doi: 10.1140/epjst/e2018-00113-4.

10. Appendices

Appendix A

Torsional stiffness test

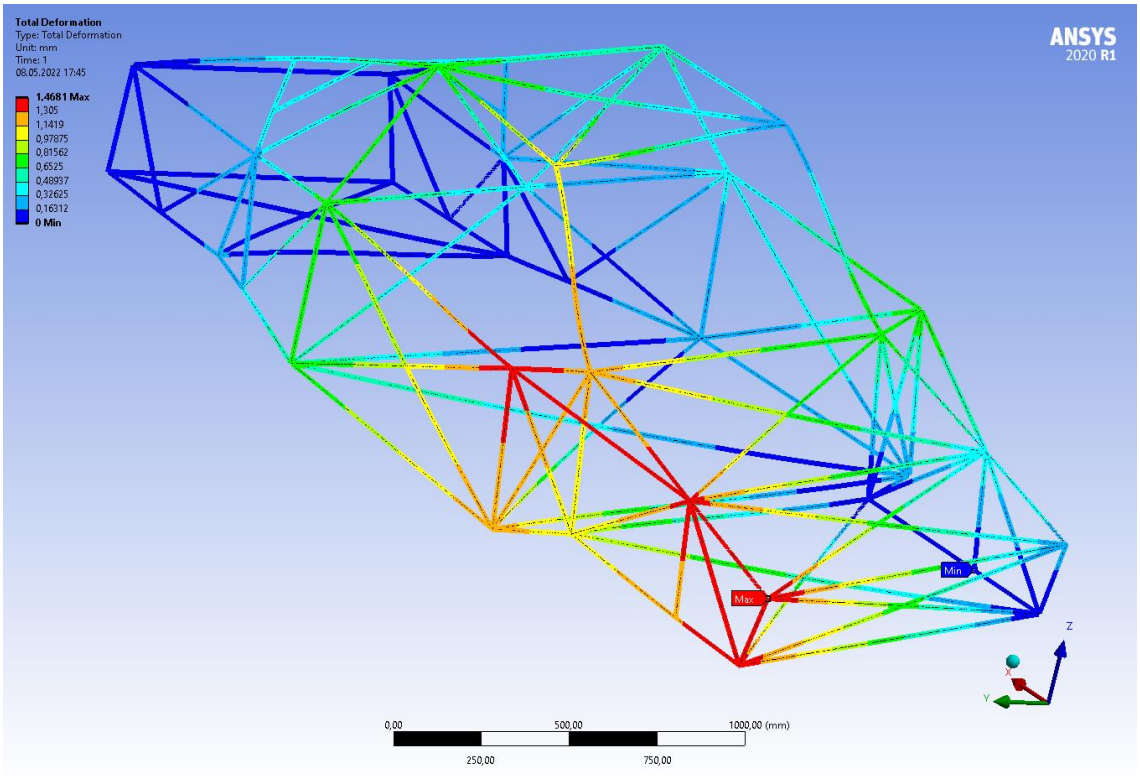

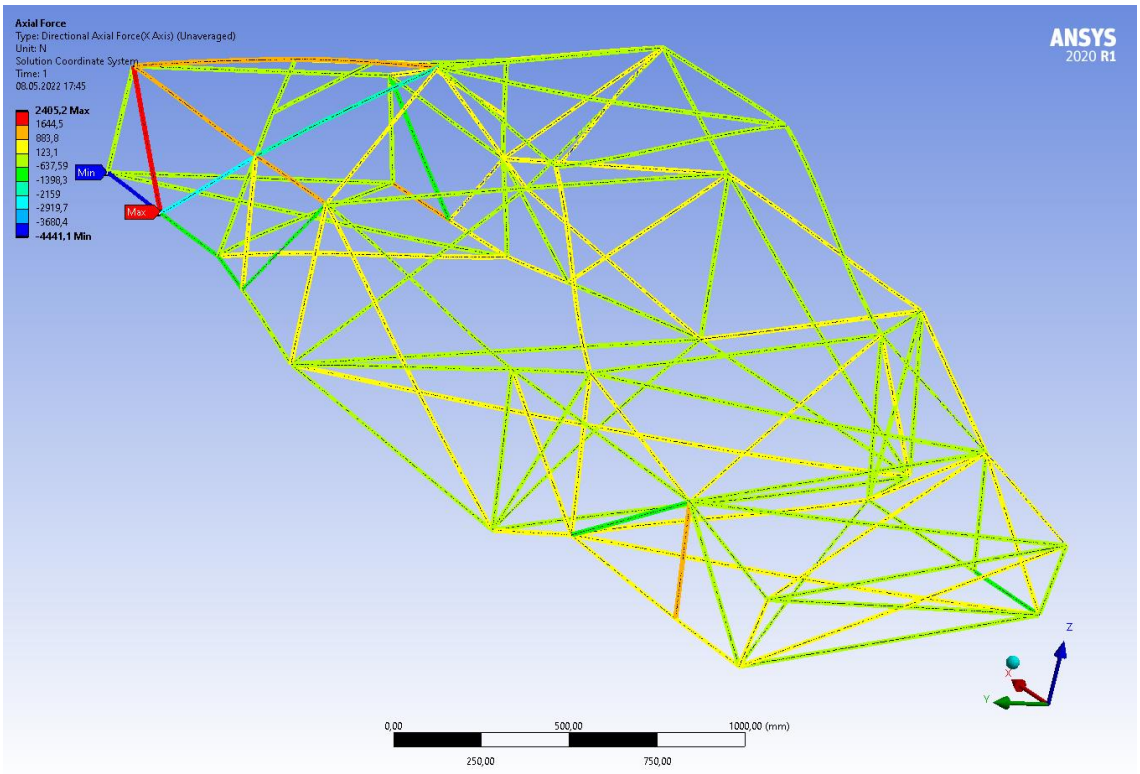
Axial Force
Type: Directional Axial Force(X Axis) (Unaveraged)
Unit: N
Solution Coordinate System
Time: 1
08.05.2022 17:45
2405,2 Max
1644,5
883,8
123,1
-637,59
-1398,3
-2159
-2919,7
-3680,4
-4441,1 Min
Min
Max
ANSYS
2020 R1
Z
X
Y
0,00
500,00
1000,00 (mm)
250,00
750,00

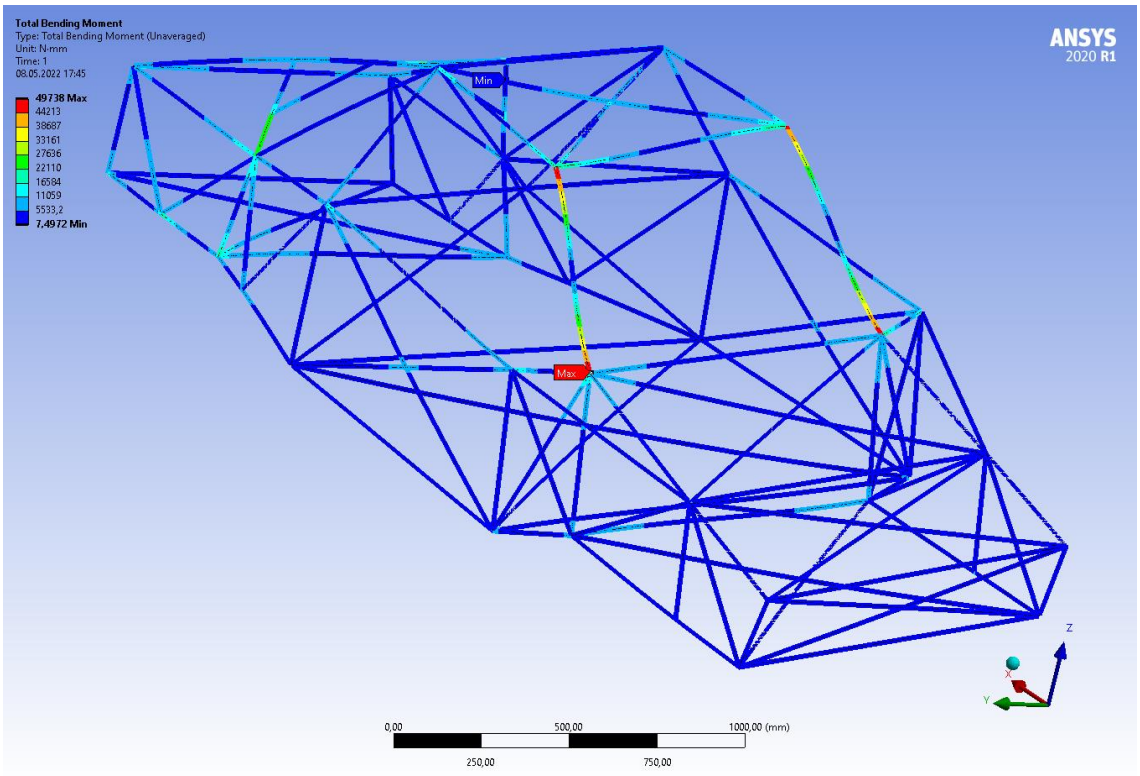
Total Bending Moment
Type: Total Bending Moment (Unaveraged)
Unit: N·mm
Time: 1
08.05.2022 17:45
49738 Max
44213
38687
33161
27636
22110
16584
11059
5533,2
7,4972 Min
Min
Max
ANSYS
2020 R1
Z
X
Y
0,00
500,00
1000,00 (mm)
250,00
750,00

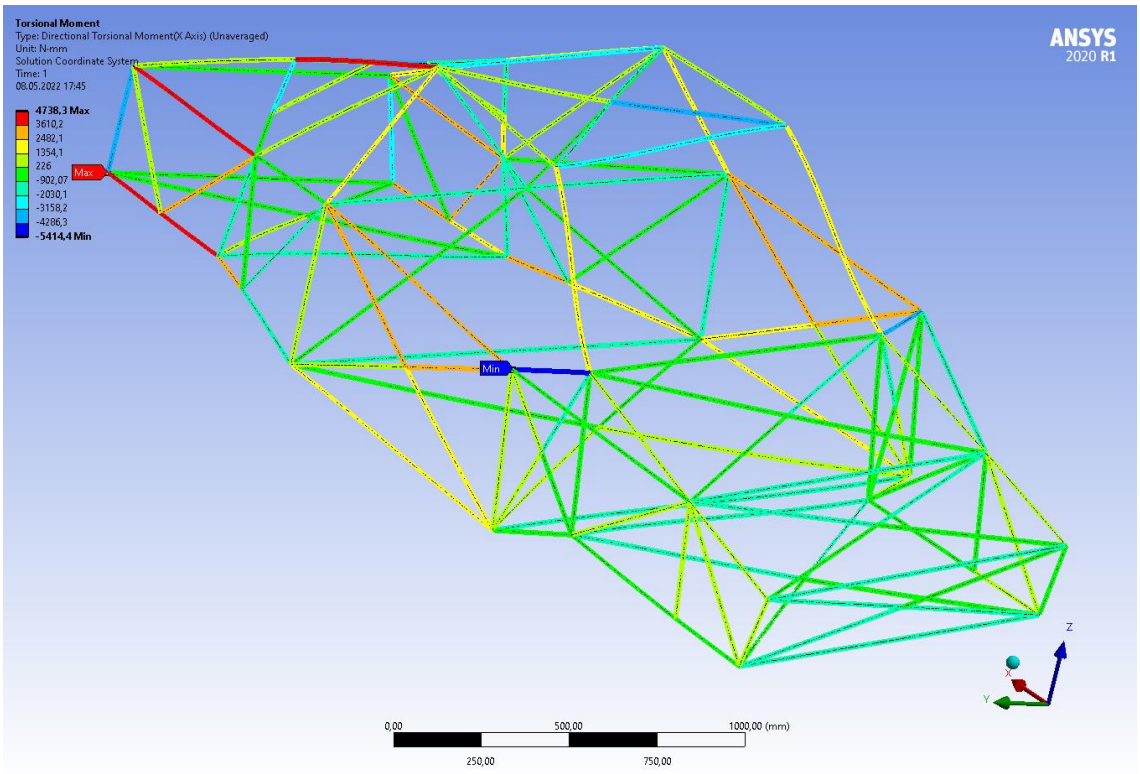
Torsional Moment
Type: Directional Torsional Moment(X Axis) (Unaveraged)
Unit: N·mm
Solution Coordinate System
Time: 1
08.05.2022 17:45
4738,3 Max
3610,2
2482,1
1354,1
226
-902,07
-2030,1
-3158,2
-4286,3
-5414,4 Min
Max
Min
ANSYS
2020 R1
0,00
500,00
1000,00 (mm)
250,00
750,00
Z
X
Y

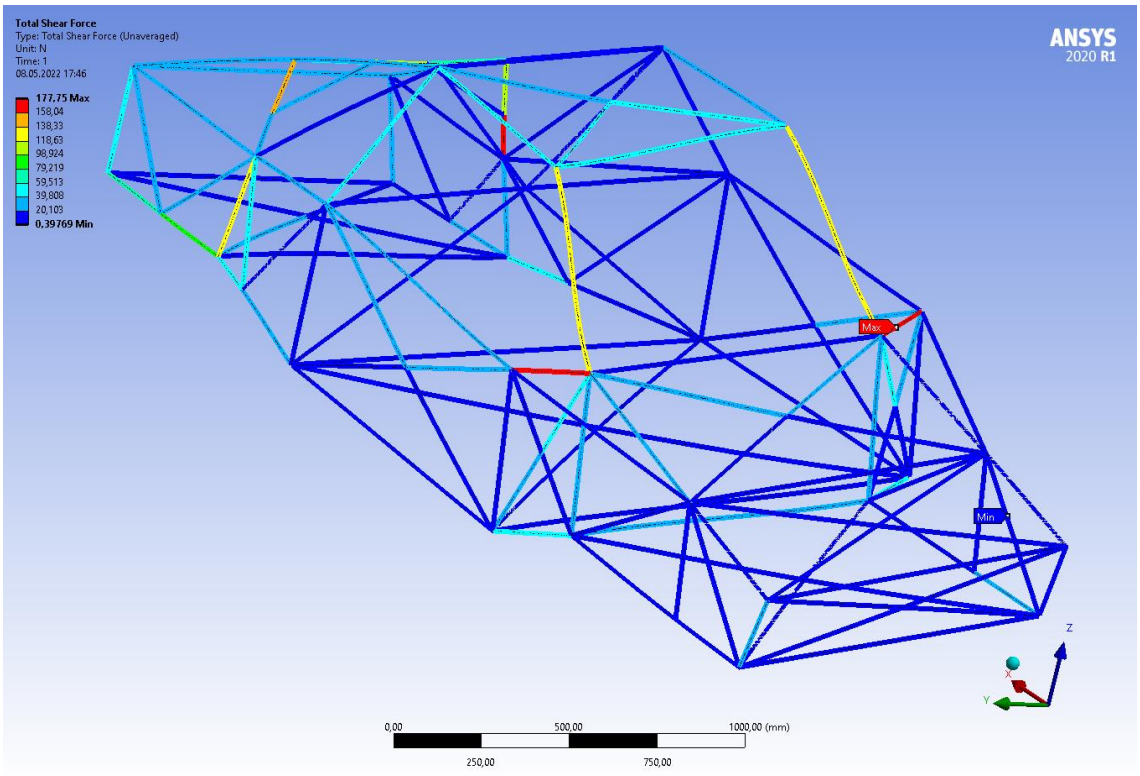
Total Shear Force
Type: Total Shear Force (Unaveraged)
Unit: N
Time: 1
08.05.2022 17:46
177,75 Max
158,04
138,33
118,63
98,924
79,219
59,513
39,808
20,103
0,39769 Min
Max
Min
ANSYS
2020 R1
0,00
500,00
1000,00 (mm)
250,00
750,00
Z
X
Y

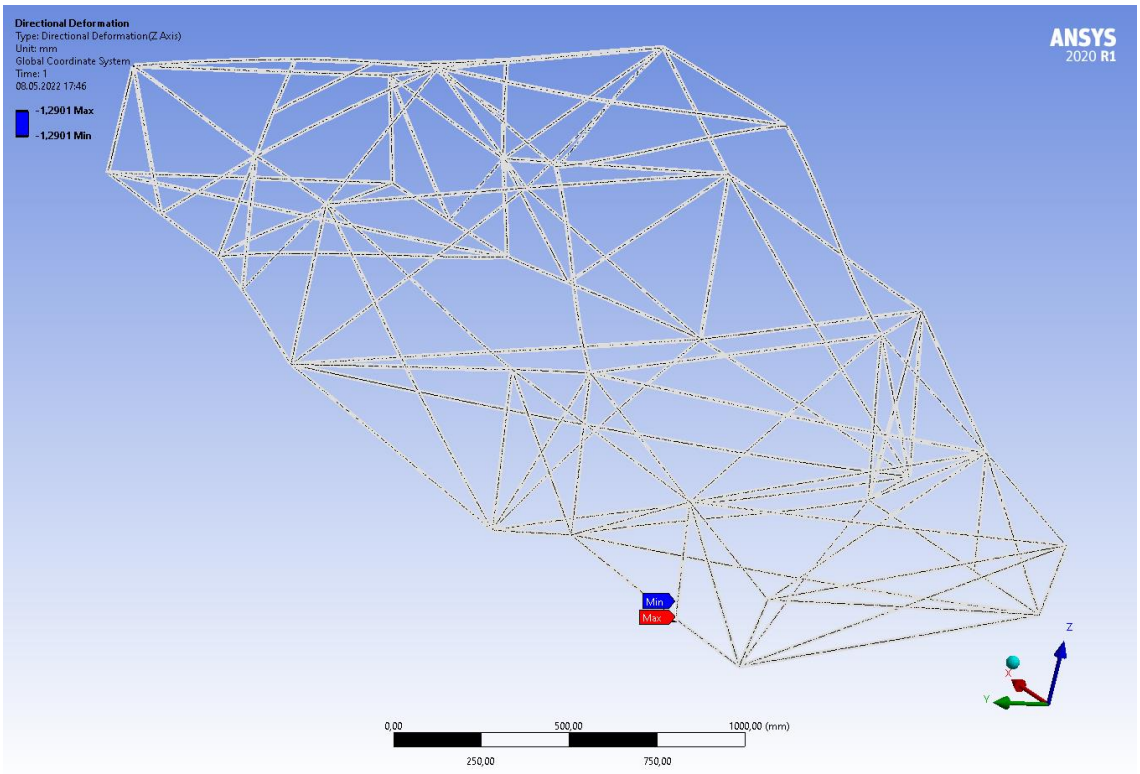
Directional Deformation
Type: Directional Deformation(Z Axis)
Unit: mm
Global Coordinate System
Time: 1
08.05.2022 17:46
-1,2901 Max
-1,2901 Min
ANSYS
2020 R1
Min
Max
Z
X
Y
0,00
500,00
1000,00 (mm)
250,00
750,00

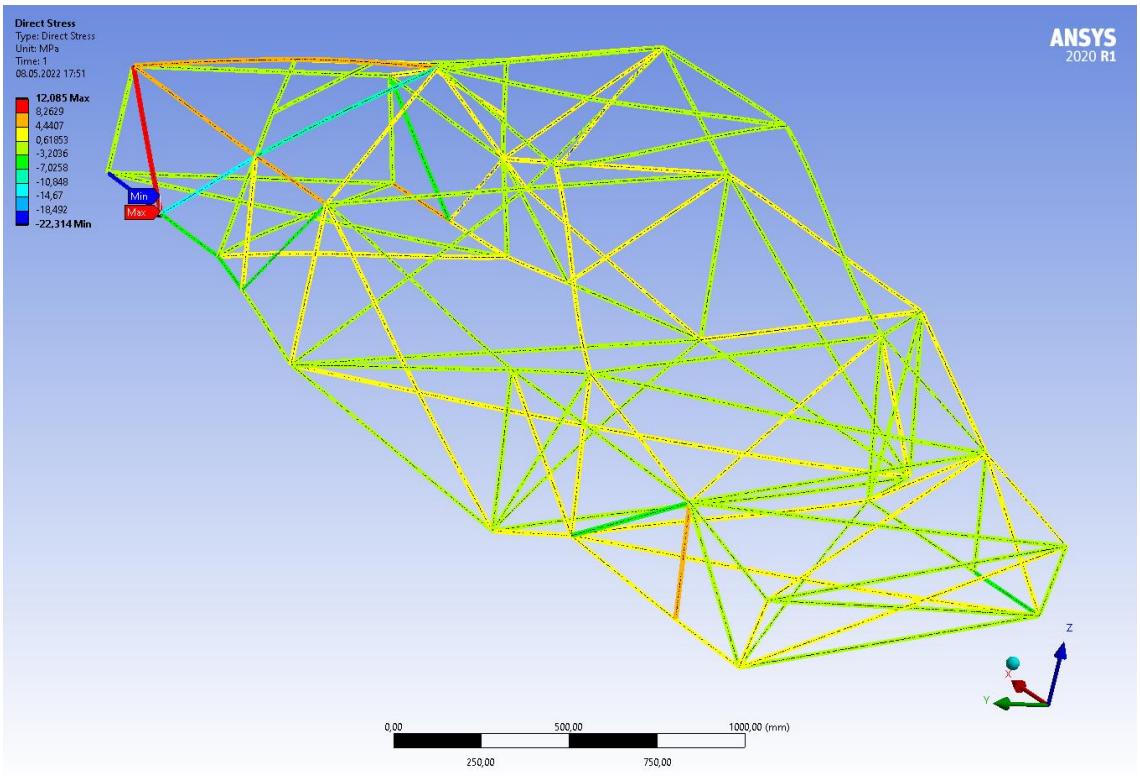
Direct Stress
Type: Direct Stress
Unit: MPa
Time: 1
08.05.2022 17:51
12,085 Max
8,2629
4,4407
0,61853
-3,2036
-7,0258
-10,848
-14,67
-18,492
-22,314 Min
ANSYS
2020 R1
Min
Max
Z
X
Y
0,00
500,00
1000,00 (mm)
250,00
750,00

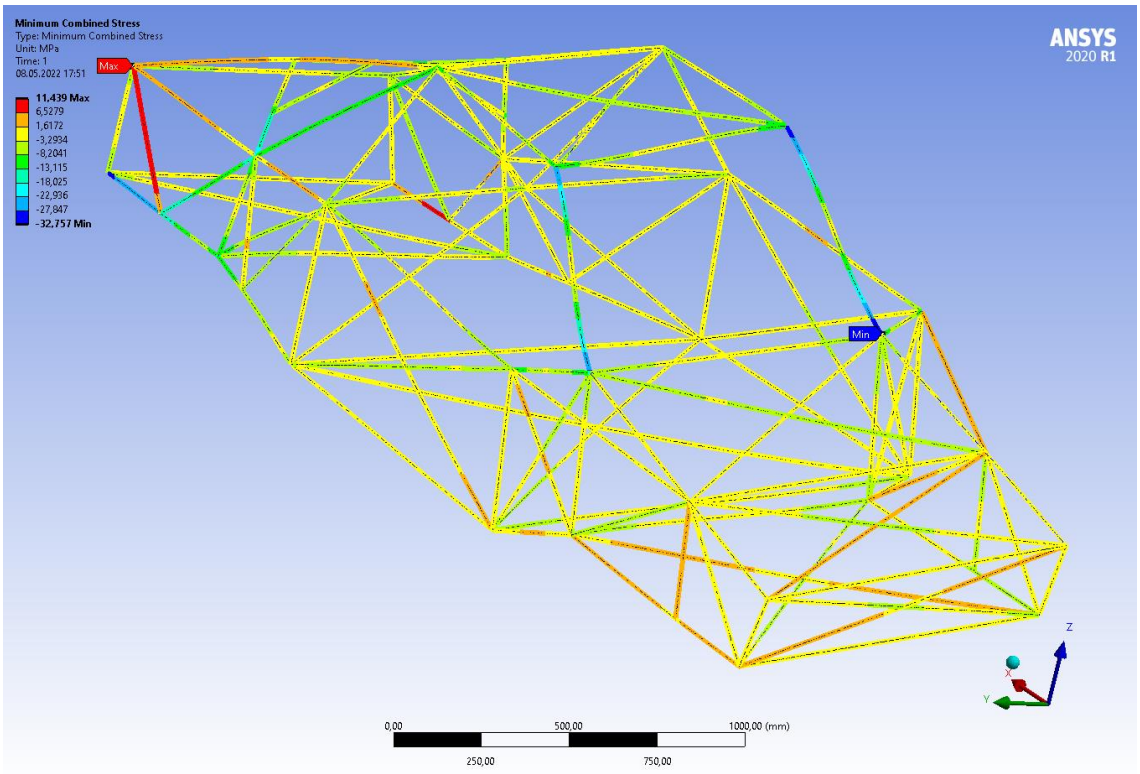
Minimum Combined Stress
Type: Minimum Combined Stress
Unit: MPa
Time: 1
08.05.2022 17:51
11,439 Max
6,5279
1,6172
-3,2934
-8,2041
-13,115
-18,025
-22,936
-27,847
-32,757 Min
Max
Min
ANSYS
2020 R1
0,00
500,00
1000,00 (mm)
250,00
750,00
Z
Y
X

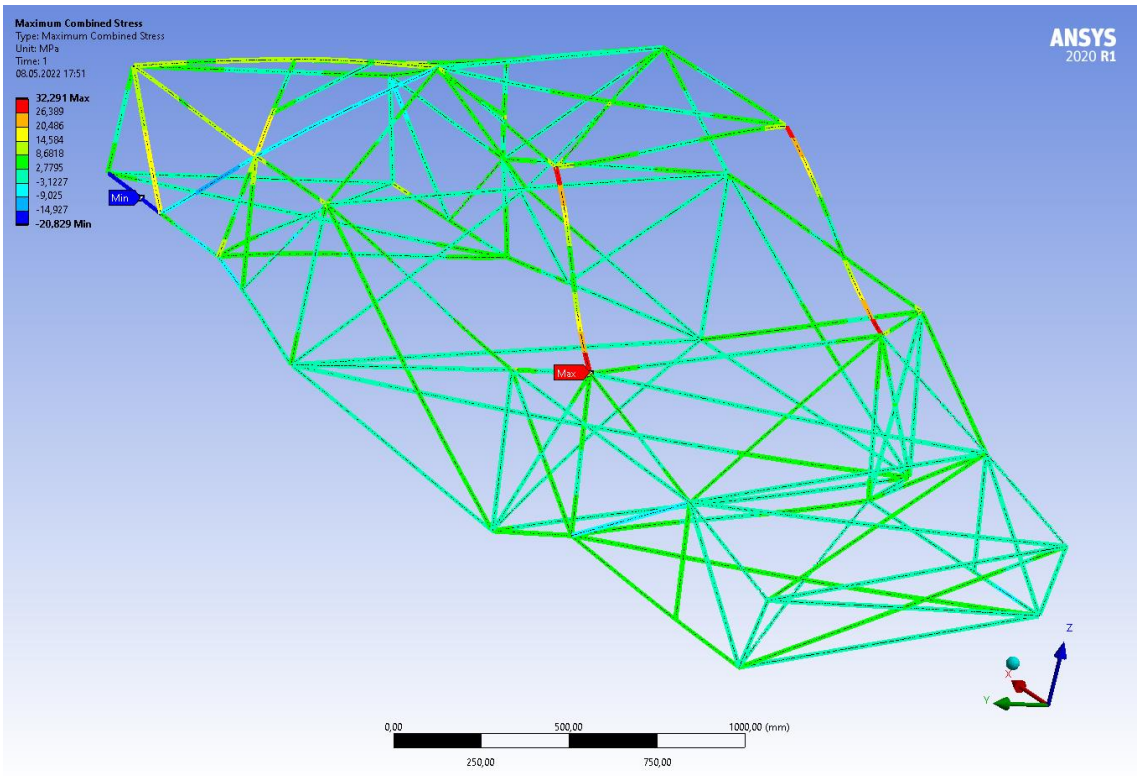
Maximum Combined Stress
Type: Maximum Combined Stress
Unit: MPa
Time: 1
08.05.2022 17:51
32,291 Max
26,389
20,486
14,584
8,6818
2,7795
-3,1227
-9,025
-14,927
-20,829 Min
Min
Max
ANSYS
2020 R1
0,00
500,00
1000,00 (mm)
250,00
750,00
Z
Y
X

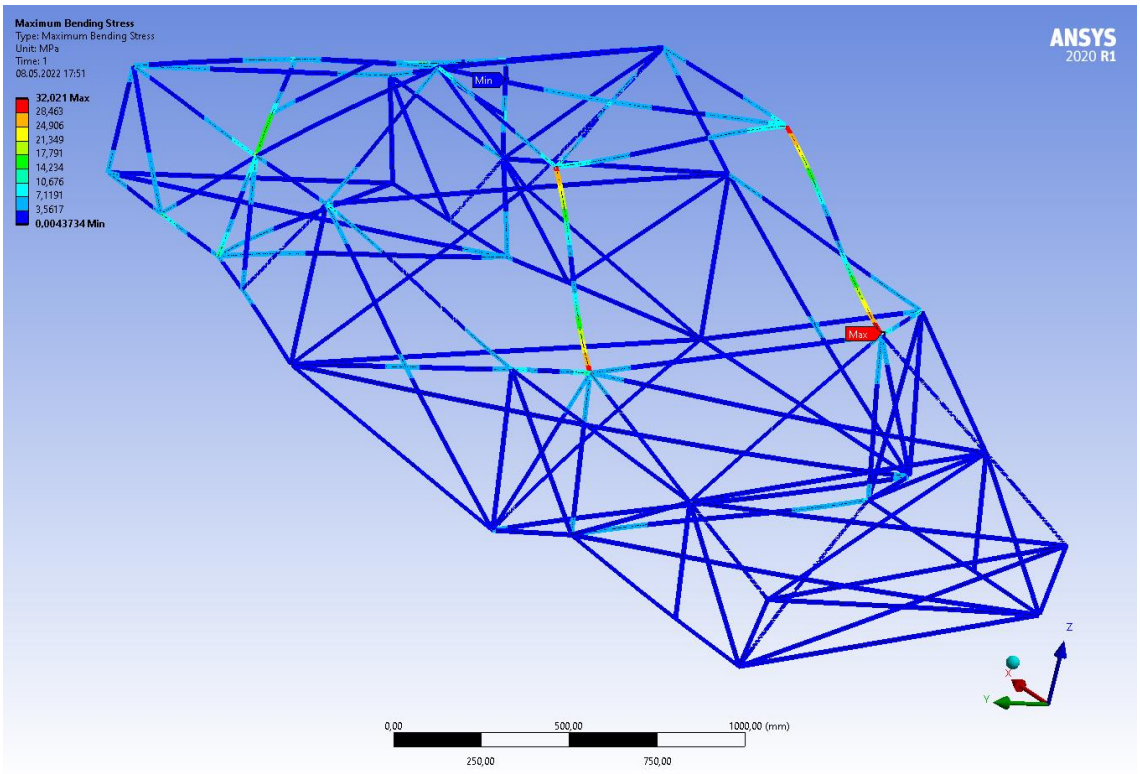
Maximum Bending Stress
Type: Maximum Bending Stress
Unit: MPa
Time: 1
08.05.2022 17:51
32,021 Max
28,463
24,906
21,349
17,791
14,234
10,676
7,1191
3,5617
0,0043734 Min
ANSYS
2020 R1
Min
Max
Z
X
Y
0,00
500,00
1000,00 (mm)
250,00
750,00

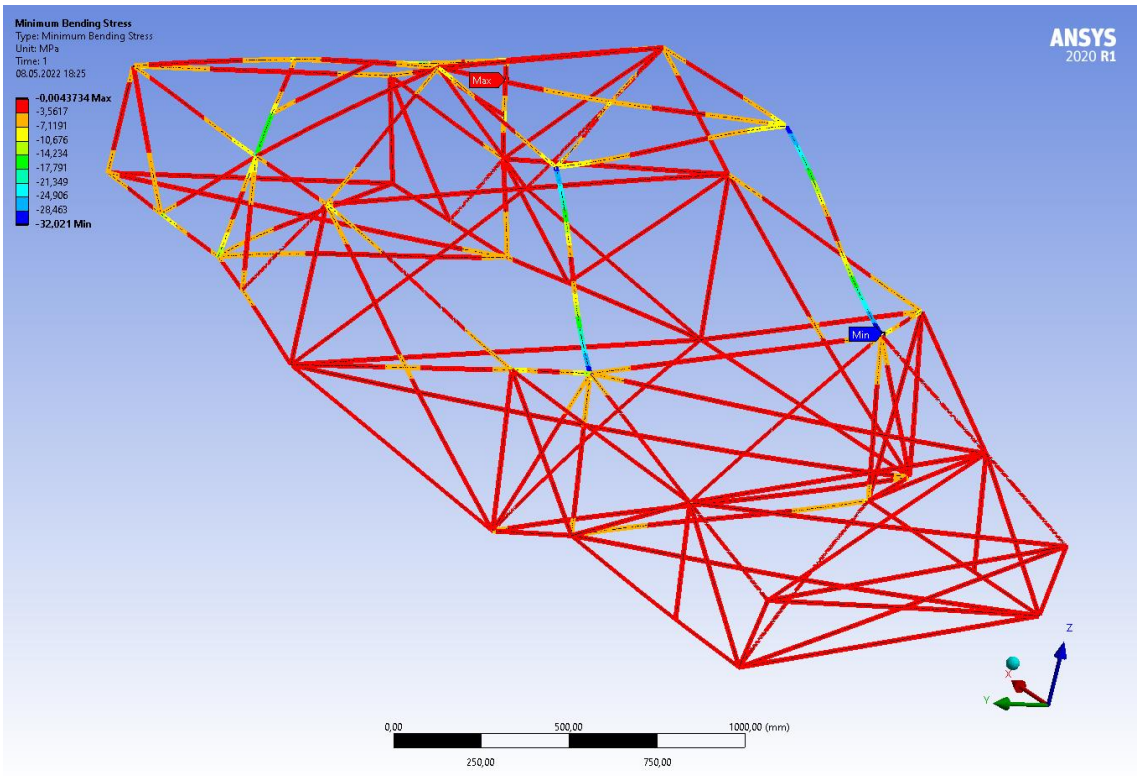
Minimum Bending Stress
Type: Minimum Bending Stress
Unit: MPa
Time: 1
08.05.2022 18:25
-0,0043734 Max
-3,5617
-7,1191
-10,676
-14,234
-17,791
-21,349
-24,906
-28,463
-32,021 Min
ANSYS
2020 R1
Max
Min
Z
X
Y
0,00
500,00
1000,00 (mm)
250,00
750,00

Appendix B

Dynamic load vertical

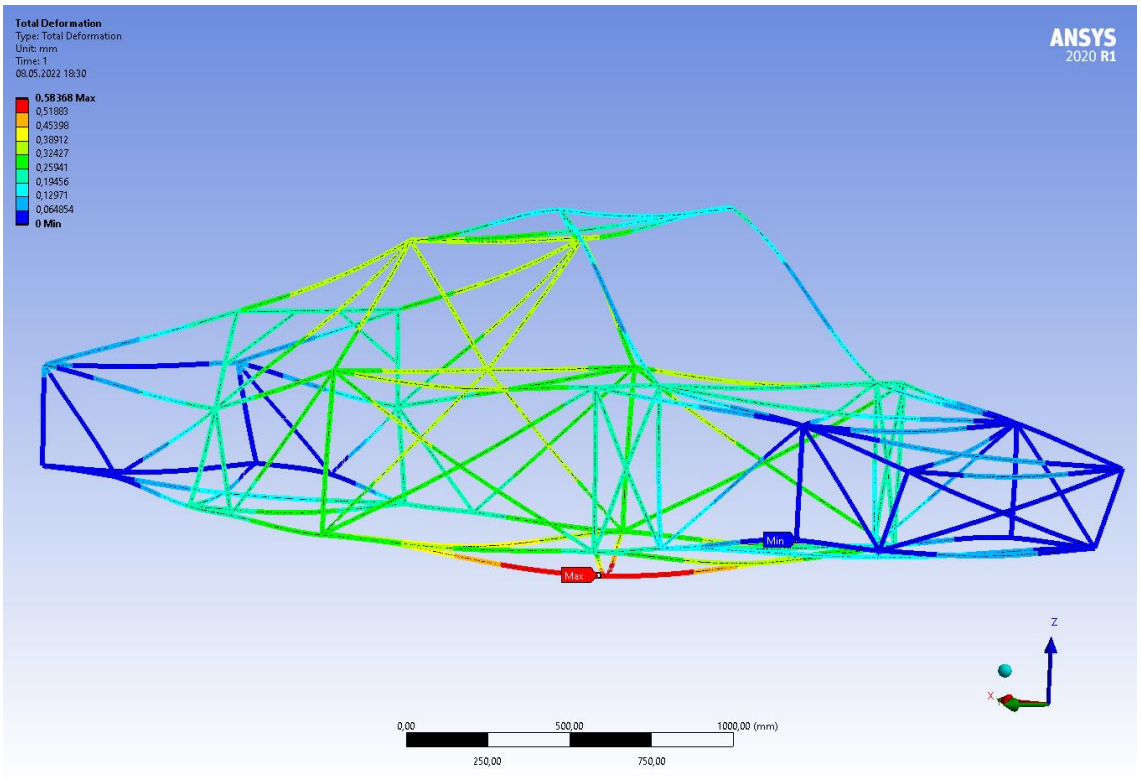

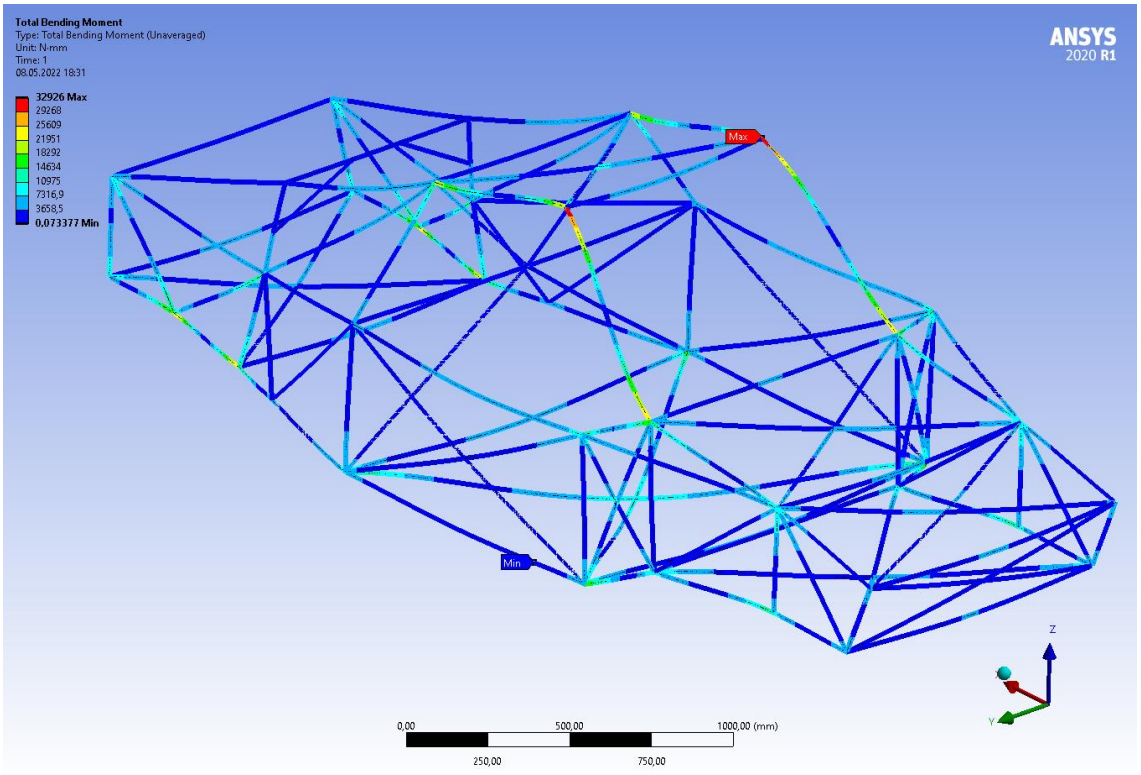

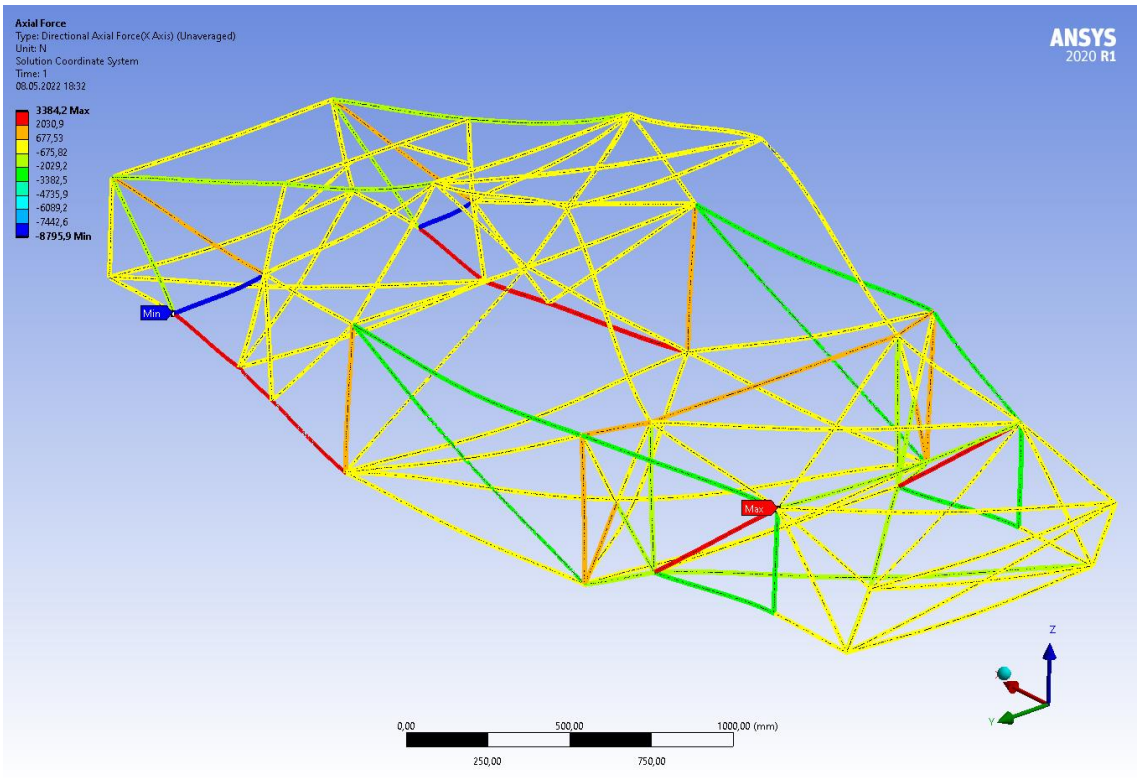
Axial Force
Type: Directional Axial Force(X Axis) (Unaveraged)
Unit: N
Solution Coordinate System
Time: 1
08.05.2022 18:32
3384,2 Max
2030,9
677,53
-675,82
-2029,2
-3382,5
-4735,9
-6089,2
-7442,6
-8795,9 Min
ANSYS
2020 R1
Min
Max
0,00
500,00
1000,00 (mm)
250,00
750,00
Z
Y

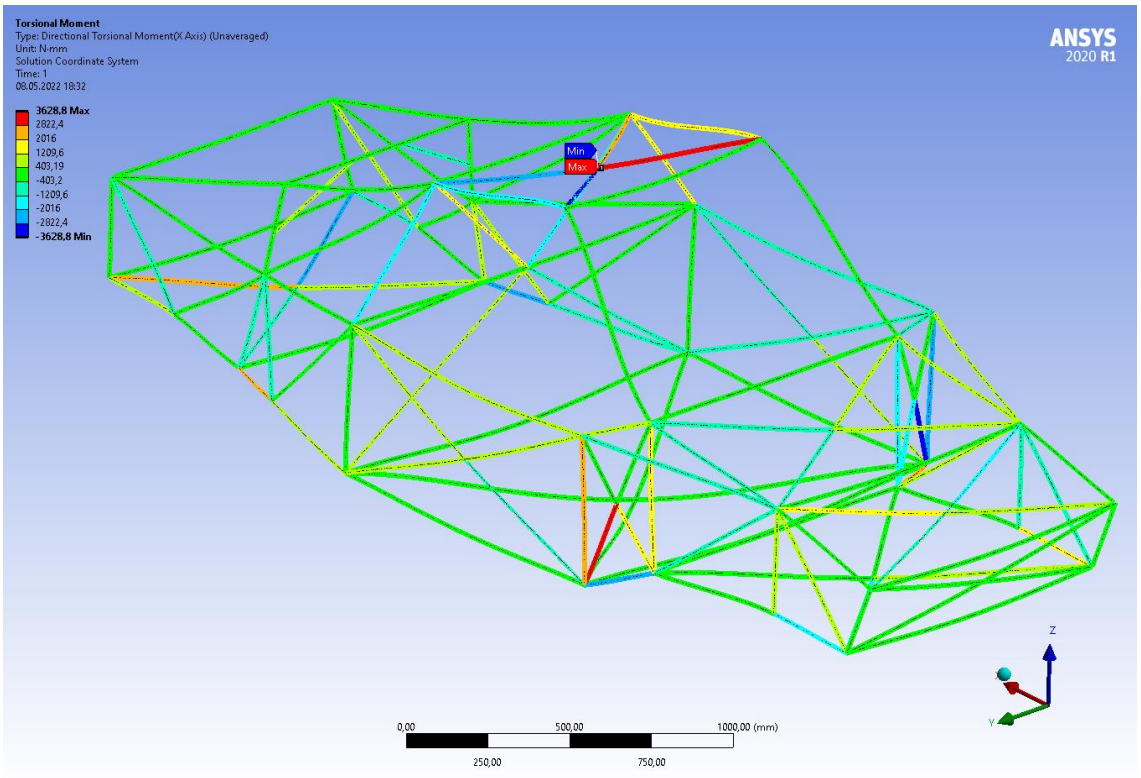
Torsional Moment
Type: Directional Torsional Moment(X Axis) (Unaveraged)
Unit: N·mm
Solution Coordinate System
Time: 1
08.05.2022 18:32
3628,8 Max
2822,4
2016
1209,6
403,19
-403,2
-1209,6
-2016
-2822,4
-3628,8 Min
ANSYS
2020 R1
Min
Max
0,00
500,00
1000,00 (mm)
250,00
750,00
Z
Y

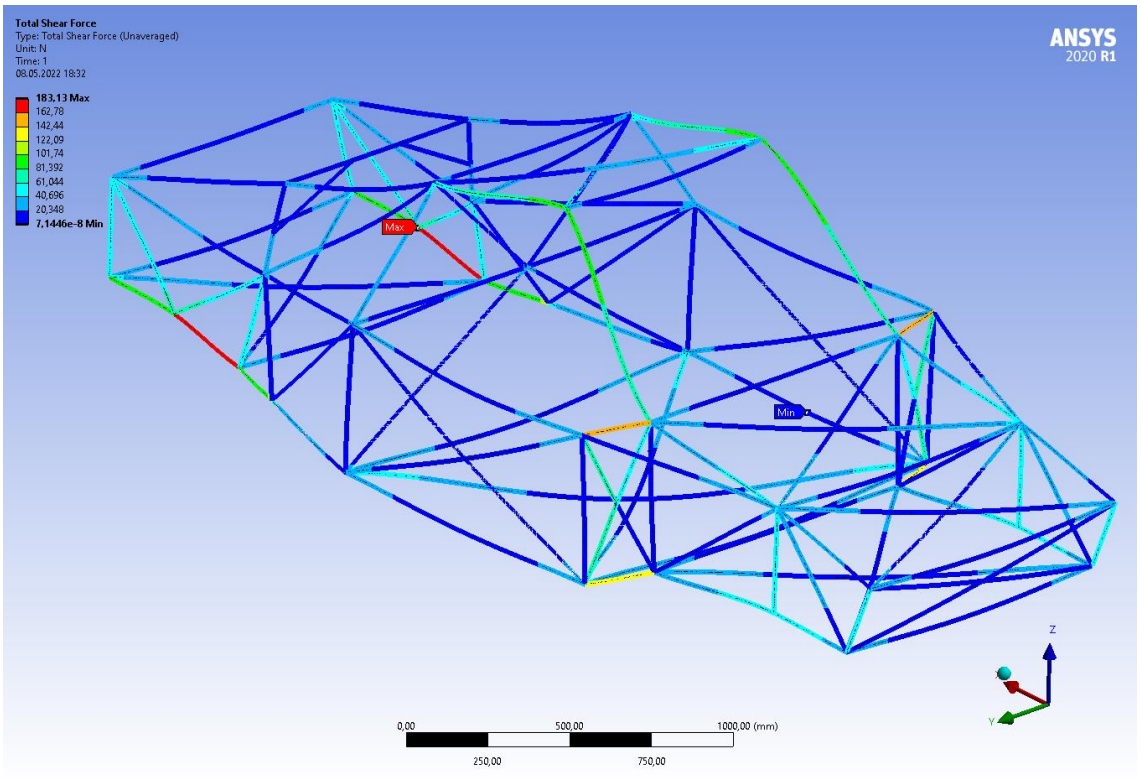
Total Shear Force
Type: Total Shear Force (Unaveraged)
Unit: N
Time: 1
08.05.2022 18:32
183,13 Max
162,78
142,44
122,09
101,74
81,392
61,044
40,696
20,348
7,1446e-8 Min
ANSYS
2020 R1
Max
Min
Z
Y
0,00
500,00
1000,00 (mm)
250,00
750,00

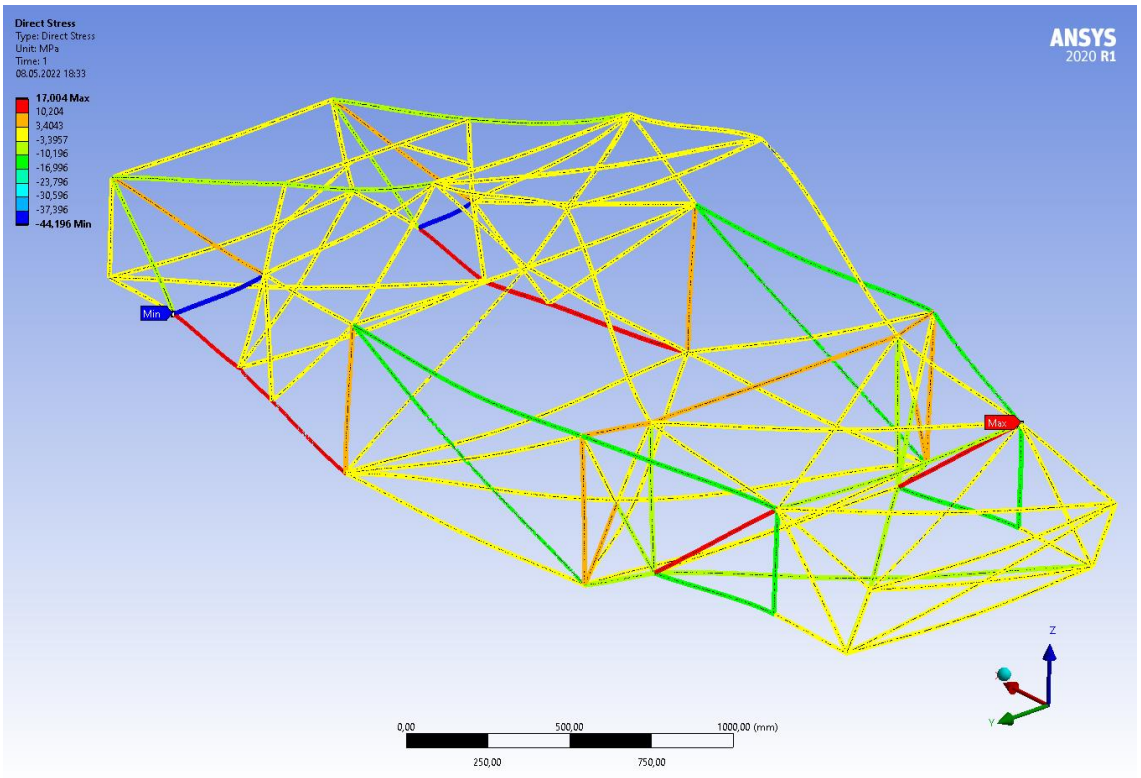
Direct Stress
Type: Direct Stress
Unit: MPa
Time: 1
08.05.2022 18:33
17,004 Max
10,204
3,4043
-3,3957
-10,196
-16,996
-23,796
-30,596
-37,396
-44,196 Min
ANSYS
2020 R1
Min
Max
Z
Y
0,00
500,00
1000,00 (mm)
250,00
750,00

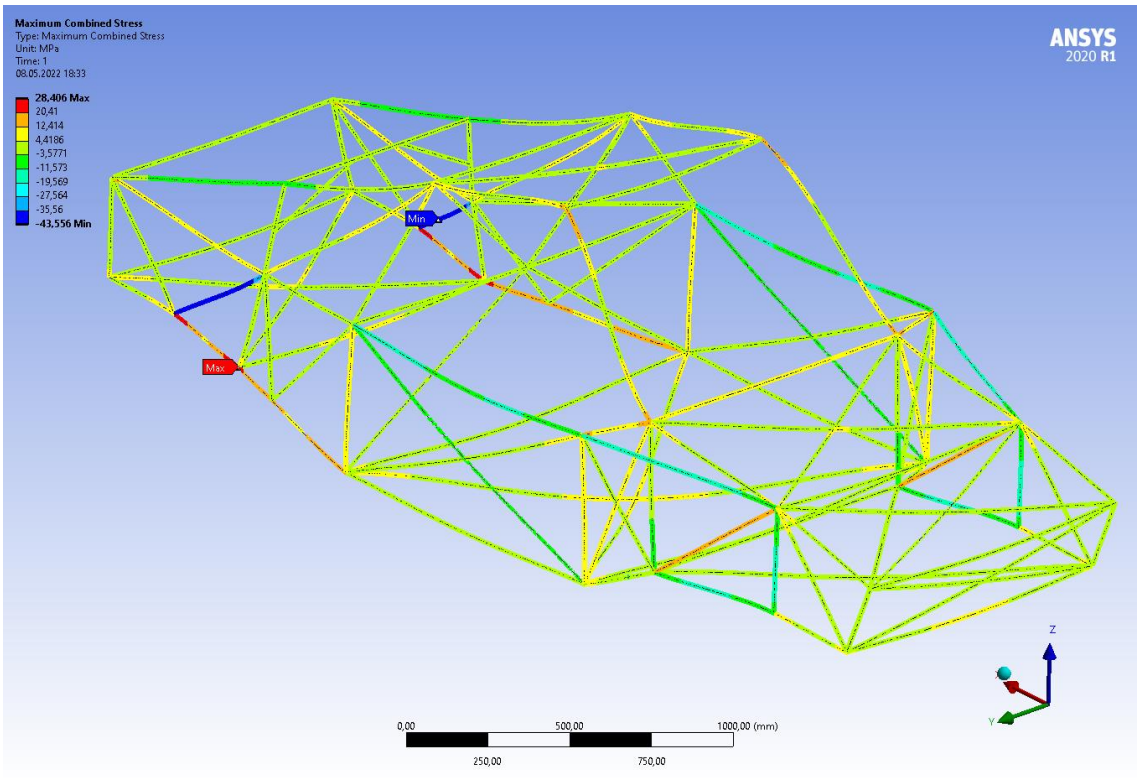
Maximum Combined Stress
Type: Maximum Combined Stress
Unit: MPa
Time: 1
08.05.2022 18:33
28,406 Max
20,41
12,414
4,4186
-3,5771
-11,573
-19,569
-27,564
-35,56
-43,556 Min
ANSYS
2020 R1
Min
Max
0,00
500,00
1000,00 (mm)
250,00
750,00
Z
Y

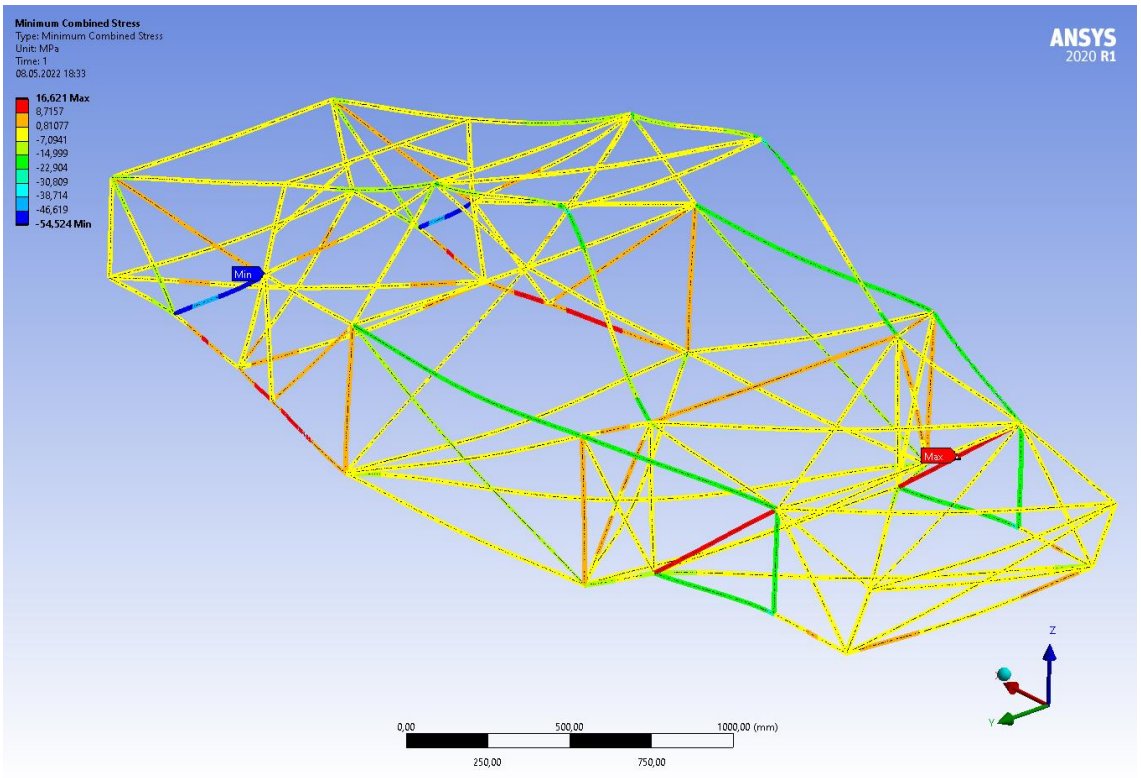
Minimum Combined Stress
Type: Minimum Combined Stress
Unit: MPa
Time: 1
08.05.2022 18:33
16,621 Max
8,7157
0,81077
-7,0941
-14,999
-22,904
-30,809
-38,714
-46,619
-54,524 Min
ANSYS
2020 R1
Min
Max
0,00
500,00
1000,00 (mm)
250,00
750,00
Z
Y

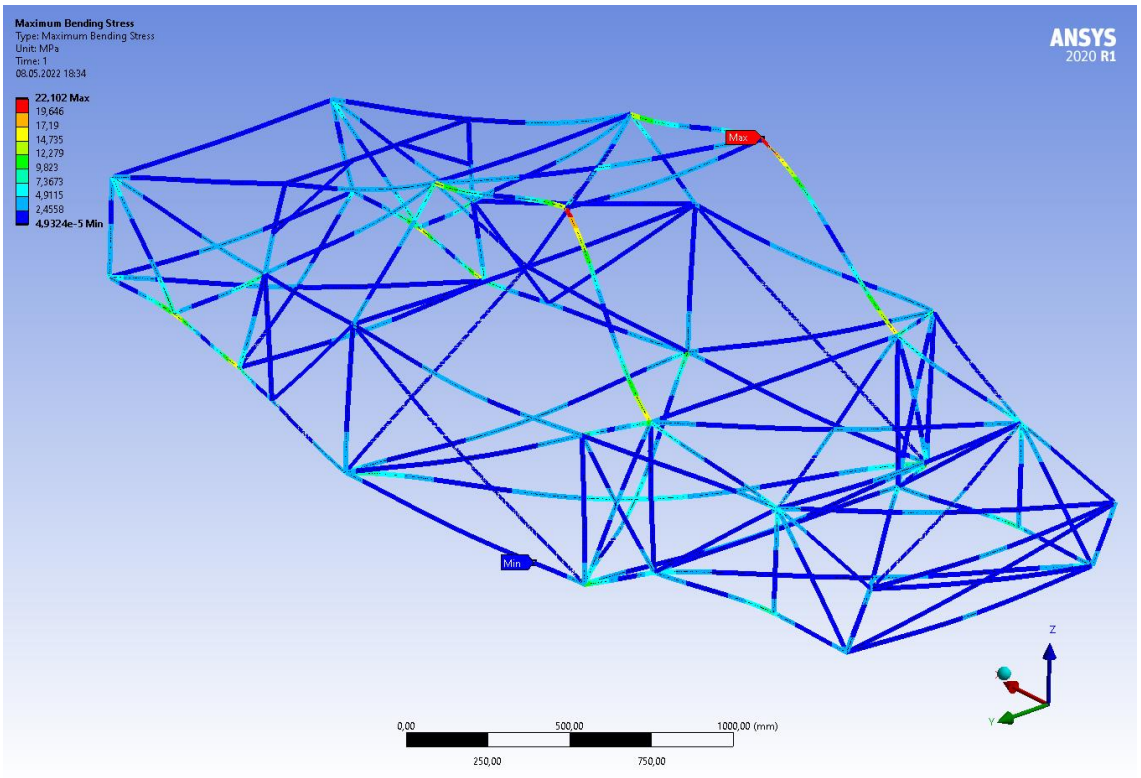
Maximum Bending Stress
Type: Maximum Bending Stress
Unit: MPa
Time: 1
08.05.2022 18:34
22,102 Max
19,646
17,19
14,735
12,279
9,823
7,3673
4,9115
2,4558
4,9324e-5 Min
ANSYS
2020 R1
Max
Min
Z
Y
0,00
500,00
1000,00 (mm)
250,00
750,00

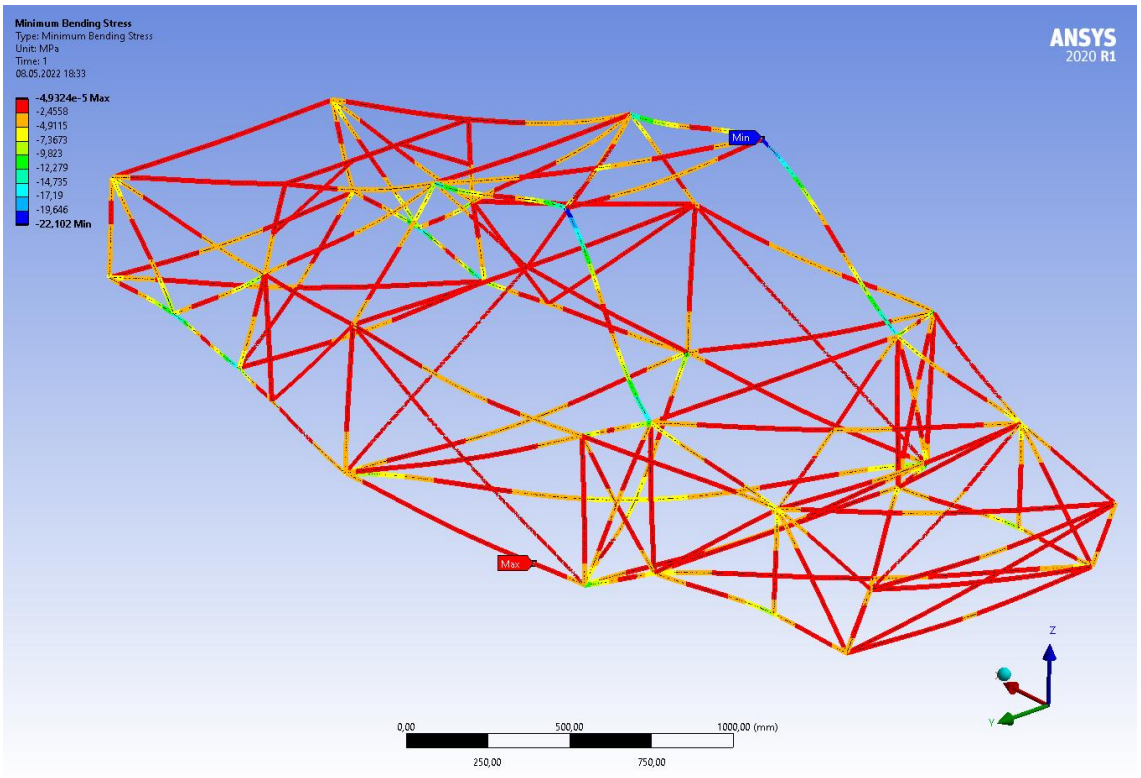
Minimum Bending Stress
Type: Minimum Bending Stress
Unit: MPa
Time: 1
08.05.2022 18:33
-4,9324e-5 Max
-2,4558
-4,9115
-7,3673
-9,823
-12,279
-14,735
-17,19
-19,646
-22,102 Min
ANSYS
2020 R1
Min
Max
Z
Y
0,00
500,00
1000,00 (mm)
250,00
750,00

Appendix C

Dynamic load lateral.

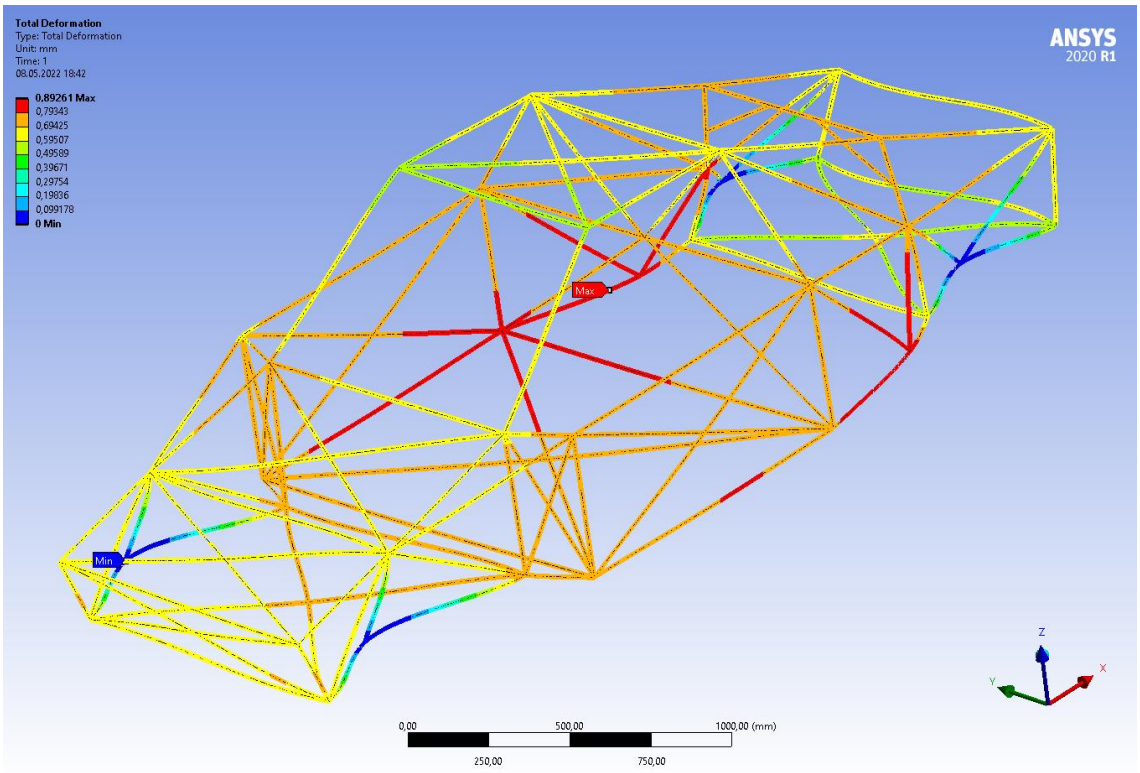

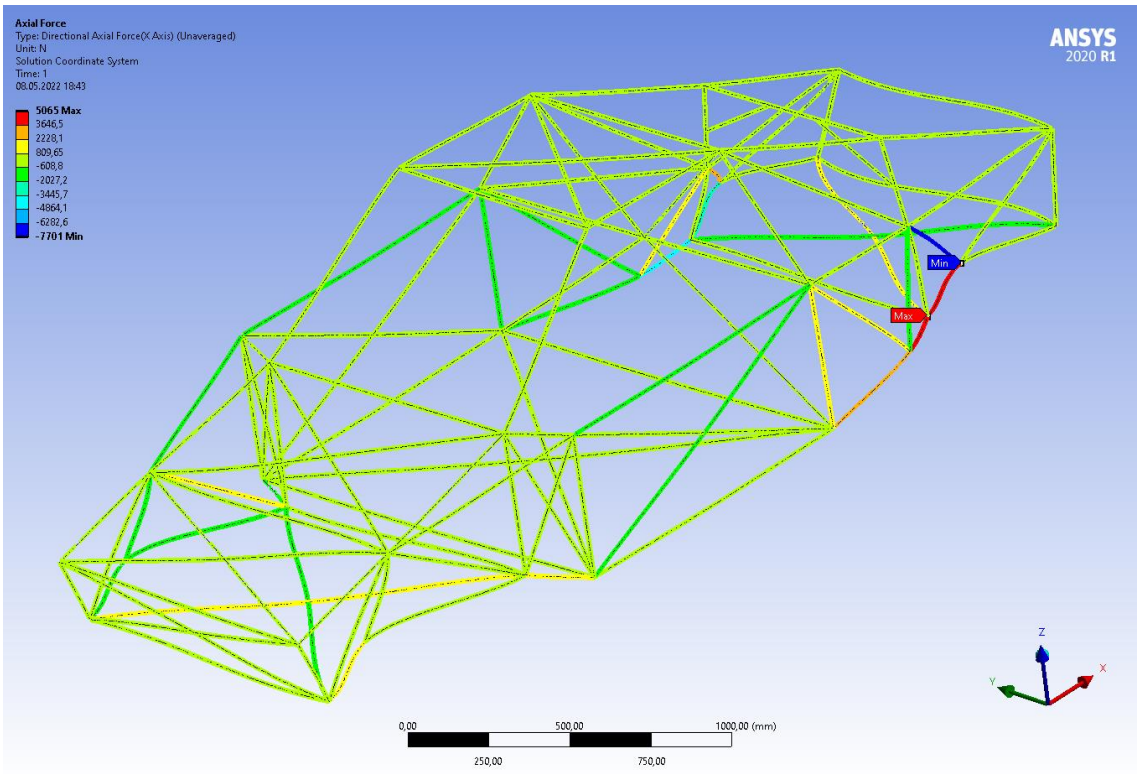

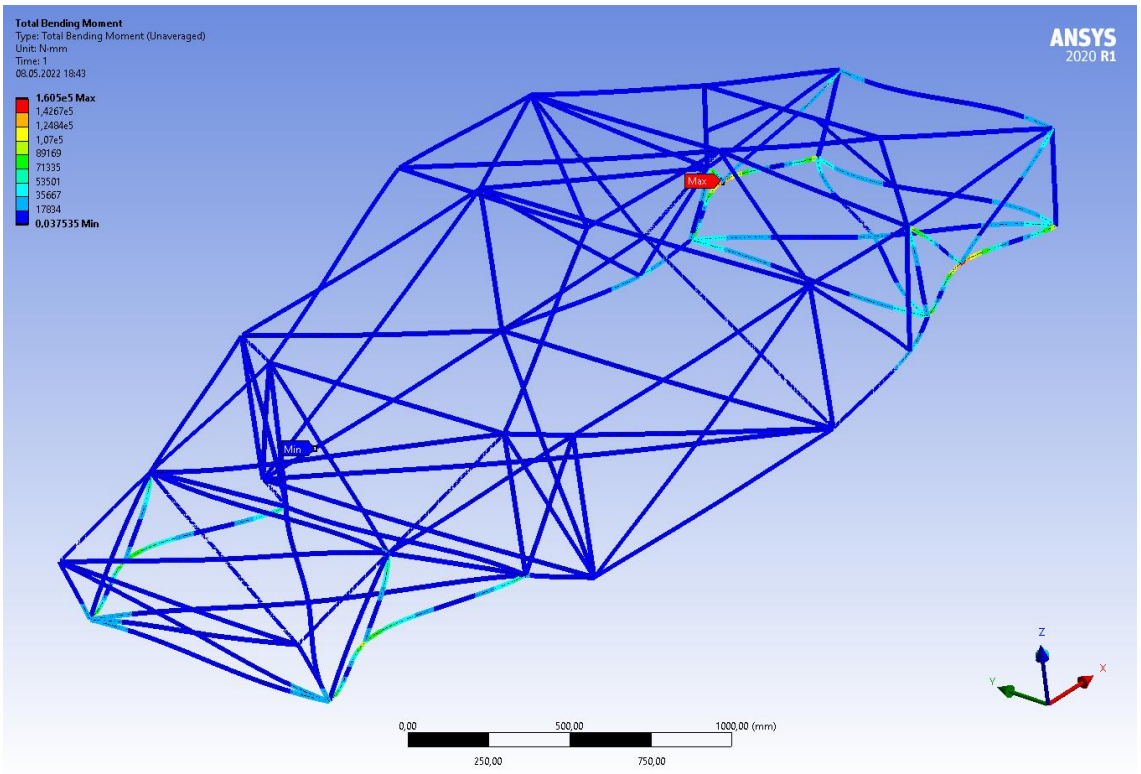
Total Bending Moment
Type: Total Bending Moment (Unaveraged)
Unit: N·mm
Time: 1
08.05.2022 18:43
1,605e5 Max
1,4267e5
1,2484e5
1,07e5
89169
71335
53501
35667
17834
0,037535 Min
ANSYS
2020 R1
Max
Min
Z
Y
X
0,00
500,00
1000,00 (mm)
250,00
750,00

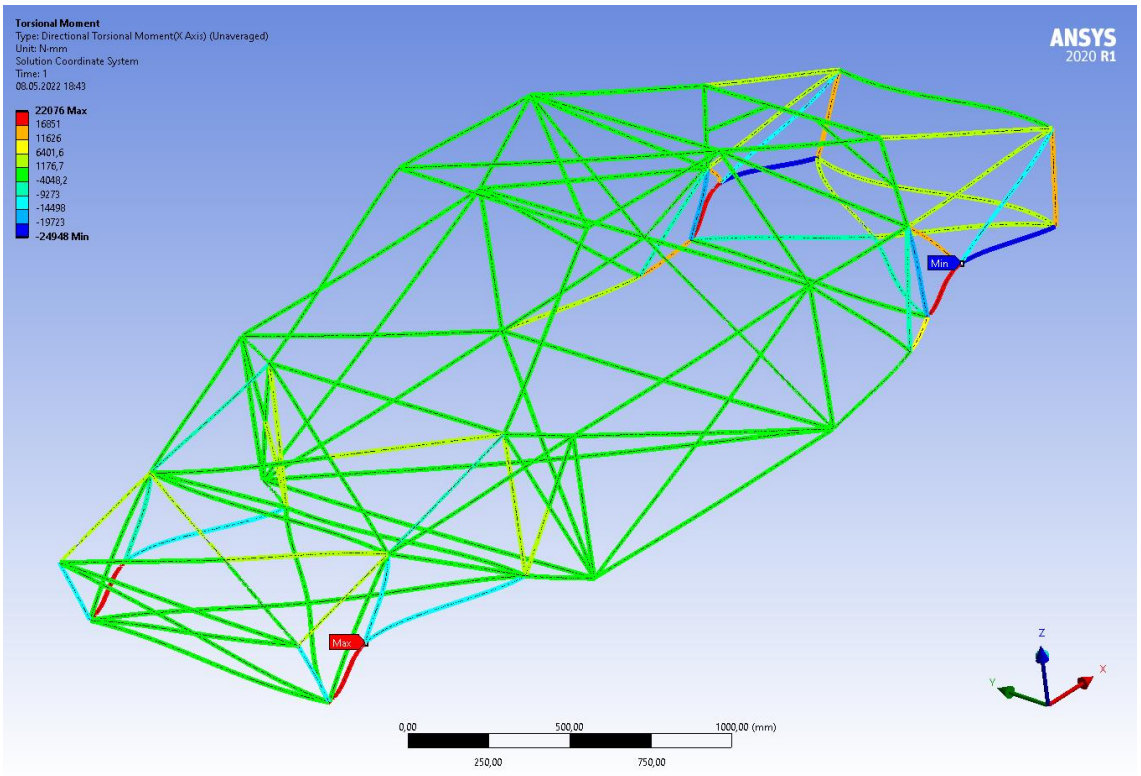
Torsional Moment
Type: Directional Torsional Moment(X Axis) (Unaveraged)
Unit: N·mm
Solution Coordinate System
Time: 1
08.05.2022 18:43
22076 Max
16851
11626
6401,6
1176,7
-4048,2
-9273
-14498
-19723
-24948 Min
ANSYS
2020 R1
Min
Max
Z
Y
X
0,00
500,00
1000,00 (mm)
250,00
750,00

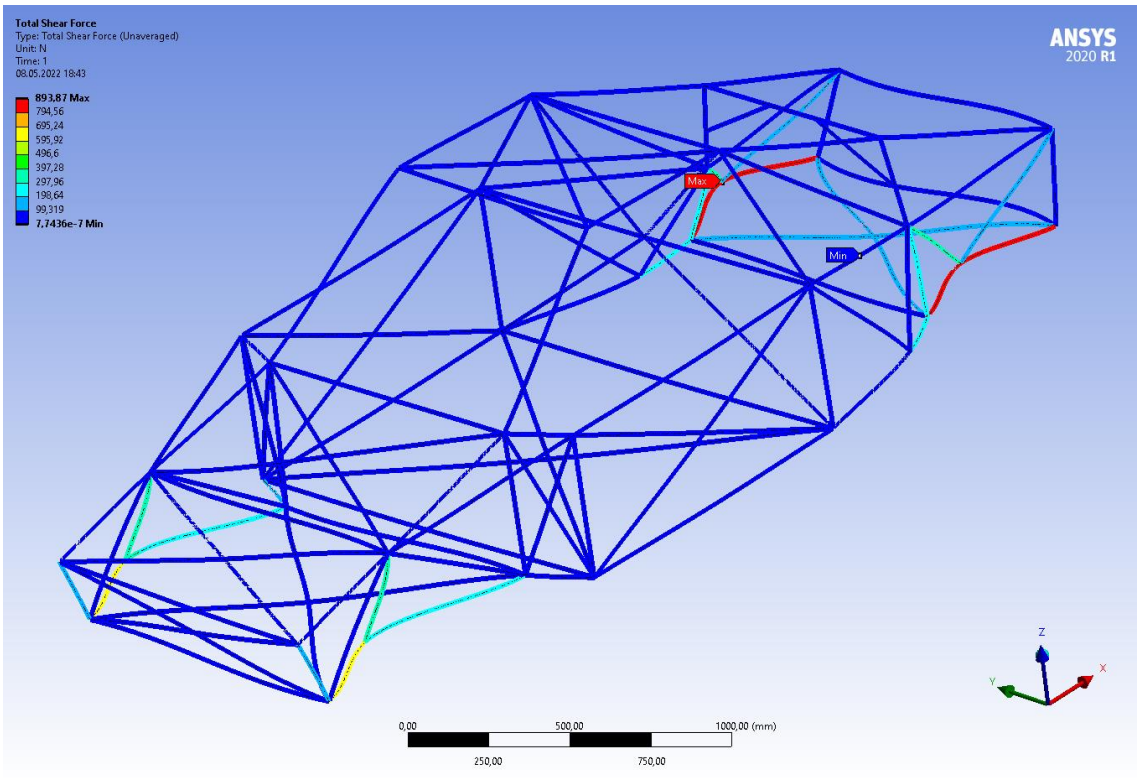
Total Shear Force
Type: Total Shear Force (Unaveraged)
Unit: N
Time: 1
08.05.2022 18:43
893,87 Max
794,56
695,24
595,92
496,6
397,28
297,96
198,64
99,319
7,7436e-7 Min
ANSYS
2020 R1
Max
Min
Z
X
Y
0,00
500,00
1000,00 (mm)
250,00
750,00

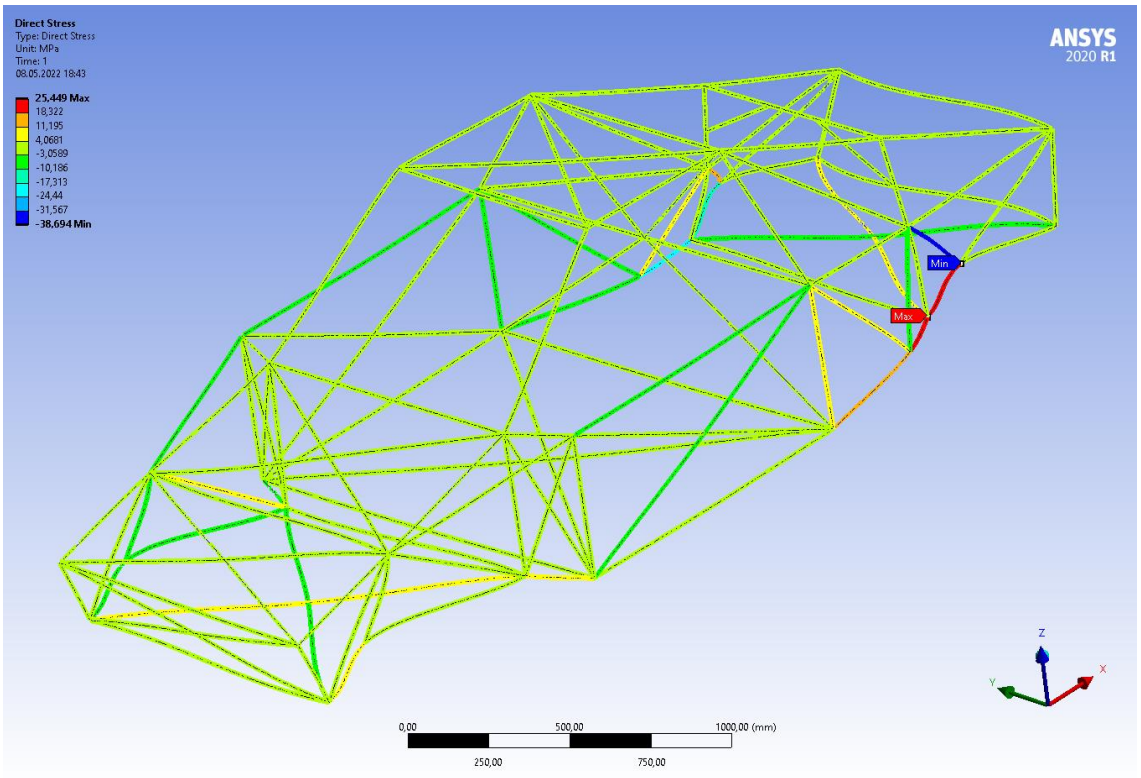
Direct Stress
Type: Direct Stress
Unit: MPa
Time: 1
08.05.2022 18:43
25,449 Max
18,322
11,195
4,0681
-3,0589
-10,186
-17,313
-24,44
-31,567
-38,694 Min
ANSYS
2020 R1
Min
Max
Z
X
Y
0,00
500,00
1000,00 (mm)
250,00
750,00

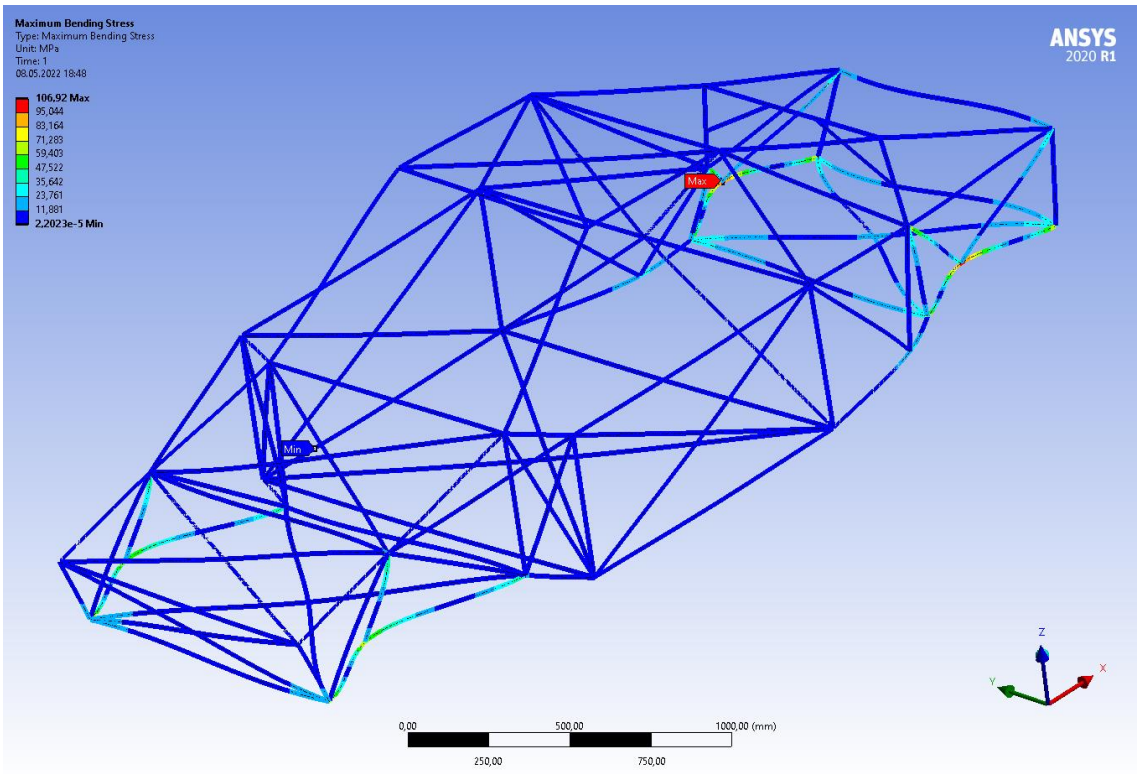
Maximum Bending Stress
Type: Maximum Bending Stress
Unit: MPa
Time: 1
08.05.2022 18:48
106,92 Max
95,044
83,164
71,283
59,403
47,522
35,642
23,761
11,881
2,2023e-5 Min
ANSYS
2020 R1
Max
Min
Z
Y
X
0,00
500,00
1000,00 (mm)
250,00
750,00

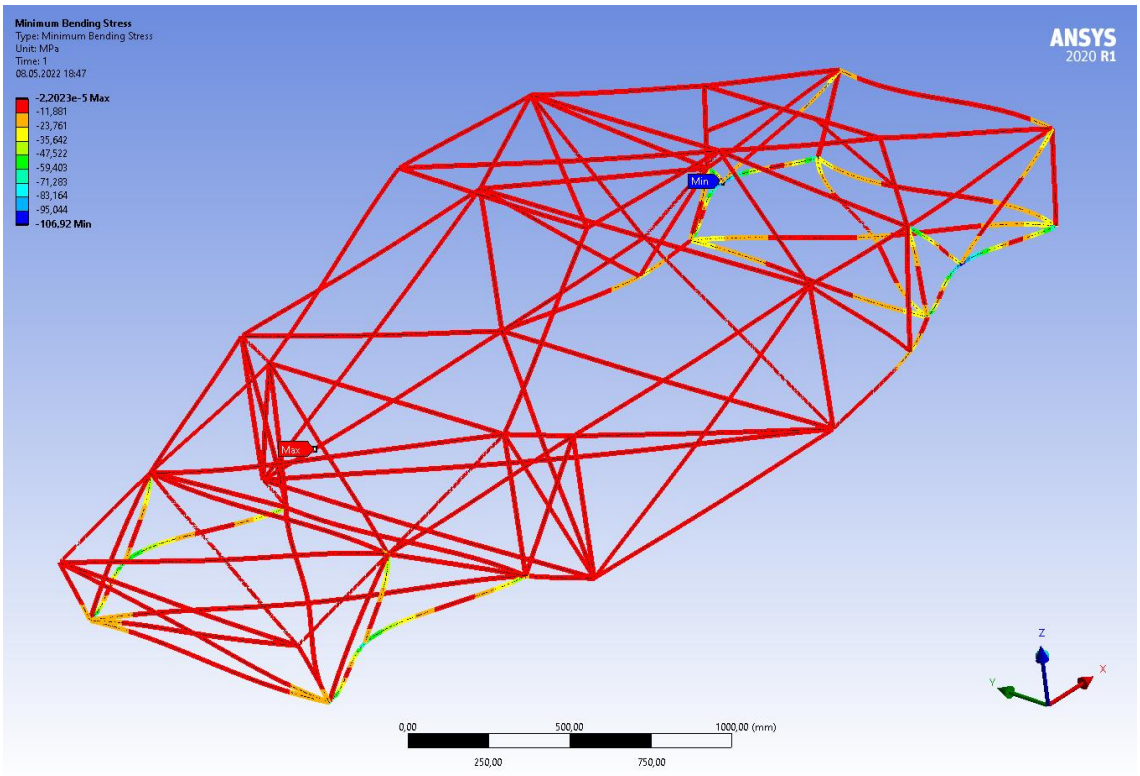
Minimum Bending Stress
Type: Minimum Bending Stress
Unit: MPa
Time: 1
08.05.2022 18:47
-2,2023e-5 Max
-11,881
-23,761
-35,642
-47,522
-59,403
-71,283
-83,164
-95,044
-106,92 Min
ANSYS
2020 R1
Min
Max
Z
Y
X
0,00
500,00
1000,00 (mm)
250,00
750,00

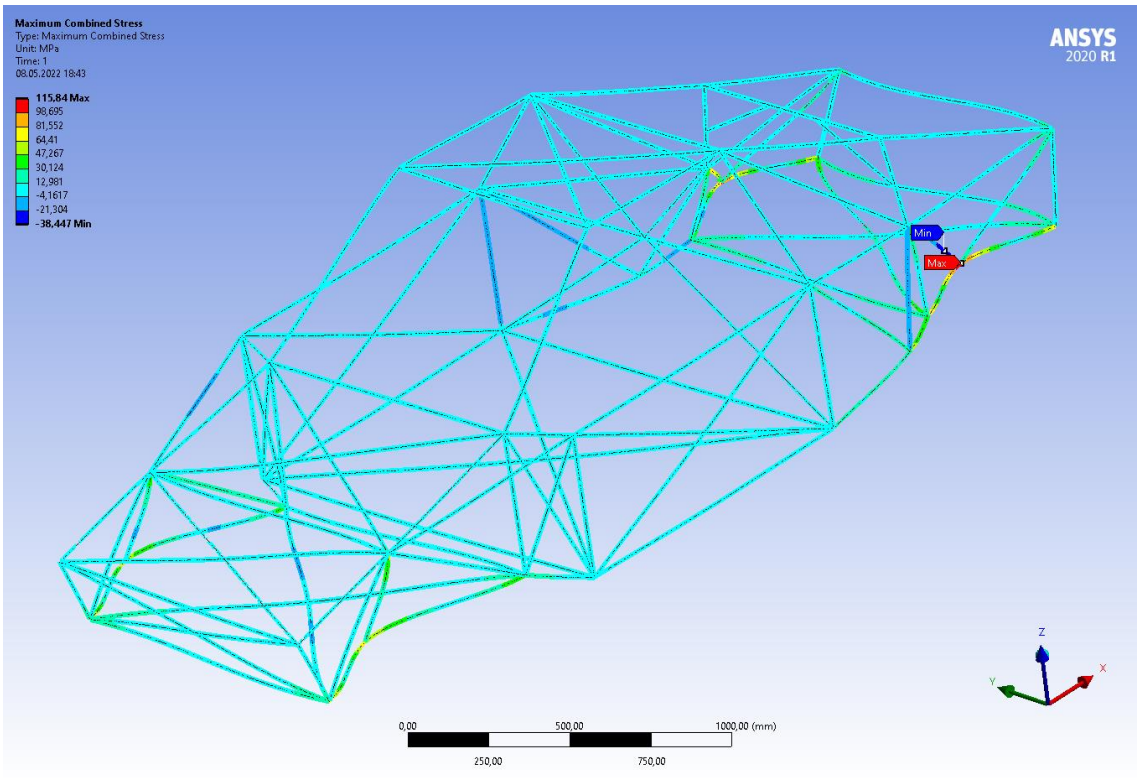
Maximum Combined Stress
Type: Maximum Combined Stress
Unit: MPa
Time: 1
08.05.2022 18:43
115,84 Max
98,695
81,552
64,41
47,267
30,124
12,981
-4,1617
-21,304
-38,447 Min
ANSYS
2020 R1
Min
Max
Z
Y
X
0,00
500,00
1000,00 (mm)
250,00
750,00

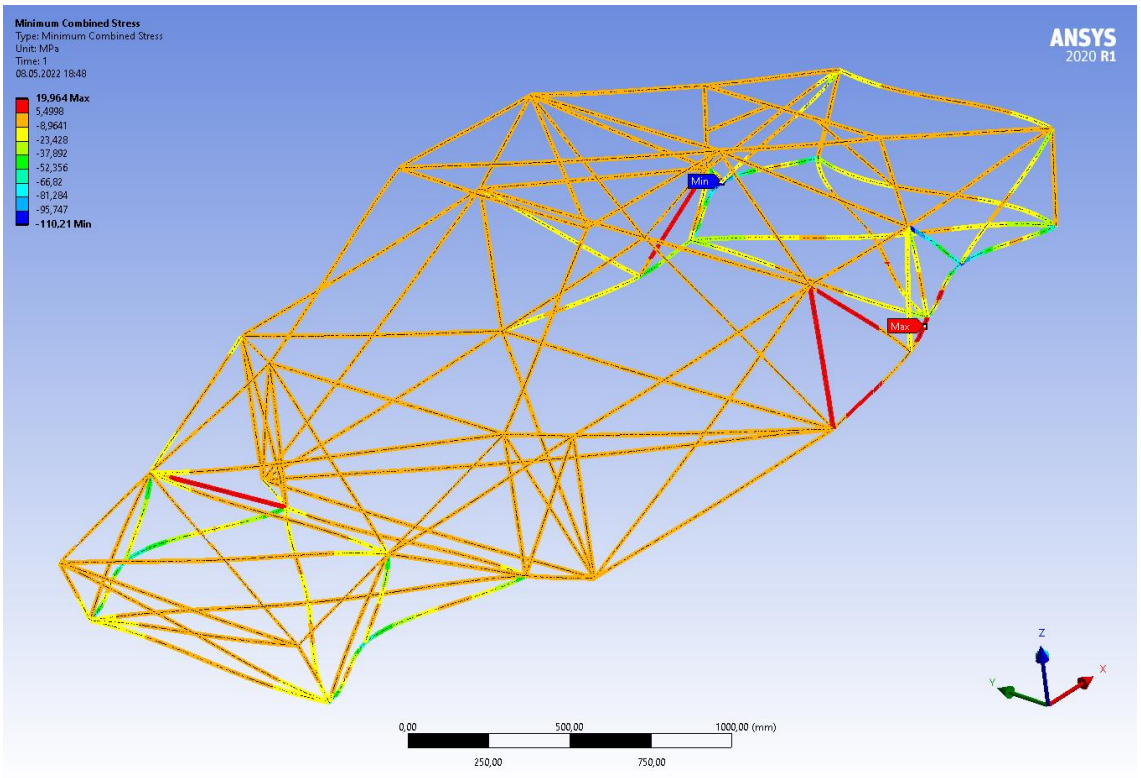
Minimum Combined Stress
Type: Minimum Combined Stress
Unit: MPa
Time: 1
08.05.2022 18:48
19,964 Max
5,4998
-8,9641
-23,428
-37,892
-52,356
-66,82
-81,284
-95,747
-110,21 Min
ANSYS
2020 R1
Min
Max
Z
Y
X
0,00
500,00
1000,00 (mm)
250,00
750,00